Dissertation zur Erlangung des Doktorgrades

der Fakultät für Chemie und Pharmazie

der Ludwig-Maximilians-Universität München

Functional analysis of the bacterial DNA repair protein complex SbcCD

Jan-Hinnerk Friedrich Fokke Saathoff

aus

Hannover, Deutschland

2018

Erklärung

Diese Dissertation wurde im Sinne von §7 der Promotionsordnung vom 28. November 2011 von Herrn Prof. Dr. Karl-Peter Hopfner betreut.

Eidesstattliche Versicherung

Diese Dissertation wurde eigenständig und ohne unerlaubte Hilfe erarbeitet.

München, den 15. Mai 2018

_____

Jan-Hinnerk FSaathoff

Dissertation eingereicht am:	17.05.2018
1. Gutachter:	Prof. Dr. rer. nat. Karl-Peter Hopfner
2. Gutachter:	Prof. Dr. rer. nat. Klaus Förstemann
Mündliche Prüfung am:	10.07.2018

Der größte Feind des Wissens ist nicht Unwissenheit,

sondern die Illusion, wissend zu sein.

Daniel J. Boorstin

This thesis was prepared from Oktober 2013 to May 2018 in the laboratory of Prof. Dr. Karl-Peter Hopfner at the Gene Center of the Ludwig-Maximilians-Universität (LMU)

Publications

During the work of this thesis, the following publication is in the process of being published:

Saathoff J.-H., Käshammer L., Lammens K., Byrne R.T., Hopfner K.-P. (2018). **The bacterial Mre11-Rad50 homolog SbcCD cleaves opposing strands of DNA by two chemically distinct nuclease reactions.** Nucleic Acids Res. 2018 Oct 2. doi: 10.1093/nar/gky878. [Epub ahead of print]

Table of Contents

1. Summary

The genomic integrity of all organisms is constantly challenged by genotoxic stress originating from endogenous and exogenous sources, with stalled replication forks (RFs) and double-strand breaks (DSBs) being among the most deleterious forms of DNA damage. Failure to properly respond to genomic distress can be highly mutagenic and lead to chromosomal aberrations. Thus, cells have evolved distinct DNA repair mechanisms.

The Mre11-Rad50-Nbs1 (MRN) complex holds a key position in the DNA damage response (DDR) and is involved in the repair of DSBs, stalled RFs and dysfunctional telomeres. MRN acts by sensing and processing these diverse DNA structures and mediates signaling *via* the kinases ATM and ATR in eukaryotes.

Although the MRN complex has been intensively studied for the last two decades, its fundamental mechanisms of action are still poorly understood. In particular, the nature of its ATP-dependent nuclease activities and how it specifically recognizes DNA ends remains unknown.

The aim of this work was to investigate the biochemical activities of the bacterial Mre11-Rad50 homolog, SbcCD. For this purpose, biochemical assays were developed and established to study and functionally connect the enzymatic activities of SbcCD.

These assays showed that SbcCD has a low basal ATPase rate. ATP hydrolysis is increasingly stimulated by (i) supercoiled DNA, (ii) double-stranded DNA and (iii) DNA ends. For its nuclease activity, SbcCD strictly requires DNA ends. SbcCD's exonuclease activity depends on ATP binding, whilst the endonuclease activity requires ATP hydrolysis. A protein-blocked DNA end stimulates SbcCD's endonuclease, which leads to internal cleavage of both DNA strands approximately 25 base pairs from the DNA end.

Upon ATP hydrolysis, SbcCD also distorts the internal structure of the DNA duplex, implying that its DNA melting and endonuclease activities are functionally coupled. The position of SbcCD's endonucleolytic cleavage is sensitive to 5 nucleotide DNA bubbles, which are cleaved on the 5' side of the bubble. Therefore, a DNA bubble could be a transient intermediate, which is required for endonucleolytic cleavage. To generate this intermediate, it appears that a native SbcD dimer interface and the plasticity of the dimer interface are important.

SbcCD cleaves the scissile phosphate on different sides, producing either 3’ or 5’ phosphates. The distinct cleavage products are determined by both the nuclease activity itself and the strand polarity. This suggests that the exo- and endonuclease activities have distinct cleavage mechanisms and could involve a geometrically flipped SbcCD complex.

The presented results provide not only a more detailed knowledge of the mechanochemical performance of the SbcCD’s enzymatic activities, but also provide an important foundation for future structural investigations.

2. Introduction

2.1 DNA damage

Deoxyribonucleic acid (DNA) carries the genetic information used in the growth, development and functioning of all known living organisms. The DNA consists of two biopolymer strands coiled around each other to form a double helix. Each strand is composed of monomer units, called nucleotides, which consist of a nucleobase, deoxyribose, and a connecting phosphate group. The latter two constitute the sugar-phosphate backbone (Watson and Crick, 1953). As DNA stores the genetic instructions of each living cell, the information needs to be well maintained. The errors in DNA are also longer lasting (if not permanent), whereas those in RNA and protein are limited by the lifetime of the molecule.

DNA damage has emerged as a major cause for many diseases related to aging and the development of cancer (Hoeijmakers, 2009). Thus, the cells have evolved mechanisms to remove different types of DNA damage. They evolved a highly coordinated cascade of events, known as the DNA damage response (DDR). The DDR senses the DNA damage, signals the presence and mediates its repair (Dexheimer, 2013).

DNA is constantly subjected to chemical and structural changes caused by extrinsic or intrinsic factors. Although DNA itself is chemically a stable compound at pH 7.5 in an aqueous solution, spontaneous acid-catalyzed hydrolysis of the N-glycosidic bond between the sugar and base occurs. These abasic sites are generated at a rate of approximately 10000 per cell per day (Lindahl and Nyberg, 1972). DNA is also susceptible to the chemical modification by reactive molecules that evolve during normal cellular metabolism, most prominently reactive oxygen species (ROS). These species not only induce a variety of base modifications, but also DNA-protein linkages and single- and double-strand breaks (Cadet et al., 1997). Unwanted DNA alkylation can also arise from endogenous sources, such as S-adenosyl-methionine. The primary sites of alkylation are the O- and N-atoms of nucleobases (De Bont and van Larebeke, 2004; Rydberg and Lindahl, 1982).

Endogenous genomic damage can also occur during cellular metabolism events, such as misincorporated nucleotides by DNA-polymerases during replication. Furthermore, chemically altered nucleotide precursors, such as 8-oxo-dGTP and dUTP, represent a significant source of replication-related DNA-damage (McCulloch and Kunkel, 2008).

In addition to endogenous sources of DNA damage, DNA is also constantly subject to exogenous or environmental DNA damaging agents. These include physical stress, such as UV-light, which induces the formation pyrimidine dimers (Ravanat et al., 2001).

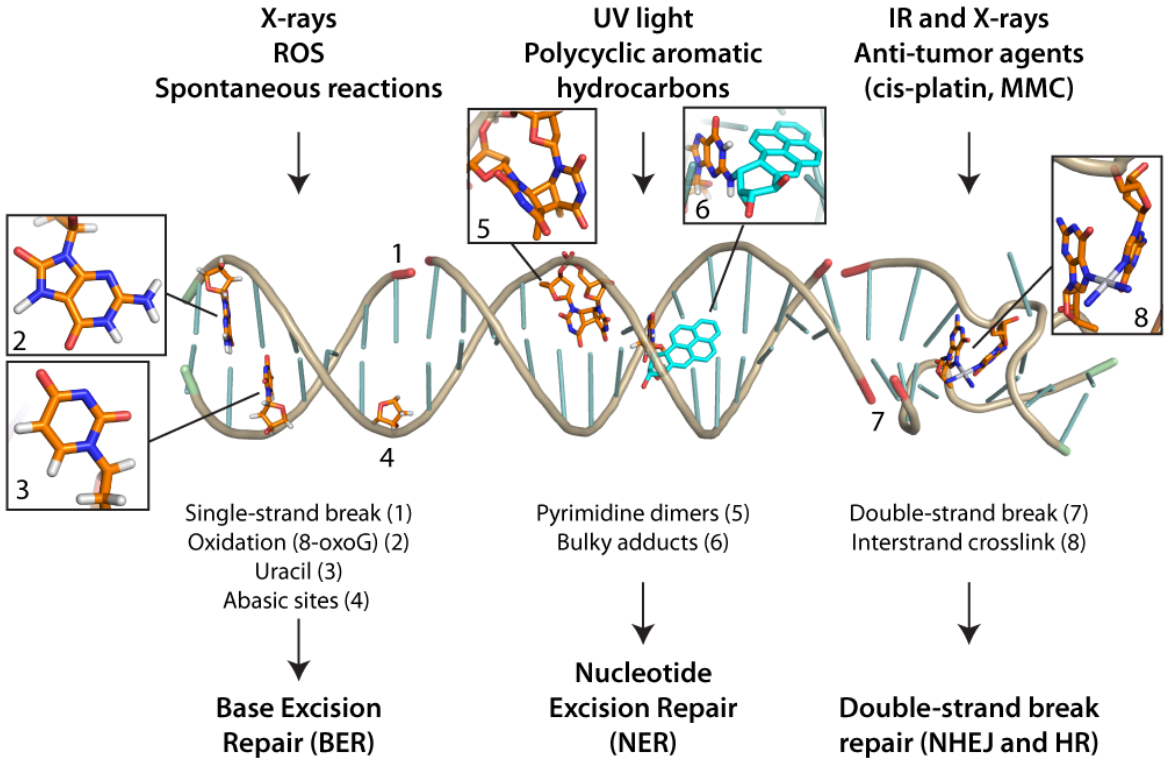

Figure 1 DNA damage and repair mechanisms. The diagram illustrates common DNA damaging agents, examples of DNA lesions caused by these agents, and the relevant DNA repair mechanism responsible for their removal. The thymine dimer (PDB code: 1T4I), the Benzo[a]pyrene adduct (5T14) and the cis-platin interstrand crosslink (1A2E) were modeled according to their crystal structures.

Cells have developed repair mechanisms, which are individually tailored to correct the different types of DNA lesions. The major repair-pathways in mammalian cells are base excision repair (BER), mismatch repair (MMR), nucleotide excision repair (NER), non-homologous end joining (NHEJ) and homologous recombination (HR).

2.2 DNA double-strand breaks

A double-strand break (DSB) occurs when both strands of the DNA duplex are severed in close proximity. They are particularly deleterious as the DNA ends can promote potentially lethal chromosomal rearrangements. These events are often associated with the development of cancer or other genomic

instability syndromes (Hoeijmakers, 2009). However, DSBs are also important intermediates in DNA metabolism processes, where they are temporarily inserted into the genome. The following chapter will give a short overview of the chances and threats posed by DSBs.

2.2.1 DNA double-strand breaks in cellular metabolism processes

In several physiological and developmental processes, DSBs are functional intermediates and required for the genetic exchange within or between chromosomes (Mehta and Haber, 2014).

For example, programmed DSBs are generated during meiosis in most sexually reproducing organisms. After alignment of homologous chromosomes in meiotic prophase I, DSBs are introduced at specific hotspots by the evolutionary conserved, topoisomerase-II-like, Spo11 protein (Keeney, 2008). The DNA crosslinked Spo11 is subsequently removed by the Mre11-Rad50-Nbs1 complex and homologous recombination events are initiated. The crossover formation results in gene conversion and therefore genetic diversification (Inagaki et al., 2010).

The introduction of DSBs is also an essential step during V(D)J recombination, a mechanism of genetic recombination to generate immunoglobulin (Igs) and the T cell receptors (TCRs) found on B cells and T cells. The diversity is obtained by the random rearrangement of variable (V), joining (J) and diversity (D) gene cassettes (Tonegawa, 1983). In mammals, it is initiated by the RAG-1/2 recombinase which introduces a single-strand nick between the coding- (V, D or J) and signal segment. The resulting 3’ hydroxyl group is positioned by RAG-1 to attack the phosphodiester bond of the opposing strand, such that a hairpin on the coding segment and a blunt end on the signal segment are formed (Schatz and Swanson, 2011). The individual coding segments are then arranged and ligated by the non-homologous end joining (NHEJ) pathway (Lu et al., 2007).

In *Saccharomyces cerevisiae*, the switching of mating type is initiated with a site-specific DSB, which is introduced by the HO-endonuclease at the MAT gene locus. Subsequently, the mating type gene is switched by unidirectional gene conversion *via* recombination with the HML or HMR gene cassette, which carries silenced copies of the mating types a and α, respectively (Haber, 2012).

DSBs also occur accidentally during essential cellular processes, such as DNA replication. As DNA does not always supply a clean template for DNA synthesis, the replisome must overcome structural obstacles, such as (i) DNA lesions (ii) DNA secondary structures and (iii) tightly bound protein-DNA complexes that induce replication stress (Zeman and Cimprich, 2014).

This replication stress can lead to a replication fork collapse, which generates the risk of incomplete DNA replication. Furthermore, the cleavage of a reversed fork ('chicken foot') by Holliday junction resolvases results in the formation of a DSB. The presence of a single-strand nick also leads to replication fork collapse and is likely to produce a free dsDNA end (Cortez, 2015). Since sister chromatid is often available as a repair template in S-phase, DSBs arising during replication are mainly repaired by the homologous recombination (HR) machinery (Errico and Costanzo, 2010).

2.2.2 Environmentally derived DNA double-strand breaks

In addition to the internal sources of DSBs, cells are challenged by various external factors that can induce DSBs.

Exposure to ionizing radiation (IR) poses a high risk of DSBs. It can originate from both natural (e.g. cosmic and gamma radiation) and artificial sources (e.g. X-rays or radiotherapy) and carries enough energy to liberate electrons from atoms or molecules. This can damage the DNA molecule directly, or indirectly by creating a high level of reactive oxygen species (ROS). Among other types of DNA damage, IR and ROS create DNA single-strand breaks (SSBs), which can convert into DSBs when introduced into complementary strands within one helical turn (Ward, 1994). IR and ROS induced breaks leave 'dirty' ends and usually require extensive processing for a proper repair (Mehta and Haber, 2014). Furthermore, UV light induces the formation of thymine dimers, which, if present during replication, induce stalled replication forks (Cordeiro-Stone et al., 1999).

In addition to physical influences, the cell must also deal with chemical sources of DNA damage. The DNA is an important target for anticancer treatment and DNA damaging agents (clastogens) have been developed as chemotherapeutic drugs (Wyrobek et al., 2005).

DNA is directly modified by DNA alkylating agents, such as methyl methanesulfonate (MMS) and temozolomide (TMZ), and crosslinking agents, such as mytomycin C and cisplatin. These compounds mostly act by introducing DNA damage that induce strong replication stress, severely affecting fast proliferating cells (Wang and Lippard, 2005). Bleomycin and phleomycin are nonribosomal peptides that directly induce DNA strand breaks but their exact mechanism of strand scission is currently not understood (Chen and Stubbe, 2005; Wyrobek et al., 2005). Another class of anti-cancer medications are topoisomerase inhibitors such as camptothecin and etoposide. These poison the topoisomerase by blocking the ligation step after DNA strand cleavage, which results in the formation of SSBs and DSBs (Koster et al., 2007).

Other well-studied DNA damaging chemicals include N-nitrosamines, heterocyclic amines, and polycyclic aromatic hydrocarbons (e.g. benzo(a)pyrene). These are commonly found in food, the latter also being present in air emissions, such as cigarette smoke and vehicle exhaust gases. In general, these types of compounds react with various sites on DNA bases to form the so-called bulky DNA adducts (Dexheimer, 2013).

2.3 DNA double-strand break repair

To counteract the impact of DSBs, cells have evolved various DNA repair mechanisms. These are conserved among the kingdoms of life, from bacteria to eukaryotes. The two major pathways are canonical NHEJ (c-NHEJ) and homologous recombination (HR). A third pathway is alternative NHEJ (alt-NHEJ), which involves minimal resection of DNA ends and requires microhomologies in the close proximity of the DSB (Thompson, 2012). Inherited defects in DSB repair leads to embryonic lethality, sterility, developmental disorders, immune deficiencies, and predisposition to neurodegenerative disease and cancer (Aguilera and Gomez-Gonzalez, 2008). This section describes the molecular mechanisms of c-NHEJ, alt-NHEJ and HR pathways and how the cell directs pathway choice.

2.3.1 Non-homologous end joining

The c-NHEJ pathway is utilized especially in G1 and early S-phase when no sister chromatid is available for recombinational repair. It promotes the direct ligation of two DNA ends, but, depending on the structure of the DSB substrate, c-NHEJ leads to a loss of between 0 and 14 base pairs (Betermier et al., 2014).

During c-NHEJ, DSB repair is mediated by a relatively small number of essential factors that are sequentially recruited to the DSB site. The initial step is recognition and binding of the DSB by the ring-shaped Ku70/Ku80 (Ku) heterodimer that encircles the DNA duplex (Walker et al., 2001). Ku has a high abundance (estimated at 400,000 molecules per cell) and a strong equilibrium dissociation constant of 1 nM to duplex DNA ends (Blier et al., 1993). Ku protects the DNA ends from premature processing and further DNA-damage and the Ku-DNA complex can be considered as a node at which the nucleases, polymerases and ligases of NHEJ can dock (Lieber, 2010). After DNA binding, Ku recruits the catalytic subunit of the DNA-dependent protein kinase (DNA-PKcs), which collocates both DNA ends. Once bound, DNA-PKcs acquires serine- and threonine kinase activity and is auto-phosphorylated, which induces the exposure of the DNA ends (DeFazio et al., 2002).

Depending on the structure of the DNA termini, the ends are made ligatable by minimal end resection or gap filling. The NHEJ-specific nuclease Artemis is recruited and activated through phosphorylation by DNA-PK (Jeggo and O'Neill, 2002). It cleaves a wide variety of DNA end structures and preferentially leaves a blunt end or a 4-nt 3' overhang (Ma et al., 2002). In order to keep sequence loss minimal and generate joining-compatible DNA ends, members of the Polymerase X family, namely μ and λ, act on the DSB site (Lieber, 2010). Further minor modification by the polynucleotide kinase (PNK) makes the DNA ends competent for ligation by adding a phosphate to the 5' end (Chappell et al., 2002).

After the processing of the DNA termini, they are religated by DNA ligase IV in conjunction with its binding partner XRCC4. The ligase activity is further stimulated by DNA-PKcs and XLF (XRCC4-like factor) (Mahaney et al., 2009).

The alt-NHEJ pathway takes advantage of microhomologies in proximity to the DSB. When several bases are nucleolytically removed from the break, the newly generated single-stranded DNA stretches hybridize through short stretches of the sequence homology. Therefore, alt-NHEJ is considered to be highly mutagenic (Haber, 2008). In this pathway, additional factors to the c-NHEJ machinery are involved and Mre11 was reported to be the main nuclease (Rahal et al., 2010).

2.3.2 Homologous recombination-mediated DSB repair

Homologous recombination does not comprise a single simple mechanism that applies to all breaks, in all organisms, at all times. This is due to the diversity and the size of DSBs, their origin, the timing in the cell cycle and the cell type (Mehta and Haber, 2014). Therefore, recombination mechanisms do not comprise a straightforward, linear process such as replication or transcription, but rather a collection of potential parallel and alternative processes (Heyer, 2015). This section mainly describes the HR pathway in human. However, the pathway and involved factors are remarkably conserved between species (Kowalczykowski, 2015).

The Mre11-Rad50-Nbs1 (MRN) complex is one of the first factors that are recruited to DNA DSBs (Stracker and Petrini, 2011). Depending on the nature of the DSB, the MRN complex needs to generate a 'clean' DNA end, which is compatible for long-range resection by processive nucleases. This is achieved by cleaving DNA with its dsDNA endonuclease activity, thereby removing the DNA-protein crosslinks (Deshpande et al., 2016; Paull and Gellert, 1998). The serine/threonine kinase ATM is recruited to the DSB and activated by MRN (Uziel et al., 2003). ATM mediates checkpoint signaling, and phosphorylates essential, HR-related factors. Furthermore, CtIP is recruited to the DSB *via* MRN in a CDK-

phosphorylation dependent manner (Sartori et al., 2007). One central role of CtIP could be the recruitment of BRCA1, which stimulates HR by the excluding the HR-inhibiting 53BP1-RIF1 complex from DSB sites (Bunting et al., 2010; Wong et al., 1998).

The chromatin structure is then altered and licensed for long-range resection, which is the determining step for HR (Hauer and Gasser, 2017). Long-range resection is either performed by DNA2, which requires RPA and a RecQ-like helicase (BLM or WRN) for activity, or by the exonuclease EXO1. The 3' overhang is immediately coated by RPA which is subsequently replaced by Rad51 forming a recombinase filament (Kowalczykowski, 2015).

This displacement is mediated by a plethora of factors, most prominently BRCA2. The simplest explanation how BRCA2 catalyzes Rad51 loading is that it displaces RPA and delivers Rad51 to ssDNA. Furthermore, BRCA2 blocks ATP hydrolysis by Rad51 thereby maintaining the active ATP-bound form of the Rad51-ssDNA ('nucleoprotein') filament (Carreira et al., 2009).

The nucleoprotein filament then executes a DNA sequence homology search, which constitutes the central reaction of HR. Once the homologous sequence is identified, Rad51 mediates DNA strand invasion by displacing the complement DNA, thereby forming a displacement loop (D-loop) structure (Sung and Klein, 2006). DNA synthesis from the 3' end of the invading strand by the Polymerase η and subsequent ligation by DNA ligase I yields a four-way junction intermediate structure known as Holliday junction (McIlwraith et al., 2005). This recombination intermediate can be resolved by three possible mechanisms: (i) dissolution mediated by BLM-TopIIIα complex, (ii) symmetrical resolution by GEN1, or (iii) asymmetric resolution by the structure-specific endonucleases MUS81-EME1 or SLX1-SLX4 (Wyatt and West, 2014). These cleavage events result in crossover or non-crossover products.

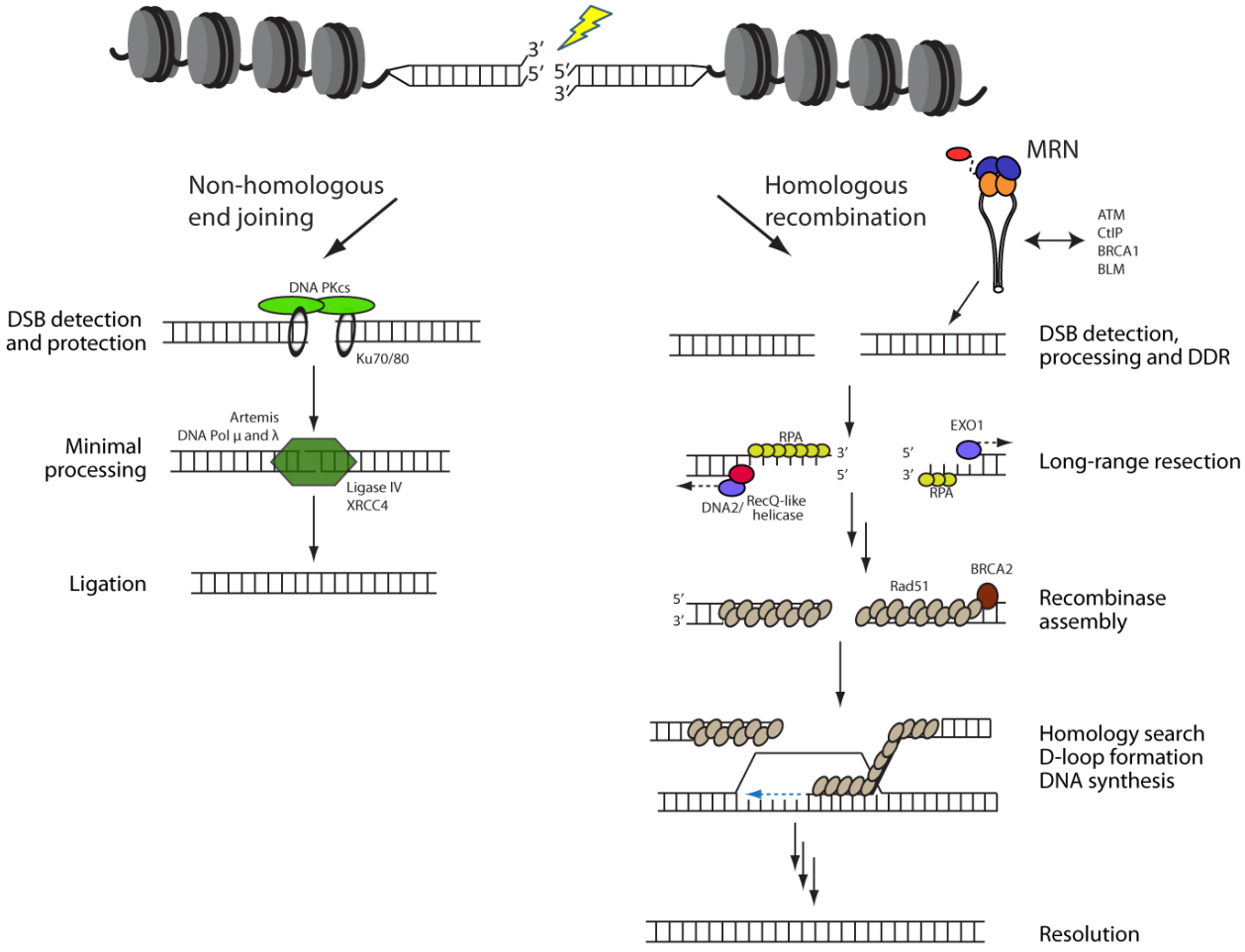

Figure 2 DSB repair by homologous recombination or non-homologous end joining. A two-ended 'clean' DSB substrate is bound by the Ku70/Ku80 heterodimer. Ku bound to DNA ends recruits DNA-PKcs to the ends and promotes their juxtaposition. If the DNA ends require processing, the nuclease Artemis and the DNA polymerase TdT, pol λ and pol μ act on the DSB. If no further processing of the ends is required, the core components of non-homologous end joining pathway, XRCC4, DNA ligase IV and XLF, mediate the rejoining reaction. DNA DSBs repaired by HR involves various steps. MRN recognizes the DSB, performs initial resection and initiates the DNA damage response by activating the ATM kinase. EXO1 and DNA2 in complex with a RecQ-like helicase perform long-range resection and create a 3' overhang which is coated by RPA. Rad51 replaces RPA with the help of BRCA2 and a nucleofilament is formed. The nucleofilament performs a search on the homologous dsDNA. Once the homologous sequence is found, the filament invades into the sister chromatid and forms a D-loop structure. DNA synthesis by Pol η resynthesizes the damaged and degraded DNA using the sister chromatid as a template.

2.3.3 DNA double-strand break repair and pathway choice in eukaryotes and mammals

In order to distinguish between NHEJ and HR, the cells have developed a cascade of mechanisms that direct the DSB repair towards one pathway. Decisive factors for the pathway choice are the nature and the size of DSBs, their origin, the timing in the cell cycle and the cell type (Mehta and Haber, 2014).

The pathway choice appears to be regulated on different levels through; (i) control of protein abundance by controlling transcription or nuclear export, (ii) tuning the activity or affinity of proteins by post-translational-modifications, and (iii) regulating the accessibility of chromatin (Hustedt and Durocher, 2016).

DNA end resection is the critical node for the regulation of DSB repair by the cell cycle. Consequently, the regulation of resection is often formulated in the context of pathway choice (Symington and Gautier, 2011).

The activity of cyclin-dependent kinases (CDKs) was found to be an essential regulator of DSB resection (Aylon et al., 2004; Ira et al., 2004). Within the cell cycle, CDKs are periodically activated and inactivated and regulate the transcription of proteins. Furthermore, they modulate crucial steps during HR and NHEJ by tuning the activity and recruitment of central HR- and NHEJ-related proteins through their kinase activities. For example, CDK activity promotes end resection directly through the phosphorylation of EXO1 and Nbs1 (Tomimatsu et al., 2014).

One of the first factors recruited to the break in HR-mediated repair is the Mre11-Rad50-Nbs1 (MRN) complex, which recruits and activates the protein kinase ATM. ATM then phosphorylates, amongst many other substrates, nucleosomes (in particular H2AX), 53BP1 and MDC1. These proteins help to transmit the damage signal to effector kinases (CHK1/Rad53 and CHK1) to trigger full checkpoint activation (Ciccia and Elledge, 2010). ATM-phosphorylated MDC1 recruits the E3 ubiquitin ligases RNF8 and RNF168 that ubiquitinate histone H2AK15. This modification, together with H4K20 di-methylation, recruits 53BP1 (Fradet-Turcotte et al., 2013), which was reported to initially accumulates at all DSB sites (Isono et al., 2017).

The role of 53BP1 was shown to prevent the long-range resection of DSBs in G1 and early S-phase and thereby promote NHEJ (Iwabuchi et al., 2006; Nakamura et al., 2006). ATM-dependent phosphorylation of the N-terminus of 53BP1 recruits PTIP and RIF1 to the breakage site, which prevents association of BRCA1 with MRN (Bunting et al., 2010). RIF1 was identified as the main factor impairing 5’ end resection involving CtIP, BLM and EXO1 (Zimmermann et al., 2013).

As cells enter late S-Phase, CDK-dependent phosphorylation of CtIP mediates the co-localization of BRCA1 with MRN after DNA damage (Sartori et al., 2007; Wong et al., 1998). There is evidence that BRCA1 functions in two distinct steps: (i) promoting the 5’ to 3’ resection of DSBs to generate a 3’ ssDNA overhang and (ii) loading of the RAD51 recombinase onto the ssDNA.

To promote resection, BRCA1 appears to antagonize 53BP1 by spatially excluding it from the proximity of DSBs (Chapman et al., 2012). This antagonism has been shown to be regulated by acetylation of histone H4K20me2, which interferes with 53BP1 binding (Tang et al., 2013). Furthermore, 53BP1 is rapidly dephosphorylated by PP4C/PP4R2, followed by RIF1 release at the time of HR progression (Isono et al., 2017).

The absence of 53BP1 then enables the re-organization of chromatin nearby the DSB by various chromatin remodelers, namely INO80, SMARCAD1 and the NuRD complex (Chen et al., 2012; Seeber et al., 2013). The recruitment of NuRD complexes to DSBs requires PARylation of the chromatin by PARP1 (Polo et al., 2010). The remodeling activity is essential to increase chromatin accessibility in order to promote Exo1- and Dna2-mediated long-range resection.

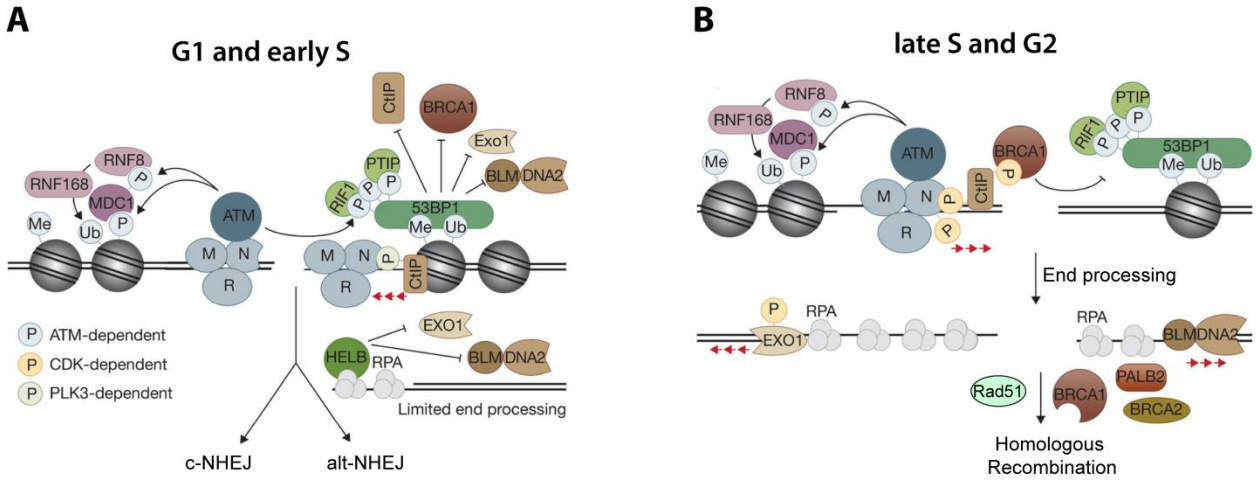

Figure 3 Regulation of DNA end resection at DSBs in dependency to cell cycle stage: (A) During G1 and early S phase, ATM is recruited to DSBs through MRN and phosphorylates targets such as H2AX (resulting in γH2AX), MDC1 and 53BP1. Histone H2A ubiquitylation by RNF168, together with H4K20 methylation, allows 53BP1 recruitment. 53BP1 creates docking sites for RIF1 and PTIP and blocks resection at DSBs, thereby channeling DSB repair towards NHEJ. P, phosphorylation; Ub, ubiquitylation; Me, methylation; red arrows, resection. **(B)** During S phase, CDK activity rises, resulting in phosphorylation of Nbs1 and CtIP. Nbs1 and CtIP phosphorylation stimulates MRN degradation and allows BRCA1 to bind to CtIP. BRCA1 counteracts 53BP1. Long-range resection proceeds through the combined action of DNA2/BLM and Exo1, also a CDK target. BRCA1 and BRCA2 promote replacement of RPA by Rad51 on ssDNA. Red arrows, resection; green arrowheads. Adapted and modified from (Hustedt and Durocher, 2016)

2.3.4 DSB resection and recombinational repair and in bacteria

Homologous recombination is the major DSB repair pathway in bacteria and it is best understood for *Escherichia coli*. DNA resection during DSB repair is performed by the RecBCD enzyme. RecF can also mediate recombinational repair in ΔrecBCD strains, but usually this pathway functions during ssDNA gap

repair (Morimatsu and Kowalczykowski, 2003; Persky and Lovett, 2008). This section focuses on the molecular mechanism of resection in the RecBCD pathway.

In contrast to archaea and eukaryotes, the bacterial Mre11-Rad50 ortholog SbcCD plays only a minor role for end resection during homologous recombination (Ayora et al., 2011). SbcCD co-localizes with the DNA replication machinery (Darmon et al., 2007) and resolves secondary structures that occur due to palindromic sequences, stalled or convergent replication forks (Bidnenko et al., 1999; Eykelenboom et al., 2008; Wendel et al., 2018). Additionally, SbcCD introduces double-strand breaks next to DNA-protein crosslinks (Connelly et al., 2003). These structures are then transformed into substrates which can be processed by RecBCD.

The physiological substrate for the RecBCD enzyme is a free blunt end or nearby duplex DNA end (Taylor and Smith, 1985). This heterotrimeric protein complex couples ATP-dependent unwinding to DNA degradation. RecB has a 3’ to 5’ helicase activity, RecD a 5’ to 3’ helicase activity and the nuclease activity is associated with the C-terminal domain of RecB. RecBCD processively degrades both DNA strands until it reaches and recognizes a Chi-site (Dillingham and Kowalczykowski, 2008; Spies et al., 2003). These are 8-bp non-palindromic sequences that are over-represented in the *E.coli* genome.

Chi recognition induces a conformational change within RecBCD that opens a latch allowing the 3’ terminated strand to bypass the RecB nuclease domain and exit the complex (Gilhooly et al., 2016; Handa et al., 2012). RecBCD is then transformed into a recombination-promoting repair enzyme. The degradation of the 3’ terminated strand is suppressed and cleavage of the 5’ strand is stimulated. Consequently, a 3’ overhang is generated and subsequently coated with RecA, generating a helical nucleoprotein filament (Anderson and Kowalczykowski, 1997; Cox, 2007).

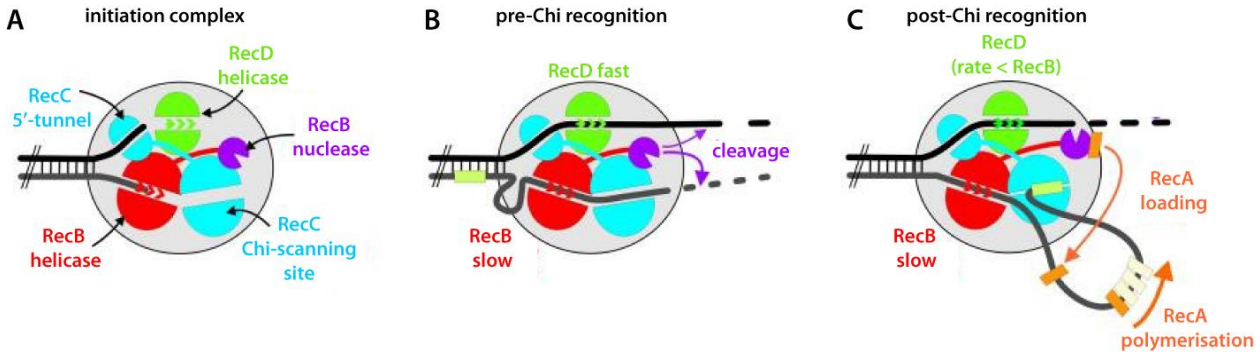

Figure 4 Model for the mechanism of RecBCD DNA resection (A) Cartoon representation of the initiation complex (B) Before encountering a Chi site, the RecBCD complex translocates along the DNA with the faster RecD motor leading, producing a loop of single-stranded DNA ahead of the complex. The RecB nuclease domain preferentially cleaves the 3'-terminated strand as it emerges from the RecC subunit and occasionally cleaves the 5'-terminated strand emerging from the RecD motor. The RecC subunit splits the DNA duplex as the DNA enters the complex, translocation is driven by the RedD and RecB helicases. **(B)** Upon encountering a Chi site in the 3'-terminated strand, the RecC subunit binds tightly to Chi and triggers several changes in the complex: disengagement of the RecD motor; preferred cleavage of the 5'-terminated strand; release of the RecB nuclease domain from the RecC interface; translocation along the 3'-terminated strand, driven by the RecB motor; and loading of RecA, mediated by the RecB nuclease domain, onto the single-stranded DNA loop as the loop is extruded through the open gate. Adapted and modified from (Dillingham and Kowalczykowski, 2008)

Single molecule studies found that homologous pairing is strongly promoted by negative supercoiling of the dsDNA (De Vlaminck et al., 2012). Homology search is performed in a 3-dimensional fashion until homologous sequences are found (Forget and Kowalczykowski, 2012). The nucleoprotein filament incorporates into the homologous DNA strand, thus, a heteroduplex forms. The previously degraded DNA strand is then newly synthesized by Polymerase I (Kowalczykowski et al., 1994) .

2.4 The Mre11-Rad50-Nbs1 (MRN) complex

The Mre11-Rad50-Nbs1 complex (MRN) complex is a major player in DNA damage response (DDR) and central for maintaining the genome integrity. It has a central function in initiating homologous recombination, and plays major roles in alternative non-homologous end joining, meiotic recombination and telomere maintenance (Stracker and Petrini, 2011). Deletion of any component of the MRN complex leads to developmental retardation or embryonic lethality in mice (Buis et al., 2008). The MRN complex senses DSBs, DNA ends and rapidly localizes to sites of damage. Once in position it activates the DNA damage checkpoint signaling cascade *via* ATM, protects and tethers the DNA ends, and performs initial nucleolytic processing of the DSB.

2.4.1 Structural architecture and functions of the individual MRN-components

The Mre11-Rad50 (MR) core complex is heterotetramer consisting of two Mre11 and two Rad50 molecules. In eukaryotes it further associates with Nbs1 (Xrs2 in *S. cerevisiae*) to form the MR(N/X) complex. Atomic force microscopy revealed an MR(N/X)-architecture of a globular head region which harbors the Mre11 dimer, the ABC-ATPase domains of Rad50 and one or two copies of Nbs1 (Figure 5A). A large helical region of Rad50 protrudes from this globular region and folds into a coiled-coil tail (de Jager et al., 2004; Moreno-Herrero et al., 2005). The Rad50 coiled-coil tail harbors an apical zinc-hook dimerization motif that allows the interaction with other MRN complexes (Hopfner et al., 2002). Due to the flexible nature of the complex, structural analysis by X-ray crystallography was limited to the individual domains of the catalytic head or truncated versions of the complex. The following sections describe the structures and activities of the individual components of the MRN complex.

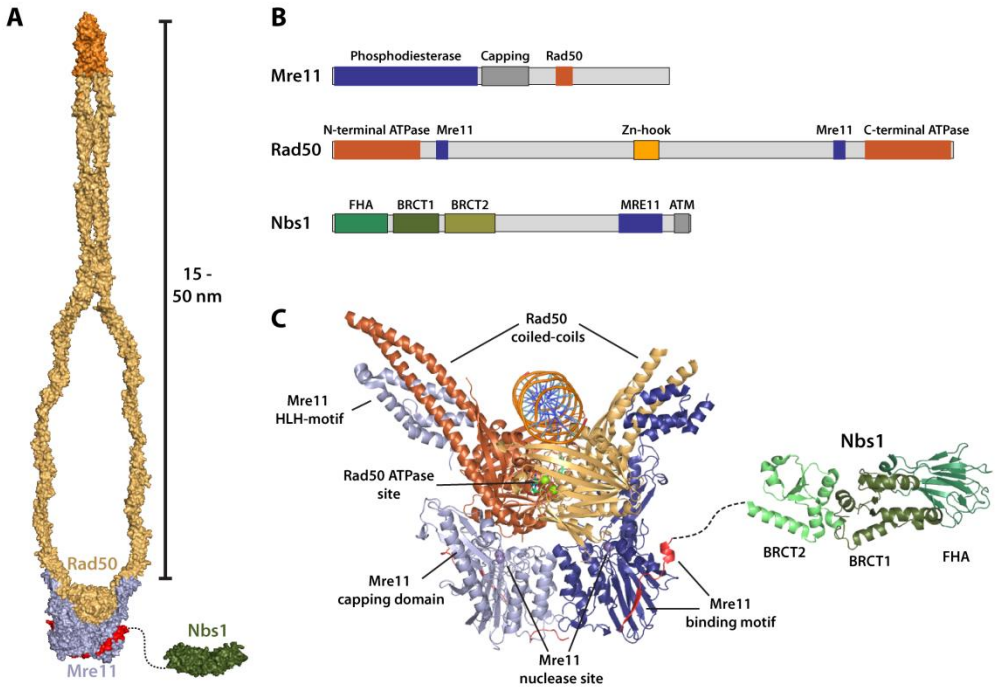

Figure 5 Global architecture and domain overview of the Mre11-Rad50-Nbs1 complex (A) Model of the full-length MR(N/X) complex. The model was built from *S. pombe* MN (PDB code 4FBW) and Nbs1 (3HUE), *M. jannaschii* MR (3AVO), *H. sapiens* Zinc-hook (5GOX) and a model of the coiled-coils. The length of the Rad50 coiled-coils can range from 15 nm in T4 bacteriophage to 50 nm in eukaryotes. **(B)** Domain architecture of Mre11-Rads50-Nbs1: Mre11 consists of a conserved N-terminal phosphodiesterase and an adjacent DNA capping domain. The C-terminal region contains a hydrophobic interaction motif for Rad50. Rad50 consists of a bipartite ABC-ATPase cassette, which is separated by a long coiled-coil region. An MRN inter-complex interaction mediating Zn-hook maps to the central coiled-coil region. Nbs1 contains an N-terminal phosphoprotein binding module, which is composed of an FHA and two BRCT domains. The C-terminus possesses interaction sites for both Mre11 and ATM. **(C)** Model of the MR(N/X) catalytic head. Crystal structures are shown as in (A), but with *C. thermophilum* Rad50 (5DA9). Individual domains are indicated.

2.4.1.1 The Mre11 subunit

Mre11 can be considered as the core of the MRN complex as it interacts with both Rad50 and Nbs1. Comparisons of Mre11 structures from the three kingdoms of life show that it has a conserved fold (Schiller et al., 2014). The N-terminal phosphoesterase domain active site coordinates two manganese ions which are essential for exo- and endonuclease activities. These are coordinated by conserved histidine-, asparagine- and aspartic acid residues (Hopfner et al., 2001; Hopfner et al., 2000a). C-terminal of the phosphoesterase domain is the capping domain, which ends into a flexibly attached helix-loop-helix (HLH) motif that acts as the main interaction site with Rad50 (Lammens et al., 2011; Williams et al., 2011).

Two Mre11 protomers form a dimer which is obtained *via* a conserved four-helix bundle structure. Mre11 of higher order species comprise a further stabilizing latching loop, which becomes ordered upon Nbs1 binding, as seen in the crystal structure of *S. pombe* (Park et al., 2011; Schiller et al., 2012; Seifert et al., 2015). Superposition of the available Mre11 structures illustrates plasticity in the dimer organization not only between species, but also within the same organism. DNA binding by *M. jannashii* Mre11 induces a rigid body rotation of the dimer, and *S. pombe* Nbs1 induces a 30° rotation in the Mre11 dimer angle towards a conformation with a narrower nuclease cleft. Human Mre11 was crystallized as a dimer crosslinked by disulfide bond that leads to an unusual dimer interface and abolished flexibility (Park et al., 2011; Schiller et al., 2012; Sung et al., 2014). The exact biochemical role of the dynamic Mre11 dimer organization has not yet been determined. An intact dimer appears to be crucial for dsDNA coordination, however, Mre11 with a disrupted dimer interface still possesses ssDNA endonuclease activity (Williams et al., 2008). *In vivo* studies showed that disruption of the Mre11 dimer phenocopied an *mre11* knockout (Schiller et al., 2012; Williams et al., 2008).

The molecular mechanism of dsDNA processing by Mre11 remains elusive so far, as structures with Mre11 bound to a DNA undergoing degradation are missing. The available Mre11-DNA structures demonstrate that dsDNA is coordinated across the Mre11 dimer. Binding by Mre11 induces minor groove widening and the the conformation of the DNA ends is shifted away from that of ideal B-form DNA (Sung et al., 2014; Williams et al., 2008). The manganese ions of Mre11 are buried in the active site and B-form DNA is 5 Å away from a position that could be considered productive for cleavage (Hopfner et al., 2001). Either the classical B-form of DNA has to be altered or Mre11 has to undergo substantial conformational changes in order that DNA is in a position which is productive for cleavage.

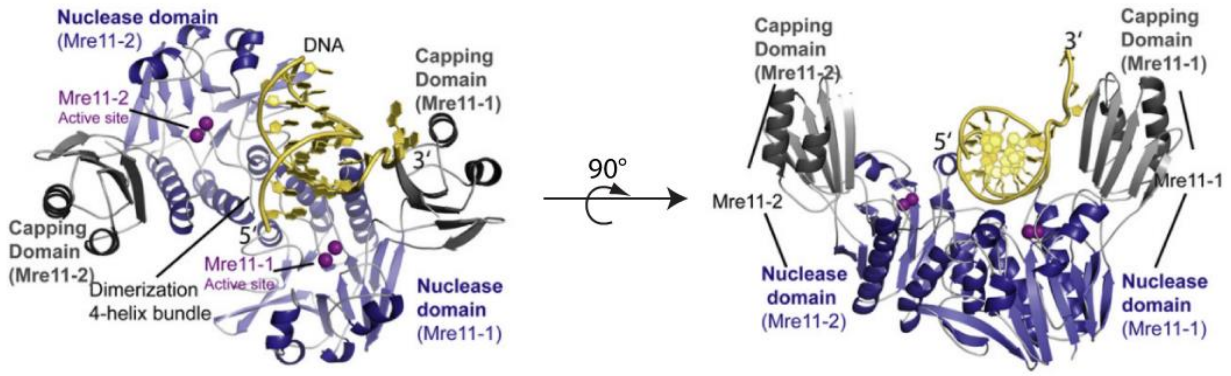

Figure 6 Mre11 binds dsDNA in an asymmetrical fashion. Upper and lower orthogonal views show that Mre11-DNA (PBD: 3DSD) binds the branched DNA substrate asymmetrically in one half of the Mre11 dimeric cleft, with both Mre11 subunits contributing to binding one dsDNA. In this conformation, dsDNA is not in a position, which is productive for a phosphate backbone cleavage. Figure adapted from (Williams et al., 2008).

2.4.1.2 The Rad50 subunit

Two copies of Rad50 polypeptides are represented in the MRN complex. Rad50 belongs to the ABC transporter superfamily, having an overall structure related to the structural maintenance of chromosomes-(SMC) protein (de Jager et al., 2004; Hopfner et al., 2001; Hopfner et al., 2000b). Binding of ATP to the Rad50 nucleotide-binding domains (NBDs) leads to the formation of a tight NBD:2ATP:NBD complex. Crystal structures of the bacterial Mre11-Rad50 'catalytic head' show an ATP-dependent conformational change from an 'open' elongated to a 'closed', more globular conformation (Figure 7A) (Lammens et al., 2011; Möckel et al., 2012). To date, this conformational change has not been validated in the context of full-length MR, as the coiled-coils could restrain the ATP-free, elongated conformation. The dimeric Rad50 harbors a positively-charged DNA binding groove formed by both monomers in the dimer. In this conformation, Mre11's nuclease site is occluded (Liu et al., 2016; Seifert et al., 2016). Until now, no conclusive molecular mechanism has been proposed which describes the coordination of DNA binding by Rad50 and DNA incision by Mre11.

From the NBDs, two anti-parallel coiled-coils protrude which extend to 15-50 nm. The length of the coiled-coils is rather conserved between closely related phylogenetic taxa but can vary considerably between different domains of life. Therefore, the length could correlate with the organization of chromatin and complexity of the organism (Schiller et al., 2014). At the apex of each coiled-coil, a conserved CXXC motif coordinates a Zn^{2+} ion that functions as a homo-dimerization interface between Rad50 subunits. The so-called Rad50 Zinc-hook can adopt an elongated or rod-shaped conformation (Hopfner et al., 2002; Park et al., 2017). Ablation of the Zinc-hook phenocopies complete Rad50

deficiency (Wiltzius et al., 2005) and mutations in close proximity to the Zinc-hook affect functions that are specific to the MRN globular domain in yeast (Hohl et al., 2015). Rotary shadowing electronic microscopy and atomic force microscopy (AFM) studies visualized the dynamic architecture of the coiled-coils. These can adopt ring-shaped or parallel orientations, which appear to be species-specific and markedly affected by ATP and DNA binding (de Jager et al., 2004; de Jager et al., 2001; Moreno-Herrero et al., 2005). These results suggest conformational changes in the hook and globular domains are transmitted *via* the extended coiled-coils of Rad50.

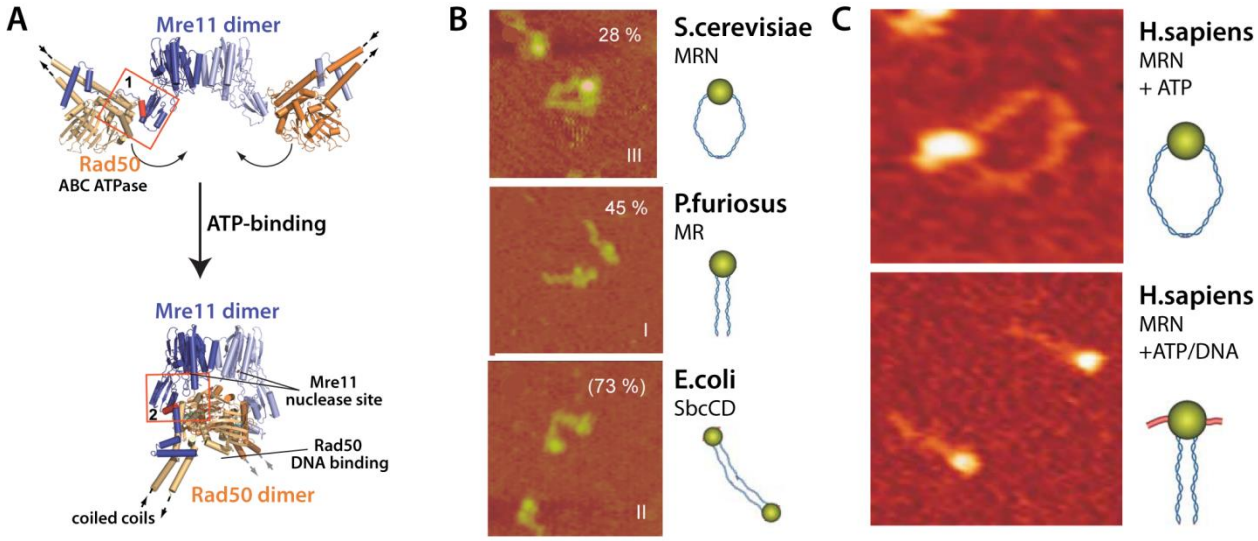

Figure 7 Conformational changes of the MR(N) complex induced by ATP and DNA binding of Rad50: (A) Conformational change of the bacterial MR catalytic head induced upon ATP binding. Adapted and modified from (Lammens et al., 2011). **(B)** Species-specific conformations of the Rad50 coiled-coils, analyzed by atomic force microscopy (AFM) **(C)** Conformational changes of the Rad50 coiled-coils induced by DNA binding. Images are at different magnifications and show single MRN complexes. (B) and (C) adapted and modified from (Moreno-Herrero et al., 2005).

2.4.1.3 The Nbs1 subunit

Nbs1 is the third component of the MRN complex. It has no enzymatic activities and fulfills scaffold and recruitment functions. The N-terminus is structured and consists of a Fork-head associated (FHA) and two consecutive BRCA1 carboxy-terminal (BRCT) domains (Lloyd et al., 2009; Williams et al., 2009). These protein folds are related to the binding of phosphoproteins. In the case of Nbs1, it was shown to recruit DSB repair factors, such as mediator of DNA damage checkpoint protein 1 (MDC1), Bloom syndrome mutated (BLM), breast cancer 1 (BRCA1) and CtBP-interacting protein (CtIP) (Chapman and Jackson, 2008; Chen et al., 2008; Xu et al., 2008).

The adjacent C-terminal region is predicted to be unstructured. A conserved NFKxFxK motif mediates interaction with Mre11 (Desai-Mehta et al., 2001; Schiller et al., 2012). However, an additional interaction site between Nbs1 and Rad50 is possible, as a stoichiometric Rad50-Nbs1 complex could be isolated *in vitro* (van der Linden et al., 2009). A C-terminal acidic patch and two FXF/Y motifs were identified as activating the ATM kinase (Falck et al., 2005; You et al., 2005).

Several studies showed that Nbs1 interaction with Mre11 is responsible for localization and proper assembly of the MR complex. A short C-terminal 108 aa peptide was sufficient to fulfill these functions in mouse (Kim et al., 2017). Additionally, nuclear localization of Mre11 (Mre11-NLS) is able to bypass several functions of Xrs2/Nbs1, including DNA end resection, meiosis and cellular resistance to clastogens in yeast *in vivo* studies. However, xrs2Δ cells exhibit defects in Tel1/ATM kinase signaling and NHEJ, which cannot be compensated by Mre11-NLS (Oh et al., 2016; Schiller et al., 2012).

2.4.2 Biochemical *in vitro* activities of the MRN complex

Biochemical *in vitro* studies with bacterial, archaeal, yeast and human MR(N/X) complex or the individual proteins showed that Mre11 possesses various Mn^{2+}-dependent nuclease activities. The dsDNA 3'-5´ exonuclease activity of Mre11 is ATP-dependent in bacteria and archaea, while the presence of ATP is not required in eukaryotes. The internal scission of ssDNA appears to be ATP-independent (Connelly et al., 1999; Furuse et al., 1998; Hopfner et al., 2000a; Paull and Gellert, 1998; Trujillo et al., 1998). Mre11 exhibits also the ability to open DNA hairpin structures on the 5' side in an ATP-dependent manner (Connelly et al., 1998; Paull and Gellert, 1999; Trujillo and Sung, 2001).

The bacterial MR complex cleaves both DNA strands next to a protein-bound DNA end in an ATP-dependent manner (Connelly et al., 2003). Recent *in vitro* studies showed that this activity is conserved in the human and yeast system, where MR(N/X) cleaves both DNA strands, with a preference for the 5' strand. The human MRN absolutely required Nbs1 for dsDNA endonuclease activity, whereas yeast MRX required phosphorylated Sae2 and Xrs2 is dispensable for activity (Anand et al., 2016; Cannavo and Cejka, 2014; Deshpande et al., 2016). Interestingly, yeast MRX-Sae2 cleavage activity is also triggered at internal protein obstacles, such as nucleosomes (Wang et al., 2017). The dsDNA endonuclease activity is believed to clean up 'dirty' DNA ends and prepare these for the long-range resection machinery. At clean DNA ends, other nucleases are able to initiate resection (Aparicio and Gautier, 2016; Paudyal et al., 2017). Studies with single-molecule DNA curtains highlighted, that MRN loads internally onto dsDNA

and diffuses in a 1-dimensional manner towards the DNA end. It was shown that it then removes Ku from the DNA ends (Myler et al., 2017).

The exact function of ATP binding and ATP hydrolysis by Rad50 was for a long time puzzling and many questions still remain. Human and yeast MR(N/X) have very low ATPase rates of less than 0.1 ATP/min. The hydrolysis rate is stimulated 20-fold for human MRN and 10-fold for yeast MRX by linear double-stranded DNA (dsDNA) in an end-dependent manner. Interestingly, protein-blocked DNA ends reduced the stimulatory effect of DNA ends (Deshpande et al., 2017; Trujillo et al., 2003). Extensive studies with the T4 bacteriophage protein revealed a similar stimulatory effect by dsDNA (Herdendorf et al., 2011).

ATP binding induces a conformational change in the MR complex to form a DNA binding groove across the Rad50 dimer (Liu et al., 2016; Rojowska et al., 2014; Seifert et al., 2015). Until now, many DNA binding studies revealed relatively low affinities for dsDNA and DNA ends, compared to other DSB sensors such as the Ku70/Ku80 complex (Liu et al., 2016; Rojowska et al., 2014; Walker et al., 2001). However, picomolar DNA binding affinities of have been measured in single-molecule fluorescence resonance energy transfer experiments with full-length human MRN (Cannon et al., 2013). It is unclear whether this difference may be explained by different experimental set-ups or due the lack or presence of the coiled-coils of Rad50. The same study with human MRN showed unwinding of dsDNA in the proximity of DNA ends. This activity required ATP binding and ATP hydrolysis (Cannon et al., 2013; Paull and Gellert, 1999).

The presence of ATP was shown to be important for tethering DNA ends, and a Rad50 signature motif mutant, which is impaired in ATP binding, lacks the ability to stimulate the checkpoint kinase ATM *in vitro* (Deshpande et al., 2014; Dupre et al., 2006; Lee and Paull, 2005). This signature motif mutant produces a phenotype equivalent to a *rad50* deletion *in vivo* (Moncalian et al., 2004).

Taken together, the ATP-related activities of Rad50 are essential for the MRN complex and its roles in DNA repair and signaling. It appears that a central purpose of ATP binding is to induce dimerization of Rad50 and therefore supply an interaction platform for dsDNA. How ATP and DNA binding translate into conformational changes of the Rad50 coiled-coils and Zinc hook is currently unknown.

The eukaryotic Nbs1 subunit has no catalytic activity itself but regulates the enzymatic activities by Mre11 and Rad50. Nbs1 stimulates DNA binding of MRN, DNA unwinding and hairpin processing (Paull and Gellert, 1999; Trujillo et al., 2003). Nbs1 appears to be crucial for a productive interaction with ATM,

as the MR complex interacts with ATM, but the presence of Nbs1 is required for the activation and autophosphorylation of ATM (Lee and Paull, 2005).

The described data point out that there is a high level of allosteric control within the MRN complex and its enzymatic functions are regulated accordingly. It is likely that an intact allosteric cascade within MRN, involving both the coiled-coils and zinc hook, is necessary for the recognition of a DNA end and subsequent activation of ATM and processing of DNA ends. This has to be taken into consideration for the design of future activity and structural studies.

2.4.3 The Mre11-Rad50-Nbs1 complex in DNA repair and DNA metabolism

The MRN complex was shown to be involved in a plethora of DNA end metabolism processes. It uses its enzymatic, regulatory and architectural features and acts in response to DSBs (i) by recognizing and processing the DNA ends, (ii) by activating the cell cycle checkpoint and (iii) by forming a physical bridge between DNA molecules (Stracker and Petrini, 2011). MRN promotes homologous recombination during meiotic and mitotic DSB repair and is involved in telomere maintenance and non-homologous end joining pathways.

2.4.3.1 Recognition and initial resection of DSBs by the MRN complex

The MR(N/X) complex is one of the first complexes that localizes to DSBs (Lisby et al., 2004). As discussed in the first chapter, DNA damage and DSBs come in a high variety of structures (Figure 1). These specific DNA structures require initial nucleolytic processing to DNA substrates that are compatible with downstream nucleases. The structure of DNA ends appears to be a major determinant of DSB repair choice. Whereas ends with normal nucleotides are efficiently channeled to NHEJ, ends with damaged nucleotides or bulky adducts are channeled to resection (Liao et al., 2016).

One prominent example of bulky DNA adducts are covalent DNA-protein crosslinks (DPCs) of the topoisomerases, whose bulkiness blocks virtually every chromatin-based process (Stingele et al., 2017). *In vitro* studies showed that MR(N/X) removes DNA-protein crosslinks from DNA ends (Cannavo and Cejka, 2014; Deshpande et al., 2016). Cells that lack Mre11 or express nuclease-deficient Mre11 are highly sensitive to topoisomerase 2 poisons (Hoa et al., 2016). During meiosis, the topoisomerase-like protein Spo11 induces a DSB. Spo11 is covalently bound to the 5’ end and the endonucleolytic removal by the MR(N/X) complex is a crucial step during meiosis (Keeney and Kleckner, 1995; Usui et al., 1998).

Several studies suggest antagonistic roles for MR(N/X) and the Ku complex in the early phase of mitotic DSB repair events. Both complexes sense and bind to DSBs, but whereas MR(N/X) is the core initiation factor for HR, the Ku complex protects DNA ends and promotes NHEJ. However, *in vitro* studies showed that MR(N/X) is capable to remove Ku complex from a DNA end by endonucleolytic incision (Myler et al., 2017; Reginato et al., 2017).

As the initial resection of DSBs by MR(N/X) is a major determinant for pathway choice, a precise control of its nuclease activity essential is to ensure correct repair. Initiation of resection by MR(N/X) depends strongly on CtIP (Sae2 in *S. cerevisiae* or Ctp1 in *S. pombe*). The phosphorylation of these proteins at a conserved serine by cyclin-dependent kinases is crucial for this step (Huertas et al., 2008; Limbo et al., 2007). Sae2 directly stimulates dsDNA exo- and endonuclease activity within the MRX complex at a protein-blocked DNA end (Cannavo and Cejka, 2014). A corresponding stimulatory effect was not observed for human MRN, but the recruitment of BRCA1 *via* CtIP is important to displace the resection inhibitor 53BP1 from chromatin. The absence of 53BP1 initiates chromatin remodeling events in the proximity to DSBs, a critical step towards resection (Adkins et al., 2013; Bunting et al., 2010; Chapman et al., 2012).

Recently reported data of *S. cerevisiae* demonstrate prolonged MRX binding to DSB in sae2Δ cells. Therefore, Sae2 was proposed to remove the MRX complex from DSBs and therefore increase the MRX-turnover at DSBs (Chen et al., 2015; Ferrari et al., 2015).

In addition to the regulation by CtIP and its orthologs, resection by MR(N/X) is also regulated by the phosphorylation state of any component of MRN. For example, Cdk1 phosphorylates Mre11 and Xrs2 as cells progress into G2-phase. The phosphorylation specifically inhibits NHEJ, whereas removal of the phosphosites in Xrs2 and Mre11 stimulates DSB repair by NHEJ (Simoneau et al., 2014).

The recruitment of Exo1 and the Sgs1-Dna2-RPA complex, as well as other nucleases and helicases, enables the long-range resection of several hundred bases to generate 3´ ssDNA. MRX in *S. cerevisiae* facilitates this recruitment of Exo1 and Dna2-Sgs1 and stimulates its nuclease activities in conjunction with RPA (Cannavo et al., 2013; Shim et al., 2010).

In addition to regulating DNA end resection, the MR(N/X) complex is also implicated as a scaffolding factor in HR, where it tethers the two DNA ends of a DSB and holds them in close proximity (Hopfner et al., 2002). This function is dependent on the Rad50 zinc-hook domain, which mediates MR(N/X) inter-complex interactions. AFM studies observed this zinc-hook dependent inter-complex formation in the presence of DNA (de Jager et al., 2001; Moreno-Herrero et al., 2005).

2.4.3.2 MRN as a mediator in checkpoint signaling

MRN not only plays a role in sensing and resecting of DSBs or as a scaffolding protein but also mediates DNA damage signaling *via* the checkpoint kinase ATM (Tel1 in yeast), an action that controls repair, induces cell cycle arrest or apoptosis (in metazoan). Although ATM localizes independently of Nbs1 or Xrs2 to DSB sites, the activation of ATM requires the presence of Nbs1 or the respective C-terminal binding site of ATM (Kim et al., 2017; Oh et al., 2016). ATM is also activated *in vitro*, where MRN stimulates the dissociation of inactive ATM dimers into active monomers (Lee and Paull, 2005).

Upon activation, ATM undergoes autophosphorylation, in human on Ser1981, which is a hallmark of its activation. Although the functional significance of ATM autophosphorylation is still unclear, it is required for the stabilization of activated ATM at DSB sites (Berkovich et al., 2007; So et al., 2009).

Once activated, ATM, in turn, phosphorylates Rad50, Mre11, and Nbs1 and regulates the resection by this phosphorylation. Mre11 was phosphorylated at Ser676 and Ser678. Cells that lacked the ability to phosphorylate these residues showed a defect in HR (Kijas et al., 2015). Further ATM phosphorylation targets are nucleosomes, in particular H2AX (resulting in yH2AX). yH2AX recruits ATM-phosphorylated MDC1, which results in further accumulation of MRN and the recruitment of the ubiquitin ligases RNF8 and RNF168. The subsequent histone H2A ubiquitylation leads to further repair protein accumulation and repair foci formation (Hustedt and Durocher, 2016). The foci formation of MRN leads to further ATM activation and an amplification of ATM-promoted checkpoint signaling *via* the downstream kinases Chk2 and effector molecules like p53 and p21 (Gobbini et al., 2013).

Other prominent ATM-phosphorylation targets are Smc1, Exo1 and the N-terminal region of 53BP1, which promotes the recruitment of Rif1 and PTIP, prominent inhibitors of resection (Bauerschmidt et al., 2010; Callen et al., 2013; Kijas et al., 2015; Zimmermann et al., 2013). The consequence of each ATM phosphorylation is cell cycle-dependent and other phosphorylations and modifications determine the individual response.

2.4.3.3 MRN in telomere maintenance and recognition of DNA secondary structures

Biochemical *in vitro* studies on eukaryotic MR(N/X) revealed a number of conserved nuclease activities for Mre11: (i) endonucleolytic cleavage of single-stranded DNA, (ii) exonucleolytic degradation of dsDNA in 3´-5´polarity, (iii) DNA hairpin opening, (iv) dsDNA cleavage next to a protein-bound DNA end, and (v) endonuclease activity towards ds- and ssDNA transitions, such as frayed DNA ends (Cannavo and Cejka, 2014; Deshpande et al., 2016; Paull and Gellert, 1999; Trujillo and Sung, 2001). It is not surprising that

MR(N/X) fulfills a function to sense and process the various structures that arise during DNA metabolism to maintain genomic integrity.

If poisoned Topoisomerases are integrated into the genome during replication, they can induce stalling of replication forks. The homologous recombination factors BRCA1, BRCA2, and Rad51 stabilize these structures and protect them from extended nucleolytic degradation (Quinet et al., 2017). The MRN complex plays an important role in mediating signaling by activation of ATR-CHK1 and recruiting TopBP1 (Kobayashi et al., 2013; Lee and Dunphy, 2013). This leads to important phosphorylation events of RPA and Rad50 that are essential for the fork restart (Gatei et al., 2014). However, MRN adopts a deleterious role in BRCA2 and Rad51 deficient cells, where reversed forks are extensively degraded by Mre11, CtIP, and EXO1, leading to genomic instability (Kolinjivadi et al., 2017).

Short inverted repeats drive the formation of large palindromic gene amplifications that lead to gross chromosomal aberrations. They are a major class of structures that are recovered in yeast cells lacking Sae2 or the Mre11 nuclease. The MRX-Sae2 complex counteracts the formation of large palindromic duplications in yeast, likely because these are hairpin-like structures that are opened and resolved by the complex (Deng et al., 2015).

Furthermore, the MR(N/X) complex plays crucial roles in maintaining and support the formation of telomere structures. Telomeres are unique nucleoprotein assemblies at the ends of eukaryotic chromosomes. They play essential roles in protecting chromosome ends from recognition by the DNA damage repair machinery and preventing degradation, fusion or recombination (Faure *et al.* 2010). They consist of G-rich sequence repeats and a terminal 3´ ssDNA tail. The tail forms a T-loop structure which is stabilized by several specific protecting factors that are summarized as the shelterin complex.

MRN, together with CtIP, promotes resection of the C-rich 5’ strand at the newly synthesized leading-strand blunt end. This generates the 3’ overhang crucial for T-loop formation at the chromosome end (Bonetti et al., 2013).

Second, the MRN is required for activating the ATM-dependent response at dysfunctional telomeres. This induces the rapid assembly of DDR components and mediates appropriate processing of the telomeres (Dimitrova and de Lange, 2009; Takai et al., 2003). Studies in *S. cerevisiae* showed that the activation of Tel1 by MRX is also required to stimulate telomerase activity to maintain a sufficient length of telomeres (Goudsouzian et al., 2006; Hirano et al., 2009). Consequently, the deletion of MRX genes or complex disrupting mutations lead to telomere shortening in yeast cells (Kironmai and Muniyappa, 1997; Schiller et al., 2012).

2.4.4 Functions of the bacterial SbcCD complex

Compared to its eukaryotic counterpart, the bacterial Mre11-Rad50 homologue, SbcCD, appears to have different roles in maintaining the genome integrity. *sbcC* was originally identified as a gene that prevents the stable propagation of palindromic sequences in *E. coli* (Chalker et al., 1988). Therefore, it interferes with the growth of lambda phage that carries long palindromes in its genomic DNA (Gibson et al., 1992). The instability of the palindromic sequences is primarily mediated by slippage on the lagging strand during replication (Davison and Leach, 1994). The subsequently formed hairpin structure is resolved by SbcCD and a double-strand break is generated (Cromie et al., 2000; Eykelenboom et al., 2008). *In vitro* studies showed that SbcCD cleaves both strands from the top of the hairpin in 10 bp intervals (Lim et al., 2015).

Furthermore, SbcCD resolves structures that occur in regions of CAG x CTG repeats, present on the lagging strand during DNA synthesis, and interferes with the propagation of these sequences (Zahra et al., 2007). The presence of trinucleotide repeats is associated with human inherited diseases, such as Huntington's disease and spinocerebellar ataxia.

Additionally, SbcCD appears to play a role in maintaining the bacterial chromatin structure in replicating cells. Fluorescence microscopy revealed that over-expressed SbcC co-localizes with the bacterial replication machinery (Darmon et al., 2007). This is consistent with the observation that SbcC interacts with the DnaG primase and replicase (Noirot and Noirot-Gros, 2004). SbcCD is implicated in the dissolution of 'chicken foot' structures that arise at reversed replication forks (Bidnenko et al., 1999). Furthermore, SbcCD, in conjunction with ExoI, is required to complete DNA replication by processing convergent replication forks, whose structure is similar to that of hairpins (Wendel et al., 2018). The SbcCD cleavage products require the subsequent processing of RecBCD in order to continue or finish replication.

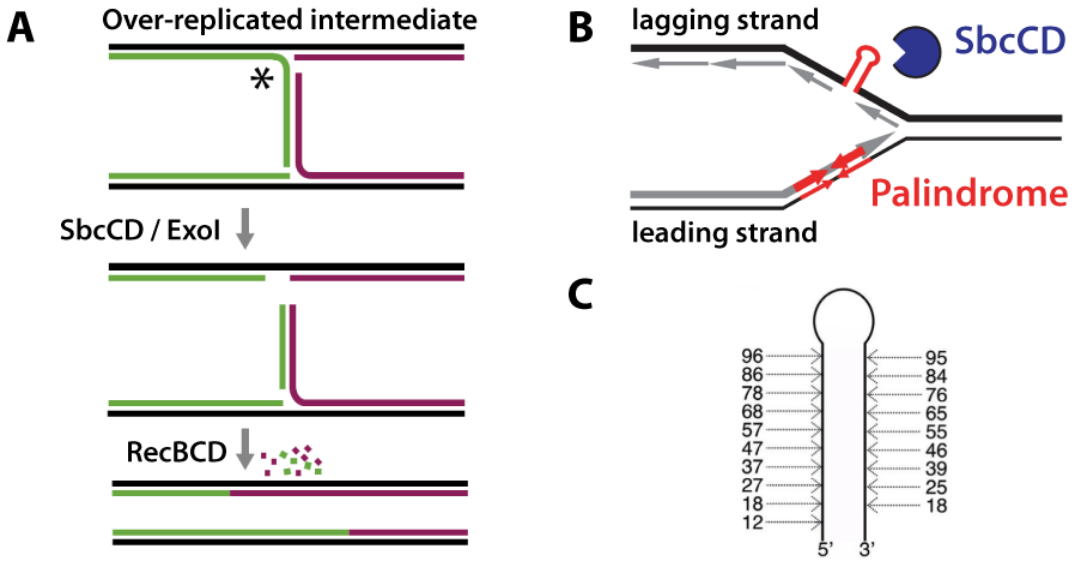

Figure 8 Secondary structures and replication intermediates that require cleavage by SbcCD (A) Model of completing replication: when replication forks continue past their meeting point, a palindromic substrate is created (top), which is cleaved and processed by SbcCD/ExoI (middle). RecBCD-mediated resection and joining of the DNA ends complete replication (bottom). Figure adapted and modified from (Wendel et al., 2018). **(B)** SbcCD cleaves a DNA hairpin formed by the palindrome on the lagging strand of replication. Figure adapted and modified from (White et al., 2008). **(C)** Cleavage pattern of hairpin processing by SbcCD. Figure adapted and modified from (Lim et al., 2015)

In vitro studies provided direct evidence that SbcCD removes proteins from a protein-bound DNA end by inserting a double-strand break (Connelly et al., 2003). In line with these results, an increased DNA-gyrase complex level could be detected in *ΔsbcCD* cells that were treated with the gyrase inhibitor quinolone. Therefore, SbcCD is involved in the processing of quinolone-trapped gyrase-DNA complexes (Aedo and Tse-Dinh, 2013). However, SbcCD appears to not cleave internal DNA-protein crosslinks, as inactivation of SbcCD did not cause hypersensitivity in cells that formed internal crosslinks between DNA and an azacytidine-methyltransferase (Krasich et al., 2015).

In summary, SbcCDs function appears to be the resolution of secondary structures that interfere with successful replication and are potentially toxic for the genomic integrity. In most of the cases, SbcCD acts upstream of RecBCD and the generated products require further nuclease processing to complete the DNA repair process.

2.5 Objectives

The MRN complex plays an important role in many DNA repair processes to ensure genome integrity. During extensive research in the past, many structural and biochemical characteristics of the MRN complex were determined. However, many fundamental functions, including the mechanisms of ATP-dependent dsDNA processing and DNA end recognition by MRN, are still poorly understood.

Most of the structural data originate from thermophilic bacteria and archaea, and the structural findings were not or could not be complemented with a biochemical characterization from the same organism. The biochemical findings from other organisms cannot be easily transferred due to species-specific differences. That is one reason why there is still a lot of incomplete knowledge about MRN.

A challenge for an in-depth characterization of full-length MRN is the unique architecture of the complex. Due to the long coiled-coils, recombinant expression and subsequent purification remain a challenging issue which limits the biochemical *in vitro* investigation. The elongated and flexible nature of the complex prevents a structural characterization of the full-length MRN complex by X-ray crystallography. However, it emerged that there is a functional connection of the MR catalytic head, the coiled-coils and the Rad50 zinc-hook and all domains of the complex are required for the proper function.

The aim of this study was to perform an in-depth biochemical characterization of the bacterial Mre11-Rad50 homolog SbcCD. A protocol had to be established to isolate recombinant full-length SbcCD in high yields and purity. Subsequent characterization requires implementation of robust biochemical assays to monitor and quantify SbcCD's ATPase, DNA binding, and nuclease activities.

To understand the SbcCD's nuclease mechanism, the shared endo- and exonuclease activities could be functionally separated by providing different DNA substrates. Further minimal DNA-modifications and the insertion of secondary structures allows screening for preferences in the process of nucleolytic degradation. Based on these data, mutants in either SbcC or SbcD could functionally connect the nuclease activity to DNA binding and ATP hydrolysis. This connection would give a comprehensive picture how SbcCD associates with and processes DNA ends.

3. Materials and Methods

3.1 Materials

All chemicals used in this work were of the highest available grade obtained from Sigma-Aldrich (Deisenhofen), Carl Roth (Karlsruhe), or Merck (Darmstadt), unless otherwise stated. Enzymes for molecular biology were purchased from Fermentas (St. Leon-Rot) or New England Biolabs (Frankfurt). Desalted oligonucleotides for molecular cloning and HPLC purified oligonucleotides for *in vitro* activity assays were obtained from Metabion (Martinsried). Chromatographic media and columns were purchased from GE Healthcare (Munich).

3.1.1 Oligonucleotides

Table 1 DNA oligonucleotides used for molecular cloning and site-directed mutagenesis. aa, amino acid; for, forward; rev, reverse; His6, hexahistidine tag; Lis1, LisH dimerization domain; PAS, Linker consisting of proline, alanine and serine.

Amplified gene fragment/mutation	Sequence (5'-3' direction)	Restriction site/Method
SbcC_for	AACCAACATATGAAAATTCTCAGCCTGCGCC	*Nde*I
SbcC_rev	AAAA GCGGCCGC TTATTTCACTGCAAACGTACTTTCC	*Not*I
SbcC_for	CCAACCATGGGCAAAATTCTCAGCCTGCGCC	NcoI
SbcD_for	AACCAACATATGCGCATCCTTCACACCTCAGAC	*Nde*I
SbcD_rev	AAAAGCGGCCGCTCATGCTTCGTGTTCTCCGGC	*Not*I
SbcD_1-340_His_6_for	GGACACCACCACCACCACCACTGAGC	blunt-end ligation
SbcD_1-340_rev	CCGACGTACCAGCAATACTTCGAC	
SbcC_K43A_for	CAACAGGTGCGGGGGCAACCACCCTGCTG	QuikChange
SbcC_K43A_rev	CAGCAGGGTGGTTGCCCCCGCACCTGTTG	QuikChange
SbcC_E983Q_for	CGCTGTTCCTTGATCAAGGTTTTGGCACG	QuikChange
SbcC_E983Q_rev	CGTGCCAAAACCTTGATCAAGGAACAGCG	QuikChange
SbcD_H84S_for	GTACTGGCAGGAAACTCTGACTCGGTCGCCAC	QuikChange
SbcD_H84S_rev	GTGGCGACCGAGTCAGAGTTTCCTGCCAGTAC	QuikChange
Lis1_for	AGAAGGAGATACTAGATGGTTCTGAGCCAGCGTCAGCGTG	In-Fusion
Lis1_20PAS_SbcD_rev	GGATGCGCATACTAGCTGCCGGAGCTGCGCTTGCT	In-Fusion
Lis1_8PAS_ SbcD _rev	GGATGCGCATACTAGCTGCAGGAGAAGCGGCAGGGCT	In-Fusion
Lis1_11PAS_ SbcD _rev	GGATGCGCATACTAGCTGCAGGAGCTGCAGGAGAAGCGG	In-Fusion

Lis1_15PAS_ SbcD _rev	GGATGCGCATACTAGCTGCGCTTGCCGGTGCAGGAGCT	In-Fusion
SbcD_V68D_for	GTTATACAACCGTTTTGTTGACAATTTACAGCAAACTGGC	QuikChange
SbcD_V68D_rev	GCCAGTTTGCTGTAAATTGTCAACAAAACGGTTGTATAAC	QuikChange
SbcD_I96E_for	GCTGAATGAATCGCGCGATGAAATGGCGTTCCTCAATACTAC	QuikChange
SbcD_I96E_rev	GTAGTATTGAGGAACGCCATTTCATCGCGCGATTCATTCAGC	QuikChange
SbcD_I96C_for	CTGAATGAATCGCGCGATTGCATGGCGTTCCTCAATAC	QuikChange
SbcD_I96C_rev	GTATTGAGGAACGCCATGCAATCGCGCGATTCATTCAG	QuikChange
SbcD_F99C_for	CGATATCATGGCGTGCCTCAATACTACCG	QuikChange
SbcD_F99C_rev	CGGTAGTATTGAGGCACGCCATGATATCG	QuikChange
SbcC_C506+509S_for	CGGGTCAGCCTTCCCCACTTTCTGGTTCCACCAG	QuikChange
SbcC_C506+509S_rev	CTGGTGGAACCAGAAAGTGGGGAAGGCTGACCCG	QuikChange
SbcC_R93E_for	GTGAAAGGTGAAGCGTACGAAGCATTCTGGAGCCAGAATC	QuikChange
SbcC_R93E_rev	GATTCTGGCTCCAGAATGCTTCGTACGCTTCACCTTTCAC	QuikChange
SbcC_R102E_for	CCAGAATCGGGCGGAAAACCAACCCGACGG	QuikChange
SbcC_R102E_rev	CCGTCGGGTTGGTTTTCCGCCCGATTCTGG	QuikChange
SbcC_K123E_for	CTGCGCCGACGGCGAAATTCTCGCCG	QuikChange
SbcC_K123E_rev	CGGCGAGAATTTCGCCGTCGGCGCAG	QuikChange
SbcC_K128E_for	CAAAATTCTCGCCGACGAAGTGAAAGATAAGC	QuikChange
SbcC_K128E_rev	GCTTATCTTTCACTTCGTCGGCGAGAATTTTG	QuikChange
SbcC_K130E_for	CTCGCCGACAAAGTGGAAGATAAGCTGGAAC	QuikChange
SbcC_K130E_rev	GTTCCAGCTTATCTTCCACTTTGTCGGCGAG	QuikChange
SbcD_S17E_for	CGGCCAGAACTTCTACGAAAAAAGCCGCGAAGCTG	QuikChange
SbcD_S17E_rev	CAGCTTCGCGGCTTTTTTCGTAGAAGTTCTGGCCG	QuikChange
SbcD_R135E_for	CATTCCGTTTTTACGTCCGGAAGACATTATTACCAGCCAG	QuikChange
SbcD_R135E_rev	CTGGCTGGTAATAATGTCTTCCGGACGTAAAAACGGAATG	QuikChange
SbcD_R197E_for	CAGTAAAAGTGACGCCGTGGAAGACATTTATATTGGCACG	QuikChange
SbcD_R197E_rev	CGTGCCAATATAAATGTCTTCCACGGCGTCACTTTTACTG	QuikChange
SbcC_E1022R_for	GTAGAAGCGATGAAAAGGCGTATTCCGGTGC	QuikChange
SbcC_E1022R_rev	GCACCGGAATACGCCTTTTCATCGCTTCTAC	QuikChange
SbcC_D995R_for	GATAGCGAAACGCTGAGGACCGCCCTTGATGC	QuikChange
SbcC_D995R_rev	GCATCAAGGGCGGTCCTCAGCGTTTCGCTATC	QuikChange
SbcC_E992R_for	CACGCTGGATAGCAGAACGCTGGATACCG	QuikChange
SbcC_E992R_rev	CGGTATCCAGCGTTCTGCTATCCAGCGTG	QuikChange

Table 2 DNA oligonucleotides used for nuclease activity assays. Fluorescently labeled oligonucleotides were PAGE purified prior to annealing. For annealing, labeled oligonucleotides were mixed with a 1.1 fold molar excess of the unlabeled oligonucleotide in annealing buffer (25 mM Tris pH 7.5, 50 mM NaCl, 10 mM $MgCl_2$). The mixed oligonucleotides were incubated in a thermocycler for 5 min at 95°C, and cooled down to 20°C at a cooling rate of 0.1°C/sec.
Labels: 6-Carboxyfluorescein (6-FAM); Biotin (Bio); Hexachlorofluorescein (HEX); Positions of phosphorothioate linkages (PTO) are indicated with an *; Positions of internally modified nucleotides are indicated by 'x'; Positions of unpaired DNA regions (bubbles) are indicated with small letters.

Name	Direc-tion	Sequence (5'–3' direction)	3' label	5' label
			internal modification	
RB22	for	CGGGTAGTAGATGAGCGCAGGGACACCGAGGTCAAGTACATTACCCTCTCATAGGAGGTG		
RB24	for	CGGGTAGTAGATGAGCGCAGGGACACCGAGGTCAAGTACATTACCCTCTCATAGGAGGTG	Bio	
RB25	for	CGGGTAGTAGATGAGCGCAGGGACACCGAGGTCAAGTACATTACCCTCTCATAGGAGGTG		Bio
RB26	for	CGGGTAGTAGATGAGCGCAGGGACACCGAGGTCAAGTACATTACCCTCTCATAGGAGGTG	Bio	Bio
RB27	rev	CACCTCCTATGAGAGGGTAATGTACTTGACCTCGGTGTCCCTGCGCTCATCTACTACCCG		
RB29	rev	CACCTCCTATGAGAGGGTAATGTACTTGACCTCGGTGTCCCTGCGCTCATCTACTACCCG	Bio	
RB30	rev	CACCTCCTATGAGAGGGTAATGTACTTGACCTCGGTGTCCCTGCGCTCATCTACTACCCG		Bio
RB31	rev	CACCTCCTATGAGAGGGTAATGTACTTGACCTCGGTGTCCCTGCGCTCATCTACTACCCG	Bio	Bio
RB49	for	CGGGTAGTAGATGAGCGCAttttttttCGAGGTCAAGTACATTACCCTCTCATAGGAGGTG	19-25 bubble	
RB50	for	CGGGTAGTAGATGAGCGtttttttttCGAGGTCAAGTACATTACCCTCTCATAGGAGGTG	17-25 bubble	
RB51	for	CGGGTAGTAGATGAGCGCAGGGtttCCGAGGTCAAGTACATTACCCTCTCATAGGAGGTG	22-24 bubble	
RB52	for	CGGGTAGTAGATGAGCGCAGtttttCCGAGGTCAAGTACATTACCCTCTCATAGGAGGTG	20-24 bubble	
RB53	for	CGGGTAGTAGATGAGCGCAGGtttACCGAGGTCAAGTACATTACCCTCTCATAGGAGGTG	21-23 bubble	
RB54	for	CGGGTAGTAGATGAGCGCAttttttACCGAGGTCAAGTACATTACCCTCTCATAGGAGGTG	19-23 bubble	
RB55	for	CGGGTAGTAGATGAGCGCAGGGACACttttttCAAGTACATTACCCTCTCATAGGAGGTG	26-30 bubble	
RB56	for	CGGGTAGTAGATGAGCGCAGGGACACCttttttCAAGTACATTACCCTCTCATAGGAGGTG	27-31 bubble	

RB66	for	CGGGTAGTAGATGAGCGCAGGGACACCGAGGTCAAGTACATTACCCTCTCATAGGAGGTG	6-FAM	
RB67	rev	CACCTCCTATGAGAGGGTAATGTACTTGACCTCGGTGTCCCTGCGCTCATCTACTACCCG		6-FAM
RB73	for	CGGGTAGTAGATGAGCGCAGGGACACCGAGGTCAAGTACATTACCCTCTCATAGGAGG'T'G	Bio	HEX
RB74	rev	CACCTCCTATGAGAGGGTAATGTACTTGACCTCGGTGTCCCTGCGCTCATCTACTACC'C'G	Bio	6-FAM
RB75	for	CGGGTAGTAGATGAGCGCAGGGACACCGAGGTCAAGTACATTACCCTCTCATAGGAGGTG		HEX
RB76	rev	CACCTCCTATGAGAGGGTAATGTACTTGACCTCGGTGTCCCTGCGCTCATCTACTACCCG	Bio	6-FAM
RB78	rev	CACCTCCTATGAGAGGGTAATGTACTTGACCTCGGCGCGCCGGCGCTCATCTACTACCCG		6-FAM
RB80	rev	CACCTCCTATGAGAGGGTAATGTACTTGACCATTAAATAATTTAGCTCATCTACTACCCG		6-FAM
RB86	for	CGGGTAGTAGATGAGCGCAGGGACACCGAGGTCAAGTACATTACCCTCTC*A*T*A*G*G*A*G*G*T*G	51-60 PTO	
RB87	rev	CACCTCCTATGAGAGGGTAATGTACTTGACCTCGGTGTCCCTGCGCTCAT*C*T*A*C*T*A*C*C*C*G	51-60 PTO	
RB90	for	CGGGTAGTAGATGAGCTAAATTATTTAATGGTCAAGTACATTACCCTCTC*A*T*A*G*G*A*G*G*T*G	51-60 PTO	
RB91	for	CGGGTAGTAGATGAGCGCCGGCGCGCCGAGGTCAAGTACATTACCCTCTC*A*T*A*G*G*A*G*G*T*G	51-60 PTO	
RB92	for	CGGGTAGTAGATGAGCGCAttttttttCGAGGTCAAGTACATTACCCTCTC*A*T*A*G*G*A*G*G*T*G	51-60 PTO	
RB93	for	CGGGTAGTAGATGAGCGCAGGGAtttCGAGGTCAAGTACATTACCCTCTC*A*T*A*G*G*A*G*G*T*G	51-60 PTO	
RB94	for	CGGGTAGTAGATGAGCGCAGGtttttCGAGGTCAAGTACATTACCCTCTC*A*T*A*G*G*A*G*G*T*G	51-60 PTO	
RB95	for	CGGGTAGTAGATGAGCGCAGGGACACCtttttCAAGTACATTACCCTCTC*A*T*A*G*G*A*G*G*T*G	51-60 PTO	
RB96	for	CGGGTAGTAGATGAGCGCAttttttACCGAGGTCAAGTACATTACCCTCTC*A*T*A*G*G*A*G*G*T*G	51-60 PTO	
RB97	for	CGGGTAGTAGATGAGCGCAGGGACACCtttttCAAGTACATTACCCTCTC*A*T*A*G*G*A*G*G*T*G	51-60 PTO	
Hin80-1	for	CGGGTAGTAGATGAGCGCAGGGACACCGAGGTCAAGTACATTACCCTCTCATAGGAGGTGCGCTTTATCAG*A*A*G*C*C*A*G*A*C	74-80 PTO	
Hin80-3	rev	GTCTGGCTTCTGATAAAGCGCACCTCCTATGAGAGGGTAATGTACTTGACCTCGGTGTCCCTGCGCTCATCTACTACCCG		Bio

Hin80-4	for	CGGGTAGTAGATGAGCGCAGGGACACCGAGGTCAAGTACATTACCCTCTCATAGGAGGTGCGCTTTATCAGAAGCCAGAC	Bio	
Hin80-5	for	CGGGTAGTAGATGAGCGCAGGGACACCGAGGTCAAGTACATTACCCTCTCATAGGAGGTGCGCTTTATCAGAAGCCAGAC		Bio
Hin80-6	rev	GTCTGGCTTCTGATAAAGCGCACCTCCTATGAGAGGGTAATGTACTTGACCTCGGTGTCCCTGCGCTCATCTACTACCCG		6-FAM

Table 3 DNA oligonucleotides used for anisotropy measurements and ATPase activity assays. For annealing, labeled oligonucleotides were mixed with a 1.1 fold molar excess of the unlabeled oligonucleotide or equimolar if both oligonucleotides were unlabeled in annealing buffer (25 mM Tris pH 7.5, 50 mM NaCl, 10 mM $MgCl_2$). The mixed oligonucleotides were incubated in a thermocycler for 5 min at 95°C, and cooled down to 20°C at a cooling rate of 0.1°C/sec. Labels: 6-Carboxyfluorescein (6-FAM)

Name	Sequence (5' -> 3')	5'- label
15nt_for	CGCTTTATCAGAAGC	
15nt_rev	GCTTCTGATAAAGCG	
20nt_for	CGCTTTATCAGAAGCCAGAC	
20nt_for_6-FAM	CGCTTTATCAGAAGCCAGAC	6-FAM
20nt_rev	GTCTGGCTTCTGATAAAGCG	
25nt_for	CGCTTTATCAGAAGCCAGACATTAA	
25nt_for_6-FAM	CGCTTTATCAGAAGCCAGACATTAA	6-FAM
25nt_rev	TTAATGTCTGGCTTCTGATAAAGCG	
30nt_for	CGCTTTATCAGAAGCCAGACATTAACGCTT	
30nt_for_6-FAM	CGCTTTATCAGAAGCCAGACATTAACGCTT	6-FAM
30nt_rev	AAGCGTTAATGTCTGGCTTCTGATAAAGCG	
35nt_for	CGCTTTATCAGAAGCCAGACATTAACGCTTCTGGA	
35nt_for_6-FAM	CGCTTTATCAGAAGCCAGACATTAACGCTTCTGGA	6-FAM
35nt_rev	TCCAGAAGCGTTAATGTCTGGCTTCTGATAAAGCG	
40nt_for	CGCTTTATCAGAAGCCAGACATTAACGCTTCTGGAGAAAC	
40nt_for_6-FAM	CGCTTTATCAGAAGCCAGACATTAACGCTTCTGGAGAAAC	6-FAM
40nt_rev	GTTTCTCCAGAAGCGTTAATGTCTGGCTTCTGATAAAGCG	
45nt_for	CGCTTTATCAGAAGCCAGACATTAACGCTTCTGGAGAAACTCAAC	
45nt_for_6-FAM	CGCTTTATCAGAAGCCAGACATTAACGCTTCTGGAGAAACTCAAC	6-FAM
45nt_rev	GTTGAGTTTCTCCAGAAGCGTTAATGTCTGGCTTCTGATAAAGCG	
50nt_for	CGCTTTATCAGAAGCCAGACATTAACGCTTCTGGAGAAACTCAACGAGCT	
50nt_for_6-FAM	CGCTTTATCAGAAGCCAGACATTAACGCTTCTGGAGAAACTCAACGAGCT	6-FAM
50nt_rev	AGCTCGTTGAGTTTCTCCAGAAGCGTTAATGTCTGGCTTCTGATAAAGCG	

55nt_for	CGCTTTATCAGAAGCCAGACATTAACGCTTCTGGAGAAACTCAACGAGCTGGACG	
55nt_rev	CGTCCAGCTCGTTGAGTTTCTCCAGAAGCGTTAATGTCTGGCTTCTGATAAAGCG	
60nt_for	CGCTTTATCAGAAGCCAGACATTAACGCTTCTGGAGAAACTCAACGAGCTGGACGCGGAT	
60nt_for_6-FAM	CGCTTTATCAGAAGCCAGACATTAACGCTTCTGGAGAAACTCAACGAGCTGGACGCGGAT	6-FAM
60nt_rev	ATCCGCGTCCAGCTCGTTGAGTTTCTCCAGAAGCGTTAATGTCTGGCTTCTGATAAAGCG	

3.1.2 Plasmids

Table 4 Plasmids used for recombinant protein expression in *E. coli*. pKP29 is based on the pET-29b vector and has a modified multiple cloning site. Eco, *Escherichia coli*; aa, amino acid; C-term-His_6, C-terminal hexahistidine tag; nc, SbcD nuclease and capping domain; *Spe*I, *Spe*I restriction site between ribosomal binding site and SbcD start codon, allows cloning of N-terminal fusion construct; Lis1, N-terminal fusion of LisH dimerization domain to SbcD; PAS, Linker between LisH domain and SbcD consisting of proline, alanine and serine (Schlapschy et al., 2013).

Construct Name	Encoded Sequence	Restriction sites	Tag	Vector
EcoSbcD_fl	EcoSbcD wt	*Not*I/*Nde*I	C-term-His_6 (SbcD)	pKP29
EcoSbcC_fl	EcoSbcC wt	*Nde*I/*Not*I	-	pKP29
EcoSbcCD_fl	EcoSbcD wt EcoSbcC wt	*NotNot*I/*Asc*I *Aar*I/*Asc*I	C-term-His_6 (SbcD)	pKP29
EcoSbcCD_H84S	EcoSbcD H84S EcoSbcC wt	*Not*I/*Asc*I *Aar*I/*Asc*I	C-term-His_6 (SbcD)	pKP29
EcoSbcCD_D48N	EcoSbcD D48N EcoSbcC wt	*Not*I/*Asc*I *Aar*I/*Asc*I	C-term-His_6 (SbcD)	pKP29
EcoSbcCD_K43A	EcoSbcD wt EcoSbcC K43A	*Not*I/*Asc*I *Aar*I/*Asc*I	C-term-His_6 (SbcD)	pKP29
EcoSbcCD_E983Q	EcoSbcD wt EcoSbcC E983Q	*Not*I/*Asc*I *Aar*I/*Asc*I	C-term-His_6 (SbcD)	pKP29
EcoSbcCD_V68D	EcoSbcD V68D EcoSbcC wt	*Not*I/*Asc*I *Aar*I/*Asc*I	C-term-His_6 (SbcD)	pKP29
EcoSbcCD_I96E	EcoSbcD I96E EcoSbcC wt	*Not*I/*Asc*I *Aar*I/*Asc*I	C-term-His_6 (SbcD)	pKP29
EcoSbcD_nc	EcoSbcD wt aa 1-340	*Not*I/*Nde*I	C-term-His_6 (SbcD)	pKP29
EcoSbcD_nc_V68D	EcoSbcD V68D aa 1-340	*Not*I/*Nde*I	C-term-His_6 (SbcD)	pKP29
EcoSbcD_nc_*Spe*I	EcoSbcD wt aa 1-340 *Spe*I	*Not*I/*Nde*I	C-term-His_6 (SbcD)	pKP29
EcoSbcD_nc_V68D_*Spe*I	EcoSbcD V68D aa 1-340 *Spe*I	*Not*I/*Nde*I	C-term-His_6 (SbcD)	pKP29
EcoSbcCD_dZn	EcoSbcD wt EcoSbcC C506S, C509S	*Not*I/*Asc*I *Aar*I/*Asc*I	C-term-His_6 (SbcD)	pKP29
EcoSbcCD_fl_*Spe*I	EcoSbcD wt *Spe*I EcoSbcC wt	*Not*I/*Asc*I *Aar*I/*Asc*I	C-term-His_6 (SbcD)	pKP29
EcoSbcCD_fl_Lis1-20PAS	EcoSbcD wt Lis1-20PAS EcoSbcC wt	*Not*I/*Asc*I *Aar*I/*Asc*I	C-term-His_6 (SbcD)	pKP29
EcoSbcCD_fl_Lis1-11PAS	EcoSbcD wt Lis1-11PAS EcoSbcC wt	*Not*I/*Asc*I *Aar*I/*Asc*I	C-term-His_6 (SbcD)	pKP29
EcoSbcCD_fl_Lis1-8PAS	EcoSbcD wt Lis1-8PAS EcoSbcC wt	*Not*I/*Asc*I *Aar*I/*Asc*I	C-term-His_6 (SbcD)	pKP29
EcoSbcD_nc_Lis1-20PAS	EcoSbcD wt aa 1-340 Lis1-20PAS	*Not*I/*Nde*I	C-term-His_6 (SbcD)	pKP29

EcoSbcD_nc_V68D_ Lis1-20PAS	EcoSbcD V68D aa 1-340 Lis1-20PAS	*Not*I/*Nde*I	C-term-His$_6$ (SbcD)	pKP29
EcoSbcCD_H84S_R93E	EcoSbcD H84S EcoSbcC R93E	*Not*I/*Asc*I *Aar*I/*Asc*I	C-term-His$_6$ (SbcD)	pKP29
EcoSbcCD_H84S_R102E	EcoSbcD H84S EcoSbcC R102E	*Not*I/*Asc*I *Aar*I/*Asc*I	C-term-His$_6$ (SbcD)	pKP29
EcoSbcCD_H84S_K128E	EcoSbcD H84S EcoSbcC K128E	*Not*I/*Asc*I *Aar*I/*Asc*I	C-term-His$_6$ (SbcD)	pKP29
EcoSbcCD_H84S_ K130E	EcoSbcD H84S EcoSbcC K130E	*Not*I/*Asc*I *Aar*I/*Asc*I	C-term-His$_6$ (SbcD)	pKP29
EcoSbcD_fl	EcoSbcD wt	*Nde*I/*Not*I	C-term-His$_6$ (SbcD)	pET-21b
EcoSbcD_V68D	EcoSbcD V68D	*Nde*I/*Not*I	C-term-His$_6$ (SbcD)	pET-21b
EcoSbcD_H84Q	EcoSbcD H84Q	*Nde*I/*Not*I	C-term-His$_6$ (SbcD)	pET-21b
EcoSbcD_cys-free	EcoSbcD_ C75A C127A C169A C238S C249A	*Not*I/*Xho*I	C-term-His$_6$ (SbcD)	pET-21b
EcoSbcC_cys-free	EcoSbcC_C50S_C78A_C118S_C483A_C709A_C725A	*Nde*I/*Not*I	-	pKP29
EcoSbcD_cys-free_F99C	EcoSbcD_ C75A C127A C169A C238S C249A_F99C	*Not*I/*Xho*I	C-term-His$_6$ (SbcD)	pET-21b
EcoSbcD_S17E	EcoSbcD S17E	*Nde*I/*Not*I	C-term-His$_6$ (SbcD)	pET-21b
EcoSbcD_R135E	EcoSbcD R135E	*Nde*I/*Not*I	C-term-His$_6$ (SbcD)	pET-21b
EcoSbcD_R197E	EcoSbcD R197E	*Nde*I/*Not*I	C-term-His$_6$ (SbcD)	pET-21b
EcoSbcC_E1022R	EcoSbcC E1022R	*Nde*I/*Not*I	-	pKP29
EcoSbcC_D995R	EcoSbcC D995R	*Nde*I/*Not*I	-	pKP29
EcoSbcC_K130E	EcoSbcC K130E	*Nde*I/*Not*I	-	pKP29

Table 5 Plasmids used for *in vitro* activity assays.

Name	**Description**	**length**	**Manufacturer**
ΦX174 RF I DNA	double-stranded, covalently closed, circular form of ΦX174 RF I DNA (supercoiled)	5386 base pairs	New England Biolabs (Frankfurt)
ΦX174 RF II DNA	double stranded, nicked, circular form of ΦX174 RFII DNA (relaxed form)	5386 base pairs	New England Biolabs (Frankfurt)
linear ΦX174 RF I DNA	double stranded, linear ΦX174 DNA (linearized with PsiI)	5386 base pairs	New England Biolabs (Frankfurt)
ΦX174 Virion	single-stranded viral DNA isolated from bacteriophage ΦX174 *am*3 *cs*70	5386 nucleotides	New England Biolabs (Frankfurt)

3.1.3 Strains

Table 6: *E. coli* strains used for molecular cloning and recombinant protein expression. The *E. coli* XL1 blue strain was used for molecular cloning. The *E. coli* Rosetta (DE3) and BL21 (DE3) strains were used for recombinant protein expression.

Strain	Genotype	Source
Xl1-Blue	recA1 endA1 gyrA96 thi-1 hsdR17 supE44 relA1 lac [F' proAB lacIqZΔM15 Tn10 (TetR)]	Stratagene (Heidelberg)
Rosetta (DE3)	F- ompT hsdSB (rB- mB-) gal dcm (DE3) pRARE (CamR)	Novagen (USA)
BL21 (DE3)	F- *ompT hsdS*B (rB-mB-) *gal dcm* (DE3)	Novagen (USA)

3.1.4 Media and antibiotics

Lysogeny Broth (LB) liquid media as well as LB agar plates (1% (w/w) NaCl, 1% (w/v) Bacto-tryptone, 0.5% (w/v) yeast extract and ± 1.5% agar) were prepared according to standard protocols (Green, 2012). Respective antibiotics were added to the media using following concentrations: ampicillin (100 µg/mL) kanamycin (50 µg/ml) and chloramphenicol (34 µg/ml).

3.2 Methods

3.2.1 Molecular biology methods

3.2.1.1 Molecular cloning

The genes encoding SbcD and SbcC were amplified by polymerase chain reaction (PCR) using a self-made mixture having the same composition as the Phusion® High-Fidelity PCR Master Mix (ThermoFisher Scientific). A typical PCR reaction contained 10-50 ng genetic template and 50 pmol of each DNA oligonucleotide in a total volume of 20 µL. The standard PCR program is shown in

Table **7**.

Table 7 PCR program used for molecular cloning. The annealing temperatures of the primers (X°C) were calculated using the OligoCalc tool (Kibbe, 2007).

Cycle step	Temperature	Time	Cycles
Initial denaturation	98°C	5 min	1
Denaturation	98°C	15 sec	30
Annealing	X°C	15 sec	
Extension	72°C	20 sec / 1 kb	
Final extension	72°C	5 min	1

The PCR products were separated ba agarose gel electrophoresis and purified using the NucleoSpin® Gel and PCR Clean-up Kit (Machery and Nagel). PCR products and Plasmid DNA were either assembled with the In-Fusion® HD Cloning Kit (Takara Bio USA) or digested with the corresponding restriction enzymes and ligated into the respective vector.

Full length SbcD was cloned into a pET21b vector using the *Nde*I and *Not*I restriction sites. Full length SbcC was cloned into a pET29b vector which had a modified multiple cloning site (MCS) that allowed polycistronic assembly of genes (internal designation: pKP29) using the *Not*I/*Asc*I and *Aar*I/*Asc*I restriction sites.

3.2.1.2 Site-directed mutagenesis

SbcC or SbcD mutants were generated by site-directed mutagenesis using the Quikchange© (Agilent) protocol and the KOD Hot Start Polymerase (Merck). Primer for site-directed mutagenesis were

designed using the PrimerX design tool (http://www.bioinformatics.org/primerx/). Typically, PCR reactions contained 5 ng DNA template and 3 pmol of each DNA oligonucleotide in a total volume of 20 µL. The standard PCR program is shown in Table 8. After digestion with *Dpn*I, 4 µL PCR reaction were transformed into 50 µL chemically competent *E. coli* cells. The presence of the mutation and the integrity of the open reading frame were confirmed using DNA sequencing.

Table 8 PCR program used for site-directed mutagenesis. Annealing temperatures were optimized for each reaction; typically an annealing temperature of 68°C was used.

Cycle step	Temperature	Time	Cycles
Initial denaturation	95°C	5 min	1
Denaturation	95°C	50 sec	18
Annealing	X°C	50 sec	
Extension	70°C	15 sec / 1 kb	
Final extension	70°C	10 min	1

3.2.1.3 Transformation of *E. coli*

Chemically competent *E. coli* cells were transformed using the following protocol: 2-5 µL In-Fusion® reaction mix, ligation mixtures or 50 ng plasmid were added to 50 µL competent cells and incubated on ice for 15 min. *E. coli* host strains are listed in Table 1. Cells were then heat-shocked for 45 sec at 42°C, followed by 2 min incubation on ice, addition of 900 µl LB medium and subsequent incubation on a thermo shaker at 37°C for 45 to 60 min to establish antibiotic resistance. Afterwards cells were plated on LB agar plates containing the respective antibiotics and incubated overnight at 37°C.

3.2.1.4 PAGE purification and crush and soak extraction of oligonucleotides

All ordered oligonucleotides required a further purification step to minimize the background signal in nuclease assays.

Oligonucleotides (100 µM in 3% Ficoll® 400) were separated on 15% native PAA gels (0.5% TBE) at 150V for 90 min. After excision of the band of interest, gel pieces were crushed into cubes (<0.5 mm) using yellow pipette tips and the oligonucleotides were extracted two times with extraction buffer (300 mM Sodium-Acetate, 1 mM EDTA). Residual gel pieces were removed by passing the supernatant through NucleoSpin® Silica membrane columns (Machery-Nagel) and the oligonucleotides were precipitated with

50% isopropanol at -20°C overnight. The oligonucleotides were dissolved in ddH_2O, the concentration was determined by measuring the absorbance at 260 nm and the oligonucleotides then frozen at -20°C.

3.2.2 Protein biochemistry methods

3.2.2.1 Protein expression in *E. coli*

Recombinant proteins were produced by transforming plasmids of interest (Table 4) into *Escherichia coli* BL-21 (DE-3) cells (Table 6). A single colony was picked and grown in LB media to an OD_{600} of 0.6 at 37°C under aerobic conditions. Recombinant protein expression was induced by addition of 0.5 mM IPTG and the cultures were grown overnight at 18°C. Cells were harvested by centrifugation (10 min at 2500 x g), frozen in liquid nitrogen and stored at -20°C until further use.

3.2.2.2 Purification of the SbcCD complex from *E. coli*

Cells containing recombinant SbcCD protein were thawed at room temperature (rt), resuspended in Lysis buffer (composition of buffers are depicted in

Table 9 and disrupted by sonication. The lysate was cleared by centrifugation for 45 min at 16 000xg and loaded onto Ni-NTA resin (Qiagen), followed by two wash steps with Lysis buffer and Wash buffer and a subsequent elution with Elution buffer. The elution fractions were applied onto a 1 mL Q HiTrap column (GE Healthcare) equilibrated with Buffer A and eluted with a linear gradient from 0-100% Buffer B. SbcCD eluted as one peak at 30% Buffer B.Peak fractions were pooled, concentrated and further purified by size-exclusion chromatography (SEC) using a Superose6 10/30 GL column (GE Healthcare) in Buffer C. Peak fractions were pooled again, concentrated to 5 mg/mL and flash-frozen in liquid nitrogen in 10-20 µL aliquots.

Table 9 Buffers used for purification, crosslinking and reconstitution of SbcD and SbcCD. Buffers were filtered and stored at 4°C, DTT and β-mercaptoethanol (β-Me) was added just before use. IMAC, immobilized metal ion affinity chromatography; IEX, ion-exchange chromatography; SEC, size-exclusion chromatography.

Name	Composition	Method
Lysis buffer	150 mM NaCl, 25 mM Tris, pH 7.5, 10 mM imidazole, 5 mM β-Me	IMAC
Wash buffer	125 mM NaCl, 25 mM Tris, pH 7.5, 20 mM imidazole, 5 mM β-Me	
Elution buffer	100 mM NaCl, 25 mM Tris, pH 7.5, 200 mM imidazole, 5 mM β-Me	
Buffer A	100 mM NaCl, 25 mM Tris, pH 7.5	IEX

Buffer B	1000 mM NaCl, 25 mM Tris, pH 7.5	
Buffer C	125 mM NaCl, 50 mM Tris, pH 7.5, 10% Glycerol, 5 mM β-Me	SEC
Buffer D	125 mM NaCl, 50 mM Tris, pH 7.5, 5 mM β-Me	
Buffer E	125 mM NaCl , 25 mM Tris, 10 mM TCEP	Cysteine-crosslinking
Buffer F	100 mM NaCl , 50 mM Hepes pH 7.4	
Buffer G	100 mM KCl, 50 mM Tris, pH 7.5, 1 mM $MnCl_2$, 2 mM DTT	SbcCD reconstitution
Buffer H	50 mM KCl, 25 mM Tris, pH 7.5, 5 mM β-Me	

3.2.2.3 Purification of SbcD from E.coli

Cells containing recombinant SbcD protein were thawed at rt, resuspended in Lysis buffer and disrupted by sonication. The lysate was cleared by centrifugation for 45 min at (16 000xg and applied onto Ni-NTA resin (Qiagen), followed by two wash steps with Lysis buffer and Wash buffer and a subsequent elution with Elution buffer. The elution fractions were pooled, concentrated and further purified by size-exclusion chromatography using a Superdex 200 16/60 column (GE Healthcare) in Buffer D. β-mercaptoethanol was omitted during SEC if SbcD was used for crosslinking experiments. SbcD eluted as a single peak. The fractions of interest were pooled, concentrated to 30 mg/mL and flash frozen in liquid nitrogen in 10-50 µL aliquots.

3.2.2.4 Covalent crosslinking of SbcD via bis-maleimidoethane (BMOE)

$SbcD^{F99C}$ was incubated in Buffer E for 30 min at 25°C and then re-buffered with degassed Buffer F using a HiTrap Desalting column (GE Healthcare). Freshly dissolved BMOE (0.5 mM) was consecutively added to $SbcD^{F99C}$ (2.4 mg/mL, 54 µM, monomer) over a period of 30 min until a protein:crosslinker ratio of 1:1 was reached. After further incubation for 30 min at 25°C, the reaction was quenched by the addition of 3 mM DTT. The crosslinked reaction was concentrated to 15 mg/mL and purified by size-exclusion chromatography using a Superdex 200 10/300 column (GE Healthcare) in Buffer D. The crosslinked SbcD fractions were identified by SDS-PAGE and concentrated to 3.5 mg/mL (39 µM, dimer) and yielded in homogenous dimeric $SbcD^{x\text{-}linked}$ protein.

3.2.2.5 Reconstitution of SbcC and SbcD

$SbcC^{wt}$ (13 µM, monomer) was incubated with $SbcD^{wt}$ (32 µM, monomer), $SbcD^{no\_cys}$ (32 µM, monomer) or $SbcD^{x\text{-}linked}$ (16 µM, dimer) in Buffer G for 2 h at rt. Reconstituted $SbcCD^{variant}$ was separated from SbcD by SEC using a Superose 6 5/150 (GE Healthcare) column in Buffer H. The peak fractions of reconstituted $SbcCD^{variant}$ heterotetramer were concentrated to 0.8 mg/mL (2.5 µM) and immediately used for further analysis.

3.2.2.6 Size-exclusion chromatography coupled right angle light scattering (RALS)

Size-exclusion coupled static light scattering was performed using an ÄKTAmicro system (GE Healthcare Life Sciences) equipped with a VE3580 Refractive Index-device and TD270 right-angle laser light scattering detector (RALS, Viscotek/Malvern Instruments) and a Superdex S200 10/300 size-exclusion column (GE Healthcare). BSA (66 kDa) was used as standard protein for calibration. Analysis of data was performed using the Viscotek Software OmniSEC.

3.2.2.7 Denaturing polyacrylamide gel electrophoresis (SDS-PAGE)

Protein samples were analyzed on RunBlue 4-20% gradient SDS polyacrylamide (PAA) gels (Expedeon) using the vertical Mini-PROTEAN 3 System (BioRad). Prior to loading, samples were mixed with 1 fold Loading Dye (25 mM Tris pH 6.8, 4% (v/v) glycerol, 1% (w/v) SDS, 1.25% (v/v) β-mercaptoethanol, 0.15% (w/v) bromphenol blue) and heated to 95°C for 5 min. Electrophoresis was performed at 180V in RunBlue TEO-Tricine buffer (Expedeon). The gels were subsequently stained and fixed in Coomassie staining solution (7% (v/v) acetic acid, 50% (v/v) ethanol, 0.2% (w/v) Coomassie Brilliant Blue R-250) and destained with water. As molecular weight standard the PageRuler™ Unstained Protein Ladder (Fermentas) was used.

3.2.3 *In vitro* activity assays of SbcC-SbcD complex

3.2.3.1 Double-stranded DNA nuclease assay

Steady state nuclease assays were carried out in assay buffer (25 mM Tris pH 7.5, 50 mM KCl, 5 mM $MgCl_2$, 1 mM $MnCl_2$, 0.1 mg/mL BSA, 1 mM DTT) with 1000 nM SbcCD (heterotetramer) and 200 nM of DNA substrate. Where indicated, reactions were supplemented with a 15 fold molar excess of Streptavidin (IBA) over DNA concentration. Reactions were started by DNA addition and incubated at

37°C for 15 min, unless specified otherwise. 10 µL of each reaction was terminated by adding equal volume of 2x loading buffer (8 M Urea, 50 mM Tris, pH 7.5, 20 mM EDTA, 6% Ficoll® 400). The zero time point was taken prior to the initiation of the reaction. Reaction products were resolved on 12% denaturing polyacrylamide gels (Rotiphorese® DNA sequencing system) in 1x TBE buffer. Gels were run 75 min at a constant power of 32W and afterwards scanned with a Typhoon fluorescence imager (GE healthcare). 6-FAM-labeled substrates were imaged with a 473 nm laser and 510 nm filter, Hex-labeled substrates with a 532 nm laser and 575 nm filter. The images were analyzed with the ImageJ software(Schneider et al., 2012).

3.2.3.2 Affinity measurement by fluorescence anisotropy

SbcCD dilutions (2 nM to 2000 nM) were prepared in 2x assay buffer (1x buffer: 25 mM Tris pH 7.5, 50 mM KCl, 5 mM $MgCl_2$, 1 mM $MnCl_2$, 1 mM DTT) and mixed with the equal volume of 6-FAM labeled DNA substrate (5 nM final assay concentration). After incubation for 20 min at 25°C, the fluorescence anisotropy was measured at an excitation wavelength of 495 nM and emission wavelength of 520 nM. Data were analyzed with Prism (GraphPad) and fit to a one site - specific binding equation.

3.2.3.3 NADH-coupled measurement of ATP hydrolysis

To monitor the ATPase activity of SbcCD, the ATP-hydrolysis was coupled to the oxidation of NADH to NAD^+, which can be monitored spectrophotometrically. The reaction buffer contained NADH (0.35 mM), pyruvate kinase/lactate dehydrogenase (20 U/mL PK, 30 U/mL LDH, Sigma-Aldrich), phosphoenol pyruvate (2 mM) and ATP (1 mM). All assays were conducted at 37°C in assay buffer (25 mM Tris pH 7.5, 50 mM KCl, 5 mM $MgCl_2$, 1 mM $MnCl_2$, 1 mM ATP, 0.1 mg/mL BSA, 1 mM DTT). The reaction was started by the addition of SbcCD. The rate of NADH oxidation was monitored fluorometrically by measuring the absorbance at 340 nm on an Infinite M1000 microplate reader (Tecan) at 37°C over a period of 20 min.

3.2.3.4 Endonuclease assay of single-stranded and double-stranded plasmid DNA

One microgram of circular single-stranded ΦX174 Virion or circular double-stranded ΦX174 RFII DNA was incubated with 500 nM of either SbcCD or SbcD in reaction buffer (25 mM Tris pH 7.5, 50 mM KCl, 5 mM $MgCl_2$, 1 mM $MnCl_2$, 0.1 mg/mL BSA, 1 mM DTT) at 37°C. 10 µL aliquots were removed at indicated time points and the reactions were stopped by the addition of 25 mM EDTA and 1% SDS. The reaction products were separated at 80V on a 0.8% agarose Tris-acetate-EDTA gel and stained with 1x GelRed (Biotium).

3.2.3.5 DNA end unwinding assay

SbcCD^{H84Q} (250 nM) was incubated with 35 base pair DNA (for: 5'-Dabcyl-CGGGTAGTAGATGAGCGCAGG GACACCGAGGTCAA-3' and rev 5'-TTGACCTCGGTGTCCCTGCGCTCATCTACTACCCG-Cy3-3', 50 nM) in assay buffer (25 mM Tris pH 7.5, 50 mM KCl, 5 mM $MgCl_2$, 1 mM $MnCl_2$, 0.1 mg/mL BSA, 1 mM DTT) in the presence of a unlabeled quencher oligo (rev sequence, 250 nM). The reaction was started by mixing protein and DNA in a 1:1 ratio to get a final volume of 200 µL. The reaction was incubated at 37°C and the development of fluorescence was instantly monitored fluorometrically by exciting at 550 nm and measuring the emission at 575 nm on an Infinite M1000 microplate reader (Tecan).

3.2.3.6 DNA internal structural distortion assay

Internal structural distortions were monitored by the reaction of potassium permanganate ($KMnO_4$) with the pyrimidine bases of distorted dsDNA (Kahl and Paule, 2009). The assay was carried out in assay buffer (25 mM Tris pH 7.5, 50 mM KCl, 5 mM $MgCl_2$, 1 mM $MnCl_2$, 0.1 mg/mL BSA, 1 mM DTT). SbcCD^{H84Q} (500 nM) was incubated with 60 bp DNA (100 nM) for 20 minutes at 37 °C in 20 µL. $KMnO_4$ (final conc.: 5 mM) was then added and the reaction was quenched after two min by the addition of β–mercaptoethanol (50 mM). The protein was digested 1 h at 50°C by the addition of SDS (0.2% w/v) and ProteinaseK (Fermentas, 2 mg/mL).

The DNA was precipitated by the addition of 90 µL of a mixture of 0.6 M sodium-acetate and 300 µg/µL linear polyacrylamid, 160 µL of Ethanol (95%, v/v) and centrifuged 30 min at 20.000 rpm at 4°C. The supernatant was removed and the pellet washed with 150 µL Ethanol (70%, v/v), centrifuged another 5 min and after removing the supernatant the pellet was dried for 5 min.

To perform the alkaline cleavage, 50 µL of Piperidine (1 M) was added to the pellet and incubated at 90°C for 30 min. To precipitate the cleaved DNA, 50 µL of the sodium-acetate and linear polyacrylamid mixture and 250 µL of Ethanol (95%) was added. The DNA was then precipitated centrifuged 30 min at 20.000 rpm at 4°C and washed with Ethanol (70%). To remove residual piperidine, 50 µL of deionized water was added and the reactions were dried in a Speed Vac for 1 h at 37°C.

4. Results

4.1 Purification and activity optimization of the SbcCD complex of *E.coli*

To get a comprehensive picture of the working mechanism of entire SbcCD complex, it is essential to have a reliable and robust purification protocol. SbcCD was expressed in *E.coli* BL-21 cells, thus, a T7 RNA polymerase system was used. This yielded soluble and over-expressed SbcCD, as shown by the intense bands for SbcD (44 kDa) and SbcC (119 kDa) in the lysate (Figure 9A). Purification *via* the plasmid-encoded C-terminal hexahistidine tag on SbcD using Ni-NTA yielded stoichiometric SbcCD complex with minor impurities at 70 and 25 kDa and DNA contaminations (A_{280}/A_{260} ratio: 0.8) from the *E.coli* lysate.

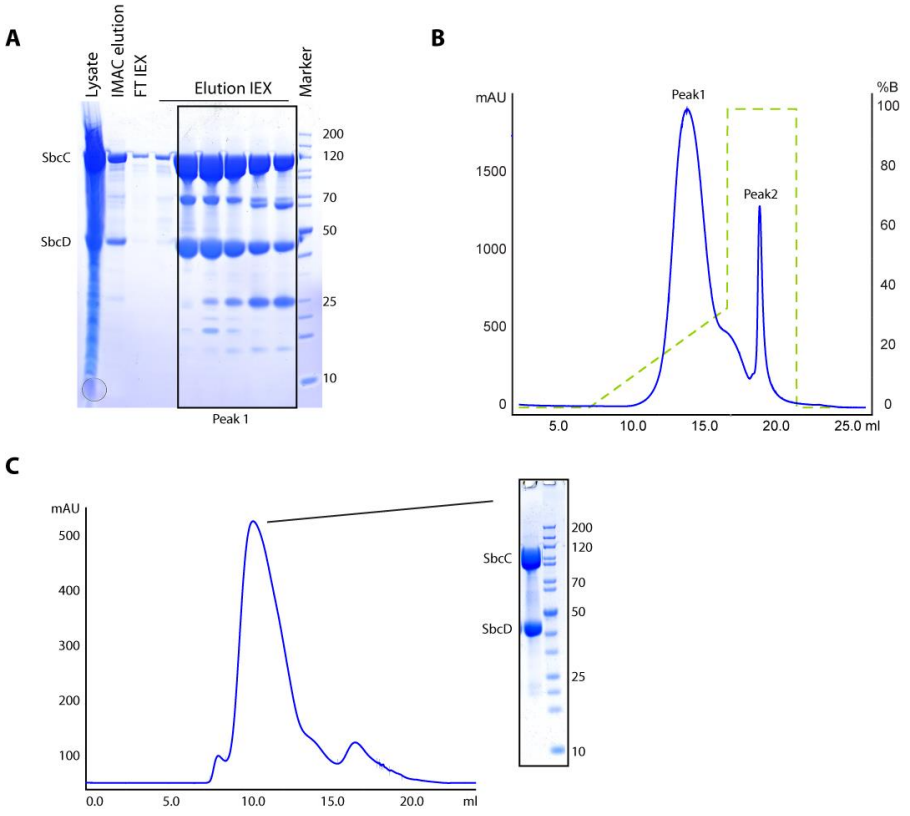

Figure 9 Purification of full-length SbcCD^{wt} protein from *E. coli:* (A) Coomassie stained SDS-PAGE-Gel of the Immobilized metal-ion affinity chromatography (IMAC) and Ion exchange chromatography (IEX) SbcCD purification. FT, Flow through. **(B)** Chromatogram of the IEX purification *via* a HiTrap Q HP column. Peak 1 corresponds to the SbcCD complex, Peak 2 corresponds to co-purified DNA. Blue color indicates A_{280}, green color the fraction of Buffer B **(C)** Chromatogram of the Size exclusion chromatography (SEC). Coomassie-stained SDS-PAGE-Gel of the pooled fractions proves the purity of the SbcCD complex after SEC.

Subsequent purification by anion-exchange chromatography (IEX) separated the DNA contamination (Peak 2) from SbcCD (Peak 1) (Figure 9B). The fractions of interest from IEX were applied on a Superose 6 column and stoichiometric SbcCD eluted at an apparent molecular weight of approximately 1.0 MDa. The difference between molecular weight (323 kDa as heterotetramer) and elution volume is due to the large stokes radius of SbcCD caused by the long coiled-coils. The protein was approximately 96% pure as validated by SDS-PAGE and the yield was 3 mg protein per liter expression culture. Therefore, SbcCD purified under these conditions is suitable for thorough biochemical and structural analysis. All mutants of SbcCD were purified with the identical protocol.

In order to conduct biochemical experiments with SbcCD, the buffer conditions need to be optimized to obtain maximal enzymatic activity. The nuclease activity on a 3' labeled 60 bp DNA substrate was monitored in dependence to rising salt concentrations, different pH values and the divalent ions of Mg^{2+} and Mn^{2+}.

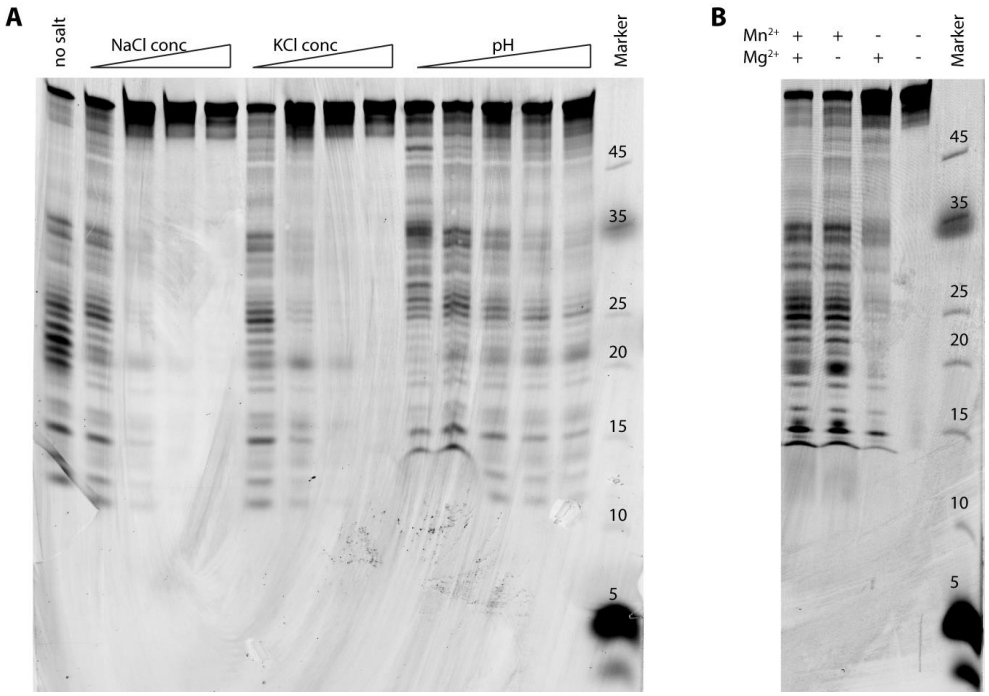

Figure 10 Buffer optimization for SbcCD nuclease activity assays (A) SbcCD was assayed in the presence of ATP, Mn^{2+} and Mg^{2+}. NaCl and KCl concentrations were 50 mM,100 mM, 150 mM and 200 mM. pH values ranged from 6.5 – 8.5 in 0.5 intervals. SbcCD and DNA were incubated for 10 minutes at 37 °C **(B)** SbcCD was assayed in the presence of 50 mM KCl, Tris pH 7.5, 1 mM ATP, dependent to the presence of 5 mM $MgCl_2$ and 1 mM $MnCl_2$.

SbcCD comprises the highest activity without any salt, 50 mM salt yielded similar SbcCD nuclease activity. Surprisingly, salt concentrations above 100 mM salt highly reduced the nuclease activity, no difference was observed between NaCl or KCl.

Screening different pH values revealed that SbcCD possesses highest nuclease activity at low pH values of 6.5 and 7.0. The pH values of 8.0 and 8.5 reduced the nuclease activity, especially the cleavage products at 25 and 35 nucleotides became less intense (Figure 10A). A salt concentration of 50 mM and a pH of 7.5 were chosen as a good compromise between high activity and physiological reaction conditions.

Screening of divalent ions showed, that the nuclease activity requires the presence of Mn^{2+} for activity. Mg^{2+} could partially compensate the absence of Mn^{2+}, in the absence of any divalent ions, SbcCD did not show any nuclease activity (Figure 10B).

4.2 ATP-dependent activities of SbcCD

SbcC belongs to the superfamily of the ATP-binding cassette (ABC) ATPases and has homologs in all kingdoms of life. In eukaryotes, the homolog of SbcC is known as Rad50. Binding of ATP to the nucleotide binding domains (NBDs) of SbcC/Rad50 leads to the formation of a tight NBD:2ATP: NBD complex, which is then able to hydrolyze ATP (Hopfner et al., 2000b). ATP binding does not only induce a large conformational change in the SbcCD's head domain, essential functions of SbcCD and its orthologs are regulated by ATP binding and subsequent hydrolysis (Schiller et al., 2014; Stracker and Petrini, 2011). Therefore, a fundamental understanding of the ATPase regulation and how an ATP-binding and ATP-hydrolysis feed back into the enzymatic and architectural activities of SbcCD is important. A thorough biochemical investigation of full-length SbcCD or is missing so far. On one hand, because previous studies were limited to thermophilic organisms and on the other hand large amounts of eukaryotic MR(N/X) are not easy to obtain for a thorough biochemical analysis.

The DNA binding of SbcCD in the presence and absence of ATP was investigated by fluorescence anisotropy measurements. This method takes advantage on the change of rotational time of a labeled molecule (DNA) when a protein associates with it and allows the precise measurement of dissociation constants (K_d) in solution. To prevent DNA-degradation during the course of experiment, the conserved histidine 84 of SbcD nuclease active was mutated to glutamine ($SbcCD^{H84Q}$).

$SbcCD^{H84Q}$ did not bind to single-stranded DNA (ssDNA) in the presence or absence of ATP. It neither bound dsDNA in the absence of ATP. In the presence of ATP, $SbcCD^{H84Q}$ bound dsDNA with a tight K_d of 42 nM. Therefore, $SbcCD^{H84Q}$ strictly required ATP-dependent dimerization of SbcC and the secondary structure of B-DNA to associate with DNA (Figure 11A)

The ATP hydrolysis of $SbcCD^{wt}$ was measured in the presence of 50 mM KCl, 5 mM Mg^{2+}, 1 mM Mn^{2+}, at a pH of 7.5. In this environment, $SbcCD^{wt}$ had a maximum ATPase velocity (k_{cat}) of 0.008 ATP/s. The addition of 60 base pair DNA stimulated ATP hydrolysis by 26-fold to a k_{cat} of 0.21 ATP/s. Single-stranded 60 nucleotide DNA did not affect the ATP hydrolysis rate (Figure 11B).

Thus, the following Michaelis-Menten kinetics were performed in the presence of 60 base-pair (bp) DNA (Figure 25). The protein and DNA concentration was kept at a constant level and the ATPase rate was determined at increasing ATP concentration.

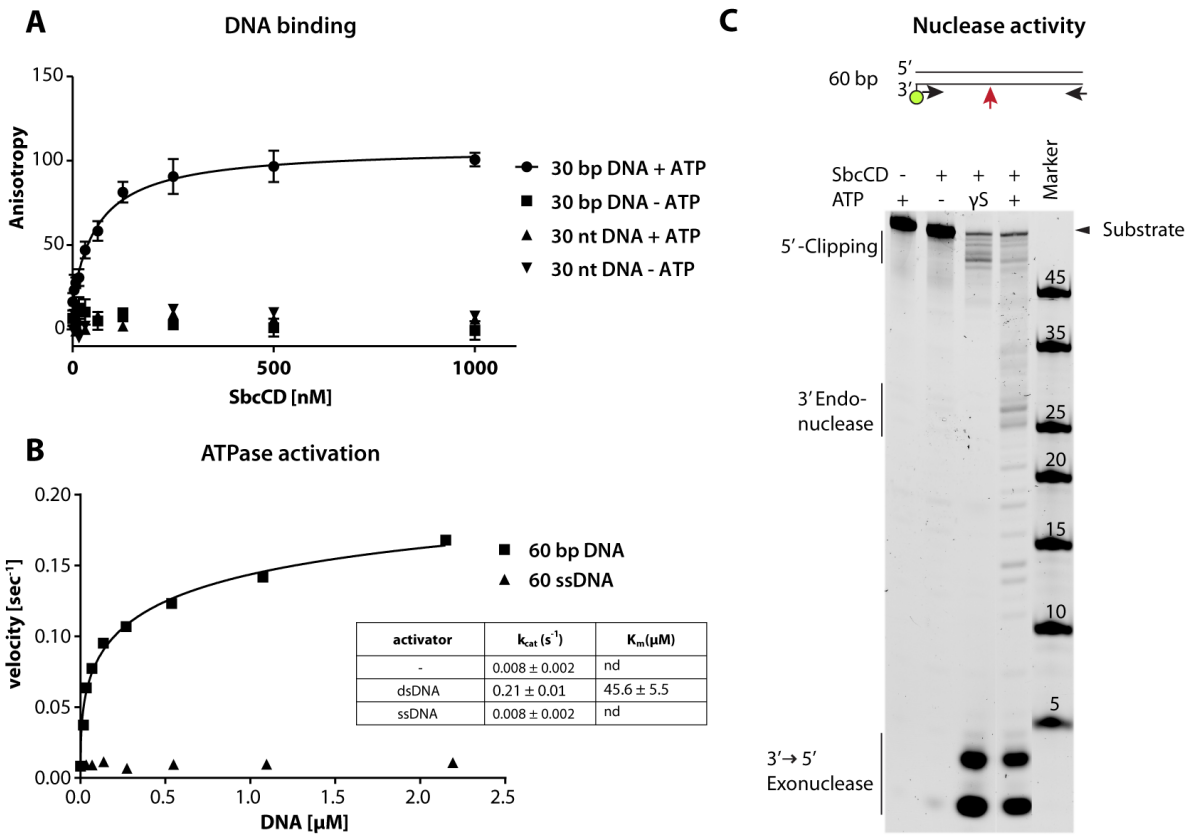

Figure 11 ATP dependent activities of SbcCD: (A) Binding of $SbcCD^{H84Q}$ to 30 base-pair or single-stranded DNA was determined using fluorescence anisotropy in the presence of 50 mM KCl, 5 mM $MgCl_2$, 1 mM $MnCl_2$, and 1 mM ATP. Measurements were done in triplicates; the error bars represent standard deviation. The data were fit to a 1 to 1 binding equation with hillslope **(B)** The steady-state ATPase hydrolysis rates of $SbcCD^{wt}$ were measured in the presence of 5 mM $MgCl_2$ and 1 mM $MnCl_2$ at 37 °C. 60 base-pair or nucleotide DNA was titrated as an activator. Data were fit to a Michaelis-Menten equation, error bars represent the standard deviation of three measurements. The table depicts k_{cat} and K_m values determined from Michaelis-Menten kinetic studies which were conducted in the presence of 1 µM 60 bp DNA **(C)** Nuclease activity of $SbcCD^{wt}$ was assayed with 3' 6-FAM-labeled 60 bp DNA under identical conditions as in (B). Reactions were started by addition of $SbcCD^{wt}$ and stopped after 15 minutes at 37 °C by addition of Urea loading dye. Cleavage products were separated on a Urea polyacrylamide gel and visualized by detecting Fluorescence at 420 nm.

SbcCD harbors two active sites and the ATP hydrolysis could be cooperative. A sigmoidal shape of the curve would indicate this fact. The ATPase rate of $SbcCD^{wt}$ was not sigmoidally dependent on the concentration of ATP and the data fit best to a Michaelis-Menten equation. Therefore, the two ATPase sites appear not to influence each other's activities. The Michaelis-Menten constant (K_m) was determined to 46 µM. Taking a physiological ATP concentration of 1.5 mM into account (Yaginuma et al., 2014), these kinetic data propose that SbcCD is predominantly in an ATP-bound conformation in a bacterial cell and requires the presence of dsDNA to hydrolyze ATP.

The nuclease activity of SbcCD was investigated in dependence of ATP binding (ATPγS) and ATP hydrolysis (Figure 11C). 60 bp DNA was used as substrate and DNA degradation was monitored by the presence of 6-Carboxyfluorescein (6-FAM) on the 3' terminus.

In the absence of ATP, no significant DNA degradation could be observed. The presence of the non-hydrolysable ATP-analogue ATPγS induced exonucleolytic degradation from the 3' terminus, shown by the appearance of cleavage products below five nucleotides. In addition, SbcCD cleaves approximately five nucleotides from the 5' terminus. In the presence of ATP, the exonuclease activity is preserved. Additional cleavage products could be detected at internal sites; the most prominent being around 25 nucleotides. Notably, the amount of utilized substrate is similar between ATPγS and ATP, therefore, ATP-hydrolysis did not enhance the exonuclease efficiency (Figure 11C). In summary, SbcCD needs ATP binding to associate and degrade DNA, but ATP-hydrolysis is required for internal dsDNA incisions.

4.3 Activities of SbcCD towards double-stranded DNA

4.3.1 ATPase activity of SbcCD in response to single-stranded and double-stranded DNA

To test the effect of a physiological relevant DNA substrate on the ATPase activation, the ATP hydrolysis in the presence of a 5.4 kilobases plasmid in (i) a closed single-stranded (ii) supercoiled (iii) relaxed and (iv) linearized state was measured. This gives information how internal DNA, DNA ends or the supercoiled state of DNA influence the ATPase hydrolysis rate of $SbcCD^{wt}$. The protein- and ATP-concentrations were kept constant; the plasmid DNA was added as an activator.

Circular single-stranded DNA did not stimulate ATP hydrolysis of $SbcCD^{wt}$. The supercoiled plasmid stimulated the ATPase by 9-fold to k_{cat} 0.072 ± 0.006 s^{-1} and the nicked plasmid by 26-fold to k_{cat} 0.207 ± 0.18 s^{-1}. Linearizing the plasmid with PsiI (generates blunt ends) did not further enhance the k_{cat} (0.200 ± 0.007 s^{-1}) compared to the nicked plasmid. However, the DNA concentration at half-maximum velocity (k_{act}) is 4-fold lower compared to nicked DNA. At 1 nM of plasmid, which would correspond to one DNA break in an *E.coli* cell (Milo et al., 2010), the ATPase was activated 7-fold. At the same concentration, supercoiled and nicked plasmid activated the ATPase 2-fold (Figure 12A).

The activation efficiency (k_{cat}/k_{act}) can compare the relative activation capability if one enzyme catalyzes the identical reaction. In this specific case, it is a good index for comparing the effectiveness of different activators. The covalently closed plasmids are in a similar range and have an activation efficiency of 15

(supercoiled) and 19 (nicked). The linear plasmid, however, has an activation efficiency of 77 (Figure 12C).

The individual ATPase rates of the nicked plasmid activation were subtracted from the linear plasmid activation. This indicates how DNA ends contribute to the SbcCD ATPase stimulation. Below a concentration of 3.5 nM plasmid, DNA ends were the main feature for ATPase activation. Above a concentration of 7 nM, the activating effect of DNA ends was outcompeted by the rising DNA concentration (Figure 12B).

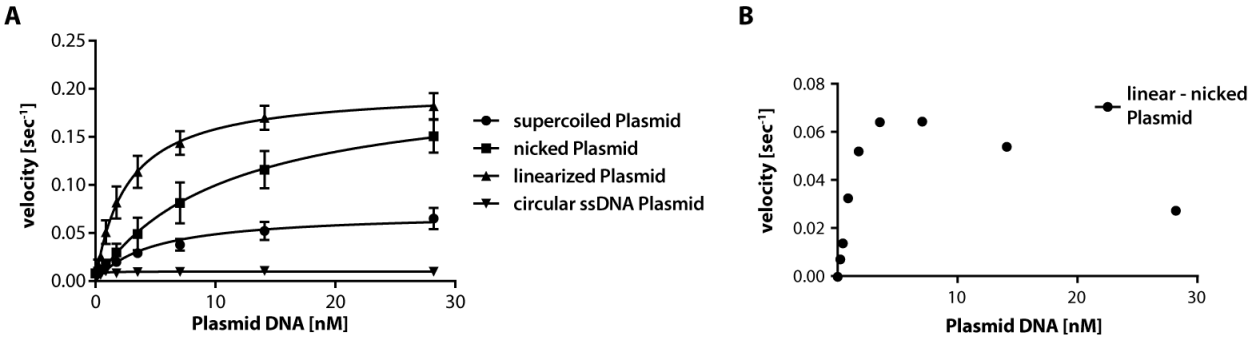

C

Plasmid	single stranded	supercoiled	nicked	linear
k_{cat} (s^{-1})	0.010 ± 0.001	0.072 ± 0.006	0.21 ± 0.02	0.200 ± 0.007
DNA-Activation	1.3	9	26	25
k_{act} (nM)	nd	4.7 ±1.1	10.8 ± 2.1	2.6 ± 0.3
k_{cat}/k_{act} ($\frac{L}{s \times \mu mol}$)	nd	15	19	77
k_{cat}/k_{act} (rel)	nd	1	1.3	5.1

Figure 12 Plasmid DNA stimulation of ATPase activity of the SbcCD^{wt} complex (A) The steady-state ATP hydrolysis rates of SbcCD^{wt} were measured in the presence of 5 mM $MgCl_2$ and 1 mM $MnCl_2$ at 37 °C. Plasmid DNA (from bacteriophage ΦX174, 5386 bp in length) was added as single-stranded, supercoiled, nicked or linear DNA at increasing concentrations. The data were fit to a Michaelis-Menten equation, error bars indicate deviation from three replicates. **(B)** The ATPase rates obtained in (A) from nicked DNA were subtracted from linear DNA. **(C)** Kinetic data that were obtained from the data-points in (A). k_{act} is the plasmid DNA concentration at half-maximum velocity of SbcCD^{wt}. k_{cat}/k_{act} represents the activation efficiency of each DNA substrate.

These results demonstrate that SbcCD ATPase is not only activated by the presence of the DNA, it is highly sensitive to DNA ends, the spatial organization and the supercoiled state of DNA. There appear to be two features that contribute to SbcCD's ATPase stimulation (i) the presence of relaxed B-DNA (ii) DNA ends.

To connect SbcCD's ATPase activation to the nuclease activity, SbcCD^{wt} was incubated with supercoiled, relaxed and linearized plasmid DNA in the presence of ATP. Furthermore, nuclease deficient *Eco*RI (EcoRInd) enzyme was added to the reactions to provide an internal protein block, since DNA end-bound proteins blocks were identified to stimulate MR(N/X)'s or SbcCD's nuclease activity (Cannavo and Cejka,

2014; Connelly et al., 2003). EcoRInd was characterized to bind specifically bind to *Eco*RI restriction sites with a picomolar affinity and halt the progression of DNA- and RNA-polymerases (Stigler et al., 2016). The plasmids were cut with nicking endonucleases that introduce nicks at specific positions into the plasmid.

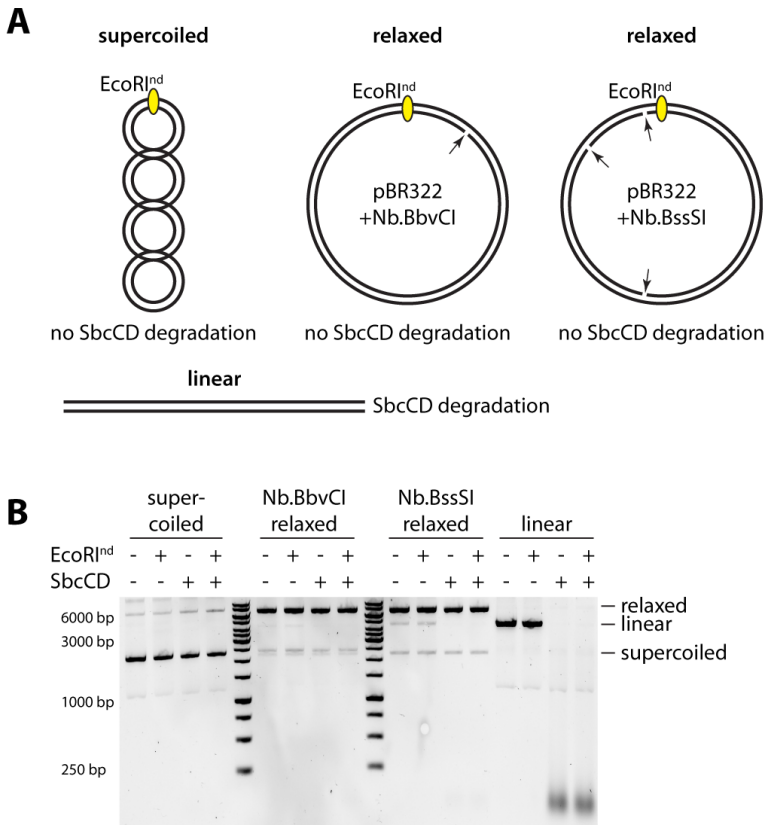

Figure 13 SbcCD^{wt} nuclease activity towards Plasmid DNA (A) Schematic overview of the plasmid substrates and incision sites of the nicking enzymes. **(B)** SbcCD^{wt} (25 nM) was assayed in the presence of 1 mM ATP, 5 mM $MgCl_2$ and 1 mM $MnCl_2$ at 37 °C for 15 min with different DNA plasmid substrates (100 ng, 1.5 nM).

The assay unambiguously showed that SbcCD^{wt} does not process circular plasmid DNA, neither in a supercoiled nor in a relaxed state. Linear DNA is rapidly processed within 5 minutes, which was tested in a time course experiment. The presence and absence of a protein block did not make a difference. Also a nick adjacent to the protein block did not stimulate endonucleolytic cleavage by SbcCD^{wt} (Figure 13).

4.3.2 Determining the ATPase activation footprint of SbcCD

So far, the minimal number of consecutive DNA base pairs required for ATPase stimulation ('activation footprint') have not been determined.

To obtain an activation footprint, the steady-state ATP hydrolysis rate of SbcCD was determined in dependence to dsDNA that ranged from 20 to 60 base pairs. Each DNA was assayed at increasing DNA concentrations and the obtained data were fit to a Michaelis-Menten equation. SbcCD was nuclease-deficient ($SbcCD^{H84Q}$), to prevent degradation during the course of the study. The SbcD H84Q mutation decreased the ATPase activity of SbcCD by approximately 15% (Figure 25) compared to the wild-type protein. This is likely due to an allosteric regulation of SbcC and SbcD within the ATP hydrolysis cycle.

A

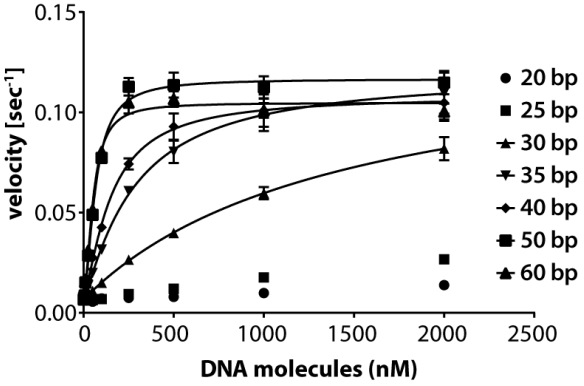

B

length (bp)	K_{act} (nM)	k_{cat} (s^{-1})
20	nd	nd
25	nd	nd
30	1700 ± 700	0.14 ± 0.03
35	280 ± 50	0.120 ± 0.008
40	152 ±19	0.108 ± 0.004
50	66 ± 5	0.117 ± 0.002
60	53 ± 4	0.105 ± 0.002

Figure 14 DNA stimulation of ATP hydrolysis by the $SbcCD^{H84Q}$ complex. (A) The steady-state ATPase hydrolysis rates of nuclease deficient $SbcCD^{H84Q}$ (500 nM) were measured in the presence of 5 mM $MgCl_2$ and 1 mM $MnCl_2$ at 37 °C. The ATPase activity was measured in the presence of dsDNA from 20 – 60 base pair lengths at increasing DNA concentrations. Error bars represent the standard deviation of three measurements. **(B)** Values were determined by fitting the data of (A) to a Michaelis-Menten equation. K_{act} indicates the DNA concentration at half-maximal velocity. Errors represent the standard Error of the fit.

The addition of 20 and 25 bp DNA did not stimulate $SbcCD^{H84Q}$'s ATPase. Just a minor increase in ATP hydrolysis could be detected for 25 bp DNA at 1000 and 2000 nM. These data could not be fitted with a Michaelis-Menten equation. From 30 bp and longer, the obtained data could be fitted and the 35 – 60 bp DNA collectively activated $SbcCD^{H84Q}$ to a maximum velocity from k_{cat} 0.105 to 120 s^{-1}. The Michaelis-Menten fit of 30 bp DNA yields a k_{cat} of 0.14 s^{-1}, which is likely due to a poor curve fit (Figure 14A and B).

30 bp DNA activated $SbcCD^{H84Q}$ with an activation constant of K_{act} 1700 ± 700 nM. When increasing the length to 35 and 40 bp the K_{act} shifted to 280 ± 50 nM and 152 ± 19 nM, respectively. Maximum ATPase stimulation was detected in the presence of 50 and 60 bp DNA, the K_{act} was increased by 2.5-fold to 66 ± 5 nM and 53 ± 5 nM, respectively (Figure 14A and B).

These data show, that a length of 30 base pairs and longer is capable to effectively activate ATPase hydrolysis by SbcCD. However, the k_{act} values indicate, that SbcCD requires 50 consecutive base pairs for efficient ATP hydrolysis activation.

The 50 and 60 bp DNA activated SbcCD^{H84Q} close to its maximal ATPase velocity at a DNA concentration of 250 nM. However, the assay concentration of heterotetrameric SbcCD^{H84Q} was 500 nM. Thus, one DNA molecule fully stimulated the ATPases of two SbcCD complexes. This is an indication that SbcCD might form arrays on DNA and two heterotetrameric SbcCD complexes could functionally influence each other.

4.3.3 SbcCD DNA binding dependent to DNA length

The MR(N/X) and MR complex can bind dsDNA *via* the Rad50 and Mre11 subunits. Depending on the study, Mre11 binds dsDNA with a K_d of 5 µM, whereas full-length MR(N) binds dsDNA in an ATP dependent manner with a K_d in the low nM range (Liu et al., 2016; Paull and Gellert, 1999; Rojowska et al., 2014; Seifert et al., 2016; Sung et al., 2014; Williams et al., 2008). The DNA binding groove of Rad50 is considered to be the main DNA binding site of the MR(N/X) complex. In the structure of *Thermotoga maritima* (*Tm*) MR^{NBD} dsDNA binds to the NBD and the coiled-coil domain of one Rad50. In the MR^{NBD} structures of *Chaetomium thermophilum* (*Ct*) and *Methanococcus jannaschii* (*Mj*) dsDNA is bound across the Rad50 dimer in an ATP dependent fashion. In all aforementioned structures, the DNA binding is sequence independent and mediated *via* the protein side-chains and the sugar-phosphate backbone of the DNA. The DNA-footprint of Rad50, which can be derived from the *Ct* and *Mj* structures, is approximately 20 bp. However, all structures are limited to Rad50 with largely truncated coiled coils (Liu et al., 2016; Rojowska et al., 2014; Seifert et al., 2016).

To obtain a DNA binding footprint, the binding constants of SbcCD^{H84Q} from 20 to 50 bp DNA were determined. Electrophoretic mobility shift assays (EMSA) was the first attempted method to study the SbcCD-DNA interaction. However, the addition of SbcCD did not induce a mobility shift despite extensive optimization in buffer composition and running conditions. Either SbcCD and DNA disassembles during the run due to high on- and off rates or ATP is missing in the agarose gel, that is a prerequisite for SbcCD-DNA complex formation.

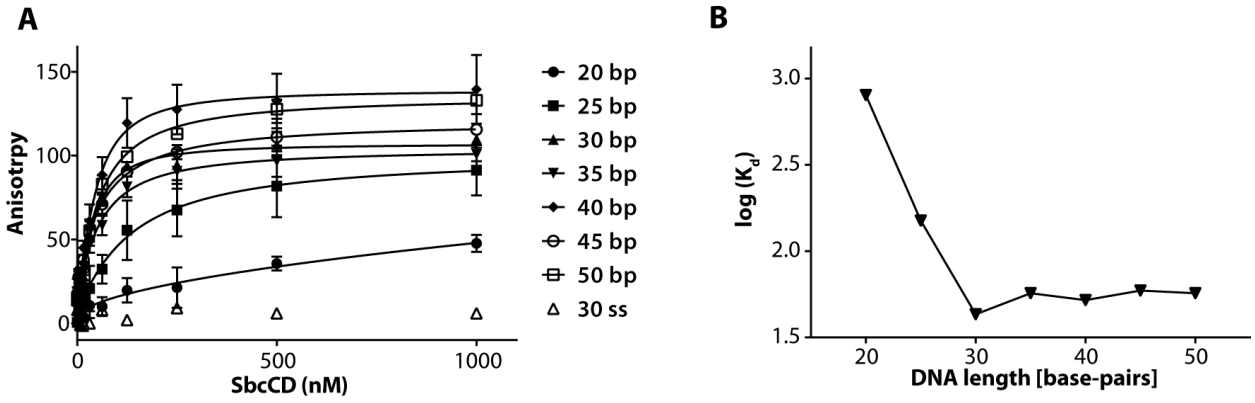

Figure 15 DNA binding of SbcCD^{H84Q} to double-stranded DNA from 20 – 50 base-pairs (A) The DNA binding of SbcCD^{H84Q} was assayed in the presence of 1 mM ATP, 5 mM $MgCl_2$ and 1 mM $MnCl_2$ at room temperature. DNA concentration was kept constant at 5 nM; the SbcCD^{H84Q} concentration ranged from 2 to 1000 nM. Data points represent the change in fluorescence anisotropy and the data were fit to a 1 to 1 binding equation. Error bars represent the deviation from three independent experiments. **(B)** Logarithmic representation of the K_d values obtained from the data fits in (A). Errors represent the standard Error of the fit.

Anisotropy experiment obtained reproducible results and was therefore the method of choice to conduct binding experiments with SbcCD and dsDNA. Previous experiments showed that SbcCD required ATP binding to associate with dsDNA. In the presence of ATPγS SbcCD bound slightly better to DNA. Nevertheless, ATP is the natural substrate for SbcCD's activity and this nucleotide was used for DNA binding assays. SbcCD^{H84Q} possesses low affinity to short DNA of 20 bp and moderate affinity to 25 bp DNA (K_d = 146 +- 46 nM). Lengthening the DNA by 5 bp to 30 bp increased the affinity to K_d = 43 ± 7 nM. Further lengthening of the DNA did not affect the K_d which remained in the range of 50 to 60 nM (Figure 15A and B).

Therefore, DNA binding and ATPase activation of SbcCD^{H84Q} share common features and still have different properties. SbcCD effectively binds dsDNA from 30 base pairs and longer. This high affinity is not increased by longer DNA. Similarly, ATPase activation is obtained by 30 bp DNA and longer. But the activation of ATP hydrolysis by SbcCD^{H84Q} appears to be a more complex process. It requires a minimal length of 30 base pairs and increases with longer DNA. The 50 and 60 bp DNAs possess certain features that induce a better ATPase activation (Figure 16). Longer DNA could offer enough space that SbcCD is able to (i) diffuse along dsDNA or (ii) form functional assemblies that are competent to hydrolyze ATP.

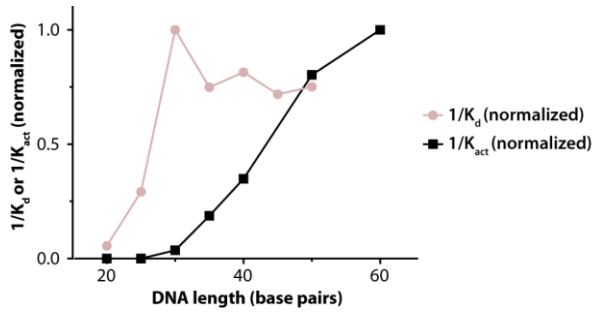

Figure 16 Comparison of length dependent DNA binding and ATP hydrolysis activity by the SbcCD^{H84Q} complex: The K_d and K_{act} values depicted in Figure 14 and Figure 15 were inversed and normalized to 1. SbcCD tightly binds dsDNA from 30 bp and longer with a K_d of approx. 50 nM.

4.4 SbcCD nuclease activity

4.4.1 SbcCD nuclease activity towards 60 base-pair DNA

MR(N/X) has a conserved 3'-5' exonuclease, ssDNA endonuclease activity and cleaves DNA secondary structures such as hairpins or 3' and 5' overhangs (Connelly et al., 1999; Lengsfeld et al., 2007; Paull and Gellert, 1998). Furthermore, MR(N/X) complex from *Saccharomyces cerevisiae* (*Sc*) and *human* process end-blocked dsDNA endonucleolytically by cleaving both strands and leaving a clean, blunt DNA end (Anand et al., 2016; Cannavo and Cejka, 2014; Deshpande et al., 2017).

The endonucleolytic incision of MR(N/X) is essential to remove covalent DNA-protein crosslinks (DPCs) on double-strand breaks. These are induced by chemotherapeutics that poison and trap topoisomerases and leave a protein bound double-strand break. DPC is also an intermediate during meiotic recombination via the topoisomerase Spo11. The processing of Spo11-induced breaks, which generate a 5' covalent attachment between Spo11 and DNA, is blocked in Mre11 nuclease deficient strains (Moreau et al., 1999). Mre11 nuclease deficiency causes a number of phenotypes that are indistinguishable to the absence of MRN in mouse, including dramatic genomic instability (Buis et al., 2008). These facts classify the nuclease activity as the central enzymatic activity of the MR(N/X) complex.

The bacterial SbcCD's architecture and enzymatic activities are highly conserved to its eukaryotic homologue. However, it is less regulated (Schiller et al., 2012). SbcCD has 3'-5' exonuclease activity, cleaves hairpin structures 5' at the loop and introduces a DSB next to protein-bound DNA ends (Connelly et al., 1999, 2003).

To get deeper insights into the mechanistic choreography of SbcCD, the nuclease activities on DNA require thorough characterization. A 5’ and 3’ labeled 60 bp DNAs were used as substrates. The effects of ATP binding and hydrolysis and the absence and presence of protein-blocked DNA end were tested.

SbcCD did not have any nuclease activity in the absence of ATP. The presence of non-hydrolysable ATPγS induced 3’-5’ exonuclease degradation by SbcCD. Clipping nucleotides from the 5’ end of DNA was also observed. However, this activity stops after approximately seven nucleotides at a rather defined band around 50-55 nucleotides (Figure 17A lanes 2-3). This clipping activity has not been reported in previous studies. Phosphorothioate protection of the opposite 3’ end reduced this activity (Figure 17C lanes 5-8). In the presence of ATP, SbcCD still comprised the exonuclease and clipping activity. Additionally, internal DNA cleavage products appeared, most prominently at a size of 27 nucleotides (3’ labeled DNA) and 23 nucleotides (5’ labeled DNA) (Figure 17A and B lane4).

SbcCD’s nuclease activity was also tested in the presence of a single-chain fragment, which has a high affinity towards fluorescein dyes (FAM-sc). This block is similar to a streptavidin-biotin conjugate and mimics a DPC, structures that often occur at DNA double-strand breaks. Binding of the fluorescein single-chain omitted the exonuclease activity of SbcCD. The bands corresponding to internal incision products appeared stronger in the presence of a protein blocked DNA end. Therefore, the conjugation of a protein block did not only omit exonuclease activity but also stimulated the endonucleolytic cleavage (Figure 17 A and B, lane 5). Next, it was aimed to determine if the distance of 27 bp is specific to the blocked or free DNA end. SbcCD cleaved a 3’ protein blocked 80 bp DNA, similarly to 60 bp DNA, 27 base pairs from the labeled DNA end. Therefore, this distance is specific and determined by a physical obstacle on a DNA end (Figure 17C lanes 1 – 4).

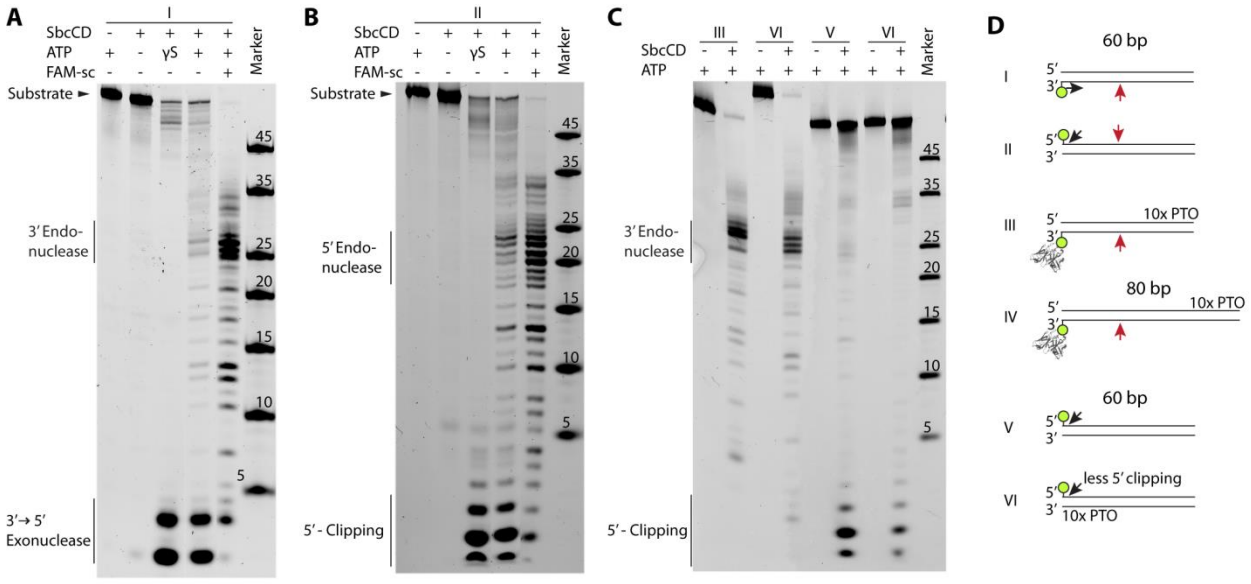

Figure 17 Nuclease activity of SbcCD^{wt} towards 60 and 80 base-pair DNA (A) SbcCD was assayed in the presence of 1 mM ATP(γS), 1 mM $MnCl_2$ and 5 mM $MgCl_2$ at 37 °C. The 60 bp DNA substrate was labeled on the 3' end with 6-FAM. FAM-sc is a single chain fragment that binds to Fluorescein dyes with a K_d of 4 nM. The cleavage products were separated by Urea-PAGE and visualized on a Typhoon scanner. The major cleavage products of SbcCD are schematized in (D). **(B)** Nuclease assay as in (A), but with 5' labeled DNA. **(C)** Nuclease assay as in (A). **(D)** Double-stranded DNA substrates that were used in (A – C) are schematized. 10x PTO describes the presence of 10 phosphorothioate linkages that protects the DNA strand from cleavage by nucleases. Arrows indicate major cleavage sites.

To conclude, SbcCD requires nucleotide binding and dimerization of the SbcC NBDs to bind DNA and process DNA from the ends. ATP hydrolysis is needed for internal incision. SbcCD preferentially incises both DNA strands around 25 base pairs from a DNA end which is stimulated by a DNA-protein conjugate. To stimulate the endonuclease activity it does not matter if the DPC is located at the 3' or 5' end. The 60 bp DNA was an optimal substrate to precisely monitor SbcCD's nuclease activities and used in the subsequent studies.

4.4.2 SbcCD nuclease activity related to dsDNA melting

It is not known how the Mre11 protein reaches the DNA which is initially bound by Rad50. It is also not known how dsDNA eventually reaches the active site of Mre11. Structures of DNA bound by Mre11 from *Pyrococcus furiosus* reveal that the manganese ions of Mre11 are concealed in the active site. B-DNA is 5 Å apart from a position which is productive for cleavage. This distance is not likely to be overcome by conformational changes of Mre11. It is more likely that the classical B-Form of DNA is altered in order to reach the active site (Hopfner et al., 2001). It has been shown in previous studies, that MR(N/X) complex unwinds dsDNA (Cannon et al., 2013; Liu et al., 2016; Paull and Gellert, 1999). But the precise purpose of

this activity could not be described in these studies. The aim of the following experiments was to correlate DNA melting activity and the presence of melted DNA stretches to SbcCD's nuclease activity.

To test if melting of dsDNA occurs during nucleolytic incision, DNA substrates with different local AT and GC contents were designed. The GC base pair has a higher thermodynamic stability than an AT base pair, mainly due to base pair stacking. Therefore, the local thermodynamic stability of B-DNA can be tuned *via* the GC/AT content (Yakovchuk et al., 2006). 60 bp DNA was modified from position 15 to 29 (counting from the FAM- dye) with (i) mixed AT/GC-content (ii) 100% AT-content (iii) 100% GC-content. The unlabelled strand was protected with phosphorothioates on the 3' end to prevent degradation. The endonuclease activity was tested in the presence and absence of a protein-bound DNA end.

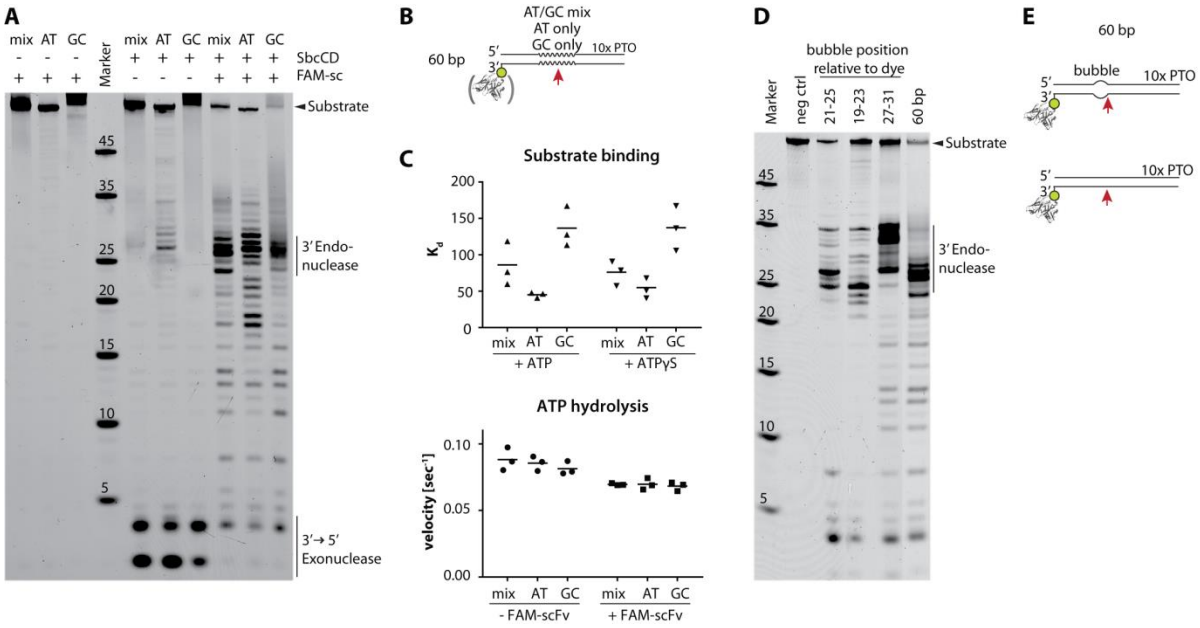

Figure 18 SbcCD cleaves double-stranded DNA dependent to the local AT/GC concentration and pre-melted DNA stretches (A) Nuclease activity of SbcCD was assayed assay in the presence 1 mM ATP, 1 mM $MnCl_2$ and 5 mM $MgCl_2$ at 37 °C towards 60 base pair DNA. The DNA was labeled on the 3' end with 6-FAM and contained different AT/GC concentrations from position 15 – 29 (counting from the dye). FAM-sc – single chain fragment that binds to fluorescein. **(B)** DNA that was used in (A) **(C)** K_d values obtained from binding of SbcCD to the DNA substrates used in (A). Values were obtained from three independent experiments, data were fit to a 1 to 1 binding equation, and errors represent the standard error of the fit. The ATP hydrolysis during nuclease assays was monitored. **(D)** Nuclease assay as in (A), but 60 base pair DNA with pre-melted DNA regions were tested. SbcCD cleaves the DNA substrates 5' to the pre-melted region. **(E)** DNA substrate that was used in (D)

As observed in previous assays, SbcCD cleaved the 60 bp DNA with mixed AT/GC content 27 base pairs from the 3' end with moderate activity. These endonuclease products became stronger with AT-rich DNA and vanished when the DNA was GC-rich (Figure 18A lanes 5-7). Therefore, SbcCD's endonuclease activity correlates to the local thermodynamic stability of B-DNA.

The cutting preference for AT-rich regions was compensated by a protein-blocked DNA end and the tested duplex DNAs were incised with similar efficiencies (Figure 18A lanes 8-10). The affinity to the tested oligos increased by 3-fold from a K_d of 132 ± 21 nM (GC-rich) to 45 ± 7 nM (AT-rich). Notably, the AT/GC content did not affect the ATPase activation under the nuclease assay conditions (Figure 18C). Therefore, destabilizing the secondary structure of DNA correlates with an increase of endonuclease activity and higher affinity. Stabilization of the dsDNA helix by GC base pairing leads to a high reduction of endonuclease activity. These data suggest that SbcCD alters the B-DNA secondary structure during the internal incision of dsDNA.

Encouraged by these findings, DNAs with mismatched stretches were designed. This interrupts the B-DNA helix structure and would mimic melted DNA, an intermediate substrate that could be generated in the course of endonucleolytic incision. The unpaired stretches (referred as bubbles) had a length of five nucleotides and were introduced 5’ and 3’ to region of the endonucleolytic cuts. The labelled DNA end was blocked with the FAM-sc to prevent exonucleolytic degradation.

The 60 bp duplex was digested in the previously characterized pattern and SbcCD cleaved the DNA substrate at 27 base pairs. Introduction of a bubble from position 27 to 31 led to incision events 3’ and 5’ to the bubble. Locating the bubble at position 19-23 leads to a major cleavage site at 25 nucleotides, position 21-25 guides the incision to 27 base-pairs (Figure 18C lanes 1-4). Therefore, SbcCD cleavage occurs at the 5’ side of unpaired DNA. Increasing the length of the bubble to 7 nucleotides reduced cutting efficiency. In the presence of non-hydrolysable ATPγS we could not detect degradation with any of the substrates (Figure 26B).

These experiments collectively showed that the endonucleolytic incision of duplex DNA by SbcCD is sensitive to the thermodynamic stability of B-DNA. Furthermore, dsDNA is incised according to the position of unpaired stretch of DNA. This highlights the importance of altering DNA structure during the endonucleolytic incision by SbcCD and its homologs.

4.4.3 Direct detection of DNA melting

Two assays were set up to monitor (i) DNA-distortion or -melting at internal sites and (ii) fraying at DNA ends.

To detect internal strand separation and structural distortions in DNA, potassium permanganate can serve as a potent probe. Potassium permanganate reacts strongly with thymine in unstacked regions and exhibits only weak reactivity towards guanine, cytosine, or adenine. It reacts with double bonds, oxidizing them to vicinal diols. Stereochemical hindrance from the base stacking prohibits reactivity of the double-stranded B-form DNA. Subsequent treatment of the oxidized product with piperidine as strong base leads to ring opening and cleavage of the phosphodiester backbone 3' to the base. The cleavage sites are then resolved by Urea-PAGE (Kahl and Paule, 2008).

This method allows detection of DNA distortions even within regions of protein-DNA complexes. The oxidation reaction is very robust, so that distorted regions can be detected even under conditions where the efficiency of DNA-protein interaction is not high (Grimes et al., 1991).

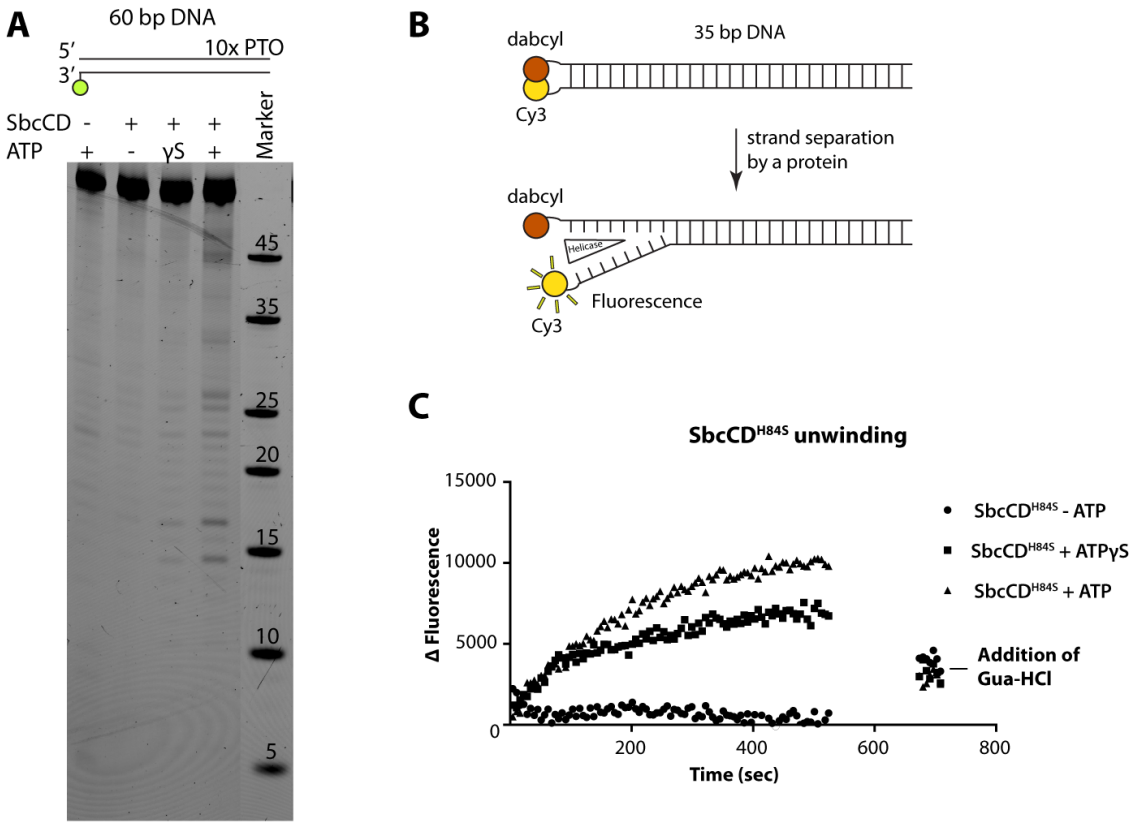

Figure 19 Direct detection of DNA melting activity of SbcCD (A) Nuclease deficient SbcCD^{H84Q} and 60 bp DNA was assayed under conditions used in nuclease assays and in the absence or presence of ATP(γS). Addition of $KMnO_4$ oxidized the nucleobases dependent on the solvent exposure. Subsequent piperidine treatment led to cleavage of the phosphate backbone adjacent to oxidized thymine nucleobases. These cleavage products were resolved on a 12% Urea Gel **(B)** DNA melting detected by fluorescence quenching. Cy3 and quencher were attached to one DNA end and the fluorescence of Cy3 was quenched by contact quenching. Cy3 and quencher form a complex in the ground state, before excitation occurs. Melting of the DNA ends releases the Cy3 fluorophore which can be detected by an increase in fluorescence. **(C)** Nuclease deficient SbcCD^{H84S} and 35 bp DNA was assayed under nuclease assay conditions in the absence or presence of ATP(γS). The change in fluorescence emission was monitored in a time-dependent manner.

60 base pair DNA and nuclease deficient SbcCD^{H84Q} were incubated at standard nuclease assay conditions and potassium permanganate was subsequently added to a final concentration of 5 mM. This concentration was not optimized and adapted from previous protocols. The treatment with piperidine and the performance of a Urea-PAGE visualized distorted regions of DNA. No DNA cleavages were observed in the absence of a protein. The presence of SbcCD^{H84Q} without ATP did not induce a structural distortion in DNA. In the presence of non-hydrolysable ATPγS, weak bands appeared around 15 nucleotides. When ATP was added, more intense bands appeared at 15, 25, 32 and 45 nucleotides (Figure 19A, lane 1-4). Since DNA affinity of SbcCD^{H84Q} was higher with ATPγS over ATP, the strand distortion did not occur passively upon DNA binding. DNA melting rather required DNA binding and a

subsequent conformational change induced by ATP hydrolysis. The band intensities did not become more intense in the presence of a block (data not shown). Therefore, a block did not stimulate DNA unwinding.

The second method to monitor DNA melting took advantage of contact fluorescence quenching. Fluorophore quenching generally occurs by one of two mechanisms: contact quenching and FRET quenching. In contact quenching, the fluorophore and quencher are in close proximity to allow direct interaction of the fluorophore with the quencher. Therefore, the absorbed light will be transferred as heat to the surrounding environment, with only a limited amount energy released as fluorescence. When the distance between the fluorophore and quencher is increased, generally to the range of 20-100 Å, FRET quenching is observed. In this mechanism, quenching efficiency is dependent upon (i) the orientation and distance between the fluorophore and quencher and (ii) the spectral overlap of the emission spectrum of the fluorophore and the absorption spectrum of the quencher (Crisalli and Kool, 2011).

A Cy3-Dabcyl fluorophore-quencher pair was applied to detect the separation of DNA strands. Dabcyl quenches the fluorescence of Cy3 by an efficiency of 95%, whereas FRET-quenching efficiency is below 70% (Marras et al., 2002). A 35 base pair 5’ Cy3 and 3’ Dabcyl labeled DNA was used as DNA substrate (Figure 19B).

This experiment was conducted with the nuclease deficient SbcCD^{H84S} mutant, which was used in the earlier stage of this PhD. SbcCD^{H84S} was pre-incubated in the presence or absence of ATP(γS) at 37 °C and the reaction was started by DNA addition. The fluorescence intensity of each sample was monitored in a time-dependent manner. A competitor DNA strand complementary to the quencher DNA strand was added in a 10-fold excess.

In the absence of ATP(γS), no increase in fluorescence, hence, no strand separation was observed. An increase in fluorescence was detected in the presence of ATP and ATPγS. The fluorescence increased to approximately 5% of the total fluorescence (Figure 19C). This could have different reasons: (i) only a small fraction of the DNA strands were separated, (ii) the emitted fluorescence was quenched by FRET quenching or (iii) the close proximity of SbcCD induces fluorescence quenching.

In order to test if the alteration of the DNA structure was permanent or dependent to binding of SbcCD, guanidinium-hydrochloride (Gua-HCl) was added to the reaction to disrupt protein-DNA interactions. Addition of Gua-HCl leveled the fluorescence of the three samples to one value. This was slightly higher

than the original value, which could be due to opening of the ends induced by high Gua-HCl concentration (Figure 19C).

These results illustrated that the melting of DNA ends required DNA binding by SbcCD^{H84S} and was not dependent on ATP hydrolysis. Since the increase of fluorescence was reversible, the competitor oligonucleotide did not anneal to the quencher strand. Consequently, DNA-end melting by SbcCD^{H84S} was not of a processive nature but is more a transient separation by SbcCD^{H84S} (Figure 19C). Interestingly, it was found that the increase in fluorescence was manganese-dependent (data not shown). Thus, the SbcD nuclease active site is either directly involved in DNA-end separation or it is due to allosteric control within the SbcCD complex.

These data correlate well to SbcCD's nuclease activities. Degradation from DNA ends requires ATP-binding as does fraying of DNA ends. However, internal distortion of DNA as well as internal incision of DNA requires ATP-hydrolysis. This indicates, that DNA processing and DNA melting are functionally coupled.

4.4.4 Chemical nature of SbcCD cleavage products

To further investigate and characterize the mode of cleavage catalysis, the cleavage products of the nuclease assays were treated with phosphatase and kinase enzymes. The addition or removal of the negatively charged phosphate changes the mobility of the oligonucleotides during electrophoresis. Therefore, the presence or absence of a phosphate group of the unlabeled 3' and 5' termini can be determined.

The endonuclease cleavage product of a 3' FAM-labeled DNA was shifted after kinase treatment and were not affected by phosphatase treatment. Thus, a free 5' OH was present and a phosphate could be transfered (Figure 20B lanes 3-5). The exonuclease products were not shifted by kinase treatment but phosphatase treatment had an effect on the electrophoretic mobility. This indicates the presence of a 5' phosphate moiety (Figure 20A lane 6-8).

Phosphatase treatment of the cleavage products of the 5' labeled 60 bp DNA induced a shift of the 5' clipping products. The internal cleavage products from 20 to 23 nucleotides were not shifted (Figure 20 A, lane 2 and 3). Therefore, the 5' clipping follows the same cleavage mechanism as endonuclease incision. The internal cleavage products have the exonuclease chemistry as observed for the 3' labeled oligo.

In Figure 20C are the FAM-labels positioned on the opposite side from the protein-blocked DNA end. Therefore, the DNA ends that were obtained after SbcCD cleavage could be visualized. The 3’ labeled as well as the 5’ labeled cleavage products were shifted by phosphatase treatment. This indicates a fully phosphorylated DNA end and is in line with the hydroxylated cleavage products that were obtained from the protein-blocked DNA end.

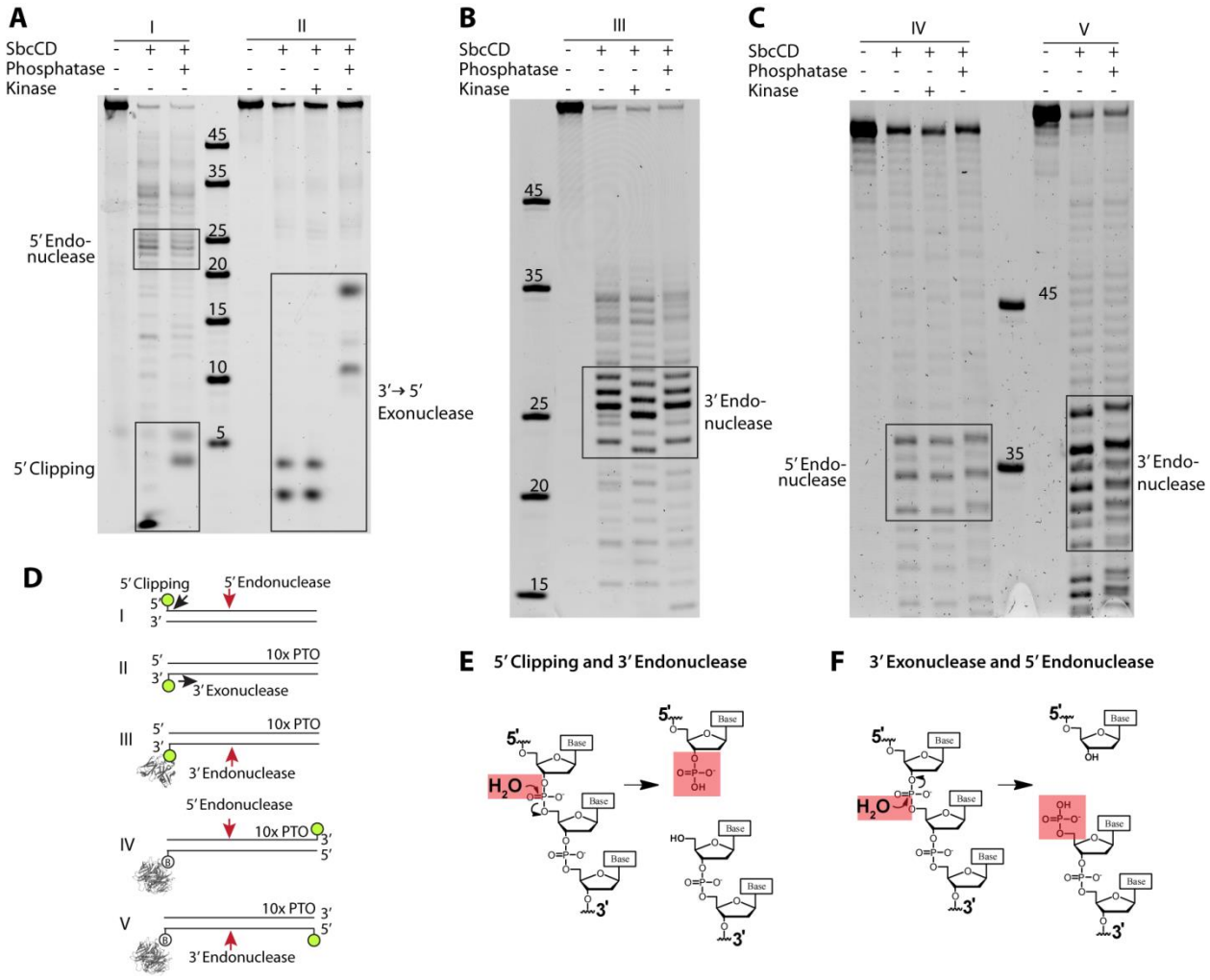

Figure 20 SbcCD performs endo- and exonuclease activity with a different cutting chemistry (A) SbcCD^{wt} was assayed in the presence of 1 mM ATP, 1 mM $MnCl_2$ and 5 mM $MgCl_2$ at 37 °C. The 60 bp DNA substrate was labeled on the 3’ end with 6-FAM. and treated with kinase and phosphatase after the nuclease reaction. Phosphate bound oligonucleotides have an increased electrophoretic mobility. **(B)** Nuclease assay as in (A) with a protein-blocked 3’ end to omit exonuclease and stimulate endonuclease activity. **(C)** Nuclease assay as in (A). Labels on the opposite side from the protein-block reveal a phosphorylated DNA end that is obtained after SbcCD cleavage. **(D)** 60 bp DNA substrates that were used in (A – C) and the cleavage position are schematized. **(E and F)** A different positioned water molecule leads to different cleavage outcomes. This is specific to determined by the nuclease activity and the strand polarity.

The data reveal two novel findings. It is the first time that the cleavage products of SbcCD or MR(N/X) are described on a chemical basis. The cleavage chemistry appears to be highly strand specific. This could be due to a symmetric coordination of the DNA and a concerted cleavage event of both protomers, each cleaving one DNA strand.

Strikingly, the cleavage of a protein-bound DNA end leaves phosphate moieties on the 3' and 5' end which is a rather unusual cleavage product and not compatible for downstream precessing enzymes, such as DNA polymerases or - ligases.

4.5 The SbcD dimer interface and its role in DNA processing

4.5.1 Analysis of the SbcD-dimer

Since the year 2000, over 20 X-ray crystallography structures of the Mre11 were published from all three domains of life (reviewed in (Schiller et al., 2014)).They all share a common fold comprising the N-terminal phosphodiesterase core and capping domain. The Helix-Loop-Helix (HLH) domain is C-terminally attached and interacts with the coiled-coil domain (Figure 21A) of Rad50. Mre11 forms a symmetric dimer. The dimer formation is mediated by conserved hydrophobic patches located in the α2 and α3 helices of each phosphodiesterase domain (Hopfner et al., 2001). This interaction motif is referred as a four-helix bundle. The Mre11-dimer of eukaryotes is further stabilized by a latching loop which is ordered upon Nbs-1 binding in *S.pombe* (Schiller et al., 2012). When superposing the crystal structures of Mre11 from different species, a dynamic dimer organization is observed including different angles between the interaction helices of each Mre11 dimer. Furthermore, DNA binding of Mre11 induces a widening of the four-helix bundle approximately 10° and rigid-body rotation of the dimer in *M.jannaschii* (Sung et al., 2014). These facts highlight the flexible nature of the Mre11 dimer.

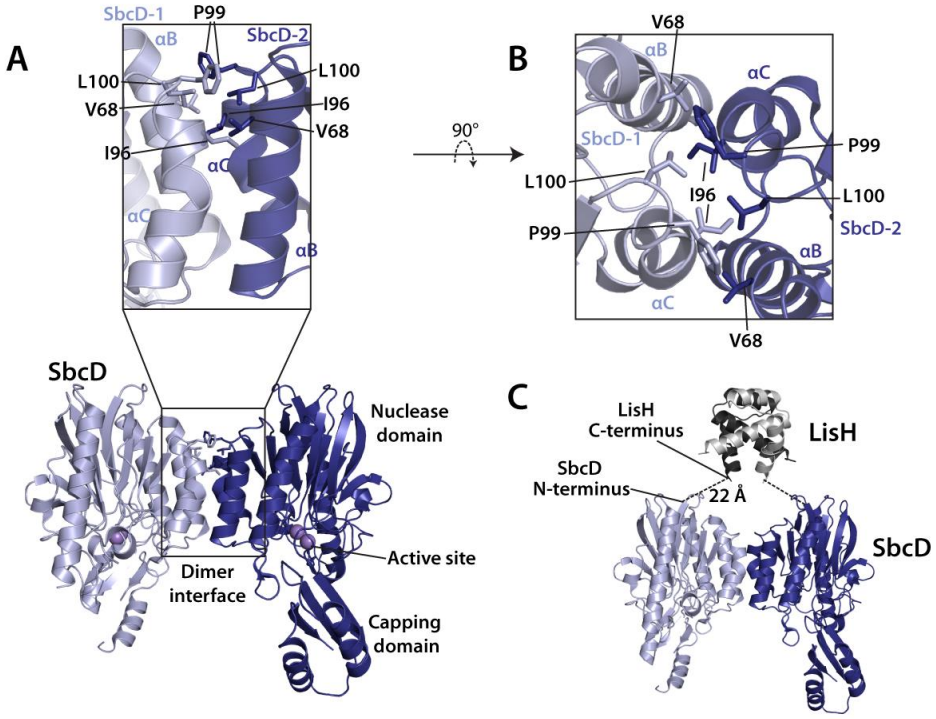

Figure 21 Crystal structure of the full-length SbcD dimer (PDB: 4M0V) (A) Ribbon representation of the overall organization of the SbcD dimer with a close-up of the 4-helix bundle motif. The main interacting residues are highlighted. **(B)** The close-up view of (A) rotated by 90°. The distance between the F99 α-carbons is 7.1 Å and therefore optimal for BMOE-crosslinking, as the crosslinker has a linker length of 8 Å. **(C)** Model of LisH dimerization domain (PDB: 1UUJ, grey) with SbcD crystal structure from (A). The LisH C-terminus was linked to the N-terminus of SbcD with a PAS-Linker (Schlapschy et al., 2013) with a length of 8 or 13 amino acids. The length between the modeled LisH C-terminus and SbcD N-terminus is 22 Å.

The dimerization of Mre11 is crucial for stable dsDNA binding (Williams et al., 2008) and different orientations of both dimers could control and regulate the nuclease activity. Moreover, Mre11-DNA complex structures served as a basis to hypothesize that dimer rotation could help DNA melting by twisting the duplex (Lafrance-Vanasse et al., 2015; Sung et al., 2014). Biochemical characterization of the T4 bacteriophage Mre11 with disrupted interface found that disruption of the Mre11 reduces the exonuclease by 10-fold and interrupts the allosteric communication between Mre11 and Rad50 during ATP hydrolysis. Therefore, the integrity of the Mre11 dimer has a functional significance within the Mre11-Rad50 complex.

The interaction between the two SbcD protomers is mainly mediated by a hydrophobic cluster consisting of Val68, Ile96, Phe99, and Leu100 (Figure 21A) on the top of the four-helix bundle. Arg60 from each SbcD forms weak Van-der-Waals interaction and is positioned by Glu92. The relatively small cluster allows a plasticity of the dimer. The Interface of its thermophilic orthologs have larger

hydrophobic clusters. For example, *Chaetomium thermophilum* dimer interaction spreads along the entire dimer interface; therefore, it has a higher stability and less plasticity (Seifert, 2015)

RALS analysis of the SbcD nuclease and capping domain showed that SbcD is mainly a monomer during size exclusion chromatography, a fraction of 4% dimeric. The introduction of the Val68Asp mutation ($SbcD^{V68D}$) induces monomerization of SbcD (Figure 22A). If SbcD is in complex with the NBD of SbcC, the main species is a heterodimer (96% dimer, 4% tetramer). Addition of ATP induces the formation of a heterotetramer (Figure 22C). Although SbcD itself appears to be a transient homodimer, the addition of a second interface by SbcC in the presence of ATP induces stable complex formation of the SbcCD – head domain.

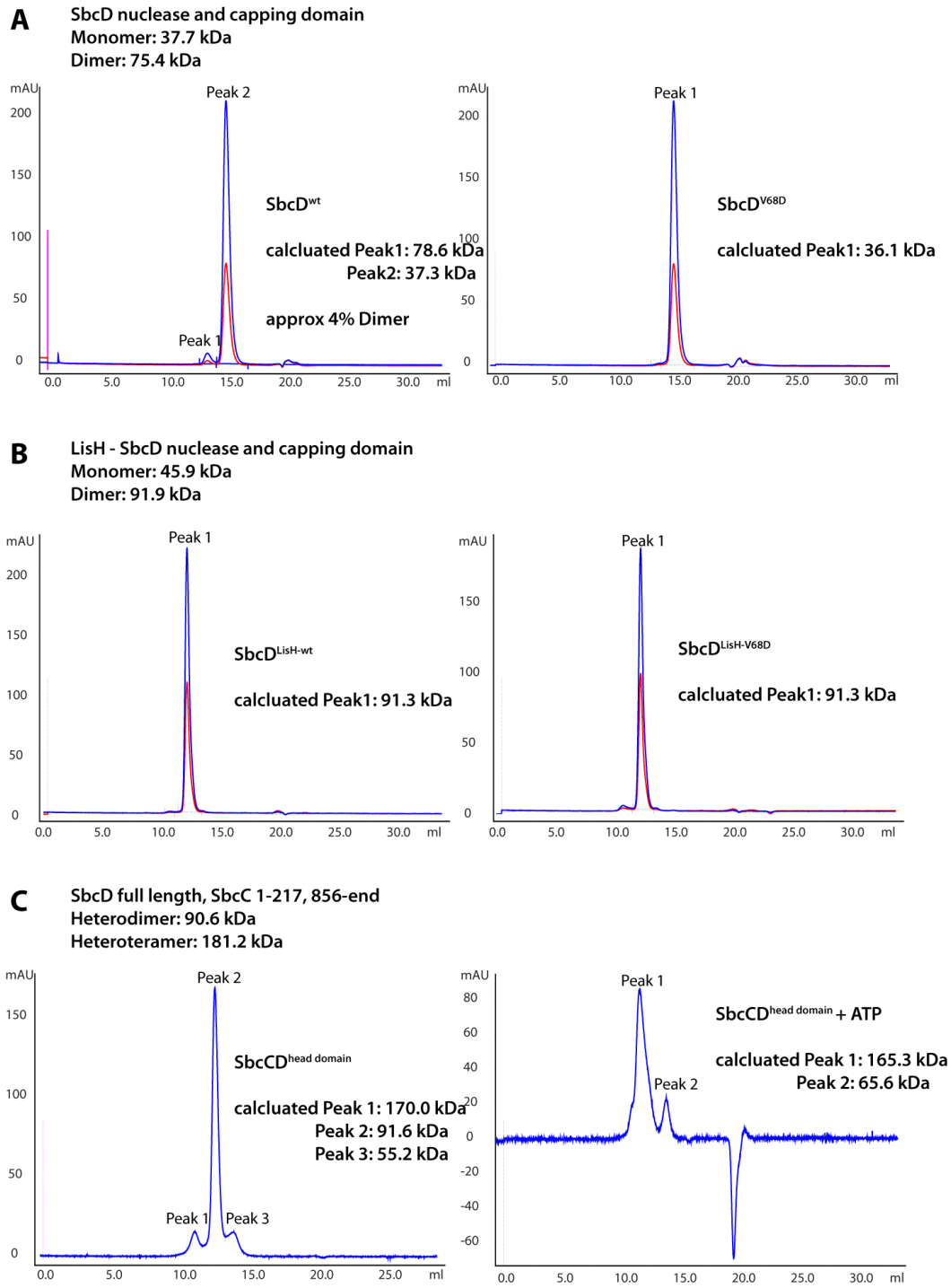

Figure 22 Right angle light scattering (RALS) analysis of SbcD nuclease and capping domain SbcCD head complex (A) SbcD nuclease and capping domain mainly forms a monomer, 4% of SbcD is a dimer. The SbcD^{V68D}-mutant induced a homogenous monomer of SbcD, therefore, a destabilization of the SbcD interface. **(B)** The N-terminal fusion of LisH induces the formation of a stable dimer of SbcD nuclease and capping domain (left), also in SbcD^{V68D} mutant (right). **(C)** Analysis of SbcD full length in complex with SbcC with shortened coiled-coils (SbcC^{scc}). SbcC^{scc}D mainly forms a heterodimer, 6% is forming a heterotetramer in the absence of ATP (left). The addition of 0.2 mM ATP in the running buffer induces the formation of a SbcC^{scc}D heterotetramer (right).

To investigate the plasticity of the SbcD dimer during nucleolytic processing, four SbcD interface versions in complex with SbcC were compared: SbcD (i) with the wild type dimer interface (ii) with a destabilized dimer interface (iii) with a covalently linked interface (iv) fused to the dimerization domain LisH.

The destabilized SbcD interface was obtained by mutating Val68 to Asp ($SbcD^{V68D}$). Val68 forms a hydrophobic interaction with Ile96. This interaction is predicted to have a large contribution to the stability of the interface. Removing the hydrophobicity and introducing charge in the interfaces leads to a reduced stability.

The stabilized SbcD interface was obtained by fusing a dimerization domain to the N-terminus of SbcD ($SbcD^{LisH}$). The dimerization domain was derived from the N-terminus of mouse Lis1 and the N-terminus comprises a LisH (Lis-homology) motif which is a globular and thermodynamically stable dimerization domain (Kim et al., 2004). Structural modulation of the LisH-SbcD fusion protein revealed the minimal linker distance of 22 Å (Figure 21C), to allow stable dimerization of LisH and not introducing conformational changes within the SbcD dimer. This distance corresponds to eight amino acids. It was shown by static light scattering, that the fusion of the LisH motif to the N-terminus of SbcD induced stable, homogenous dimerization of SbcD (Figure 22 B). The linker length could be modified to allow certain grades of flexibility within the SbcD dimer interface.

The covalent linkage of SbcD was obtained by engineering a cysteine-free version of SbcD and subsequent introduction of a cysteine into the interface (Phe99Cys). Crosslinking with bis-maleimidoethane (BMOE) and subsequent purification by size-exclusion chromatography yields a covalently linked dimer of SbcD. This was reconstituted with full-length SbcC and the complex purified by size exclusion chromatography.

The comparison of these four versions of SbcCD allows conclusions of the role of the SbcD dimer during nucleolytic cleavage of DNA.

4.5.2 Activities of SbcD with a destabilized interface

Dimerization variant $SbcCD^{V68D}$ was compared to $SbcCD^{wt}$ with regards to nuclease and ATPase activity. $SbcCD^{V68D}$ had a 3-fold reduced k_{cat} and the K_M was 6 times higher compared to $SbcCD^{wt}$. Interestingly, $SbcCD^{V68D}$ had similar ATPase rates to SbcC alone. Combining $SbcCD^{V68D}$ with an N-terminal fusion of the dimerization domain LisH restores the proximity of the two NBDs of SbcC. This restored the K_M, k_{cat} was still 3-fold reduced (Figure 25). Therefore, an intact SbcD dimer brings the NBDs of SbcC into close

proximity and facilitates ATP binding. Furthermore, it appears to allosterically regulate the ATP hydrolysis cycle of SbcC.

Next, the endonuclease activity towards a covalently closed single-stranded plasmid DNA was examined. The nuclease and capping domain of SbcD^{V68D} cleaves ssDNA with a similar efficiency to SbcD^{wt}. The assays were performed at a protein concentration, where the SbcD nuclease and capping domain is a monomer in solution. N-terminal LisH fusion to SbcD ensured stable dimerization of SbcD. LisH fusion increased ssDNA endonuclease activity for both proteins by a similar level. Full-length SbcCD^{wt} and SbcCD^{V68D} required ATP for ssDNA cleavage. In the presence of ATP both protein cleaved ssDNA with a similar efficiency. Interestingly, ATPγS slightly diminished endonuclease activity of SbcCD^{wt}, whereas the endonuclease of SbcCD^{V68D} was ablated (Figure 23A).

The nuclease activity of SbcCD^{V68D} towards dsDNA was tested. SbcCD^{wt} cleaved 60 bp DNA in the previously characterized pattern (Figure 23C lane 2). SbcCD^{V68D} retained full exonuclease activity (Figure 23C lane 3). Therefore, the association between DNA and SbcCD^{V68D} and the 3-dimensional fold of SbcD appears to be intact. However, the SbcD dimerization variant was deficient in endonuclease activity, also in the presence of a protein block. The exonuclease activity was ablated in the presence of ATPγS (Figure 26).

Introduction of a bubble re-established the endonuclease activity. The positions of the incision were identical to SbcCD^{wt}, however, the cutting efficiency was lower (Figure 23C lane 6 and Figure 26). In the absence of a block, the cutting efficiency was enhanced 3-fold compared to SbcCD^{wt}. Therefore, destabilizing the dimerization interface of SbcD correlated with the loss of endonuclease activity of SbcCD. The presence of unpaired DNA re-established the endo-activity.

The ATPase data illustrate that the dimerization variant SbcCD^{V68D} introduced a defect in the ATP hydrolysis cycle and the k_{cat} was reduced to the level of SbcC alone. This suggests that there is an allosteric cascade within SbcCD between DNA binding and endonucleolytical cleavage. The destabilized SbcD-dimer could interrupt this cascade. This defect could lead to a dysfunction of SbcCD to generate a DNA substrate which is competent for endonucleolytic cleavage. Introduction of a pre-melted stretch compensates this defect and SbcCD^{V68D} regains endonuclease activity.

Therefore, (i) the reduced ATP hydrolysis could induce a defect that SbcCD is not able to modify the DNA structure. (ii) The destabilized SbcD could induce a mis-coordination of dsDNA towards the SbcD active site. (iii) An intact SbcD interface induces dsDNA binding by SbcD and plasticity in the dimer interface translates into structural distortions of B-DNA.

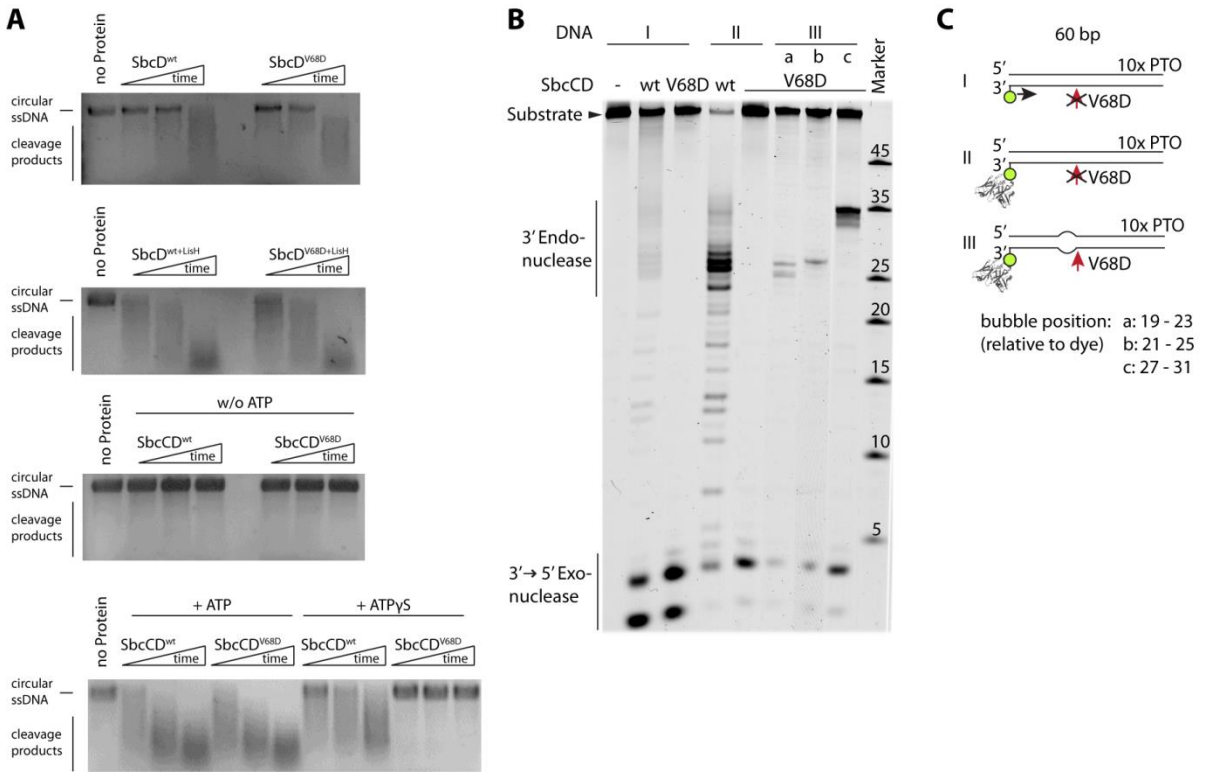

Figure 23 Nuclease activity of the SbcD dimer interface variant SbcCD^{V68D} (A) Nuclease activity of SbcD and SbcCD variants towards circular, single stranded plasmid DNA was tested. Protein (250 nM) and Phi174 virion DNA (100 ng) were mixed and reaction stopped as described in materials and methods. Cleavage products were separated on a 0.8% agarose gel. **(B)** The nuclease activity of SbcCD^{wt} and SbcCD^{V68D} was assayed towards a 3' labeled 60 bp DNA. Destabilization of the SbcD interface leads to a deficiency of endonuclease activity, but not 3'-> 5'exonuclease (Lane 6 and 7) and pseudo 5' -> 3' exonuclease activity (Lane 2 and 3). **(C)** DNA substrates used in (B)

4.5.3 Activities of SbcD with a stabilized interface

The stabilization of the SbcD interface was obtained by fusing a dimerization domain to the N-terminus of SbcD. The dimerization domain was obtained from the N-terminus of mouse Lis1. The N-terminus comprises a LisH (Lis-homology) motif which is a globular and thermodynamically very stable dimerization domain (Kim et al., 2004). The N-terminal fusion of LisH to SbcD allows plasticity within the SbcD dimer, however, macromolecular conformational changes are omitted. As linker, an 8 (SbcCD$^{LisH-8aa}$) and 13 (SbcCD$^{LisH-13aa}$) amino-acid long Pro-Ala-Ser linker was applied which is resistant to degradtation and not forming secondary structures (Schlapschy et al., 2013).

The exonuclease products of SbcCD$^{LisH-8aa}$ appeared 3-fold less intense, the endonuclease products of a protein blocked duplex DNA are 5-fold less intense compared to SbcCD^{wt}. SbcCD$^{LisH-13aa}$ exonuclease is 1.3-fold reduced, the endonuclease is 1.7-fold reduced compared to SbcCD^{wt} (Figure 24A lanes 1-8). The presence of a bubble rescues the endonuclease activity of both SbcCD^{LisH} constructs.

These data suggest that plasticity of the SbcD dimer is crucial for exo- and for endonuclease activity. These data contradict an opening of the SbcD dimer during endonuclease incision, as the LisH domain would block this conformational change.

To get a deeper knowledge of the SbcD dimer dynamics it was covalently crosslinked. The covalent linkage of SbcD was obtained by engineering a cysteine-free version of SbcD and introducing a cysteine at the edge of the interface (SbcD^{F99C}). Cross linking with bis-maleimidoethane (BMOE) and subsequent reconstitution with full length SbcC yielded in a high-purity SbcCD$^{x\text{-}linked}$ complex.

The crosslink was located at the edge of the hydrophobic patch which traps the SbcD dimer in the conformation observed in the crystal structure (PDB: 4M0V). The rotational plasticity is limited and an opening of the Mre11 dimer is fully omitted due to the covalent linkage.

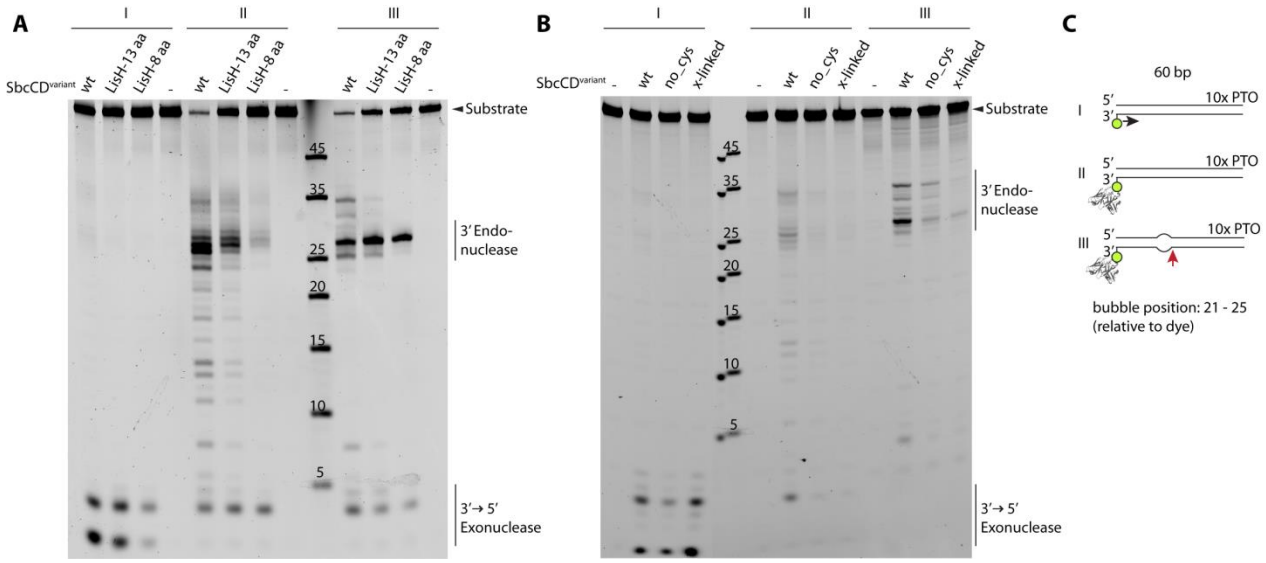

Figure 24 Nuclease activities of SbcCD complexes with SbcD having stabilized dimer interfaces: (A) Nuclease assay of SbcCD^{wt} and SbcCD with a linked SbcD interface. The dimerization domain LisH was N-terminally fused to SbcD with an 8 and 13 amino acid linker (SbcCD$^{LisH\text{-}8aa}$ and SbcCD$^{LisH\text{-}13aa}$). The linker lengths allow different flexibility grades of the SbcD dimer. **(B)** Nuclease assay of reconstituted SbcCD^{wt} and SbcCD with a crosslinked SbcD dimer interface. The cysteins from SbcD were removed (SbcD^{no_cys}) and a cysteine introduced in the SbcD dimer (SbcD^{F99C}). This version was crosslinked with BMOE (SbcD$^{x\text{-}linked}$) and reconstituted with SbcC. **(C)** DNA substrates that were used in (A and B) with indicated cleavage sites.

The nuclease activity was mildly affected by the removal of the cysteins in SbcD (SbcCD^{no_cys}). The band pattern is identical, the corresponding intensities are slightly reduced (Figure **24** B lanes 2 and 3). A crosslinked SbcD dimer (SbcCD$^{x\text{-}linked}$) increases the exonuclease of SbcCD by 2-fold. The endonuclease is reduced by 5-fold (3' labeled DNA) or 3-fold (3' label + bubble). Thus, the presence of pre-melted DNA could partially re-establish the endonuclease of SbcCD$^{x\text{-}linked}$ (Figure 24B lanes 10 – 13).

These biochemical data provide the first evidence that a dynamic SbcD dimer conformation is important for the endonucleolytic cleavage. The exonuclease activity was robust in all nuclease experiments and therefore never affected by a mutation in the SbcD interface. Crosslinking of the SbcD interface increased exonuclease activity. In contrast, the endonuclease activity was affected by all mutations affecting the SbcD dimer interface. The presence of a pre-melted stretch positively affected the endonuclease activity of all SbcD dimer versions.

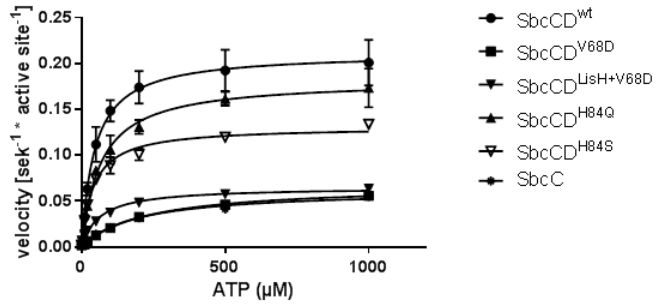

	k_{cat} (s^{-1})	K_m (µM)
SbcCD^{wt}	0.212 ± 0.006	46 ± 6
SbcCD^{H84Q}	0.182 ± 0.006	66 ± 8
SbcCD^{H84S}	0.131 ± 0.003	41 ± 4
SbcCD^{V68D}	0.068 ± 0.003	222 ± 25
SbcCD$^{LisH+V68D}$	0.065 ± 0.003	63 ± 12
SbcC	0.062 ± 0.004	190 ± 35

Figure 25 Michaelis Menten Kinetics with different SbcCD variants: ATP hydrolysis of SbcCD variants were tested at 37 °C in the presence of 1 mM $MnCl_2$, 5 mM $MgCl_2$ and 1000 nM 60 bp DNA as activator. The data were fit to a Michaelis Menten equation.

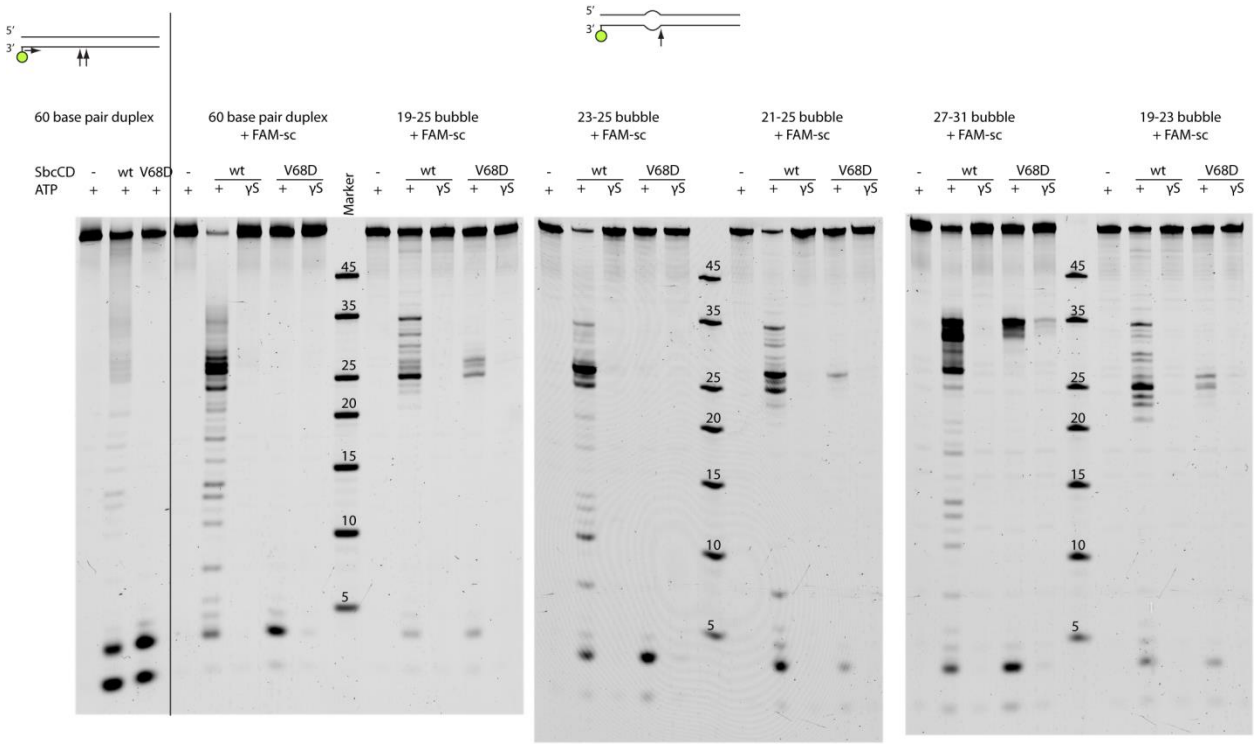

Figure 26 Nuclease assay with SbcCD^{wt}, SbcCD^{V68D} and DNA containing a bubble at different positions from the label. SbcCD was assayed under standard nuclease assays conditions. The presence of a bubble re-establishes endonuclease. The endonuclease cuts of SbcCD^{wt} appear more intense as of SbcCD^{V68D}.

5. Discussion

5.1 SbcCD as a model protein to study molecular mechanisms of the MR(N/X) complex

The mechanism of ATP-dependent dsDNA processing by MRN has been elusive for many years. The contradiction that ATP-binding triggers DNA binding but blocks the Mre11 nuclease site is a not resolved riddle. The aim of this thesis was to gain mechanistic insights how the MR(N/X) complex processes DNA.

Up to now, deciphering the molecular mechanism of MRN was mostly focused on structural studies. Over 40 structures of single subunits or truncated versions of MR(N/X) have been solved by X-ray crystallography until now. The proteins mostly originated from thermophilic organisms and that's why structural findings were often not complemented with a biochemical characterization.

MR(N/X) appears to adopt transient functional conformations during DNA processing which are dependent on the integrity of the full-length complex. Particularly the Rad50 coiled-coil and zinc-hook domains are indispensable for the proper function of MR(N/X) (Hohl et al., 2015; Hohl et al., 2011; Wiltzius et al., 2005). The MR(N/X) complexes are structurally and biochemically highly conserved and one can assume that the mechanisms of DNA-binding and DNA-incision are similar between species

To obtain a comprehensive picture of DNA processing, it is essential to work with full-length MR(N/X). At the beginning of this thesis, the MRN complex from *Chaetomium thermophilum* was expressed in *S. cerevisiae* and isolated by a three-step purification. Initial biochemical investigations showed that it had nuclease, ATP-hydrolysis, and DNA binding activity. However, the isolated amount was small and not sufficient to conduct a thorough biochemical characterization. Furthermore, most of the assays required elevated temperatures of 45 – 50 °C to obtain enzymatic activity. It is also known that the activities of eukaryotic MR(N/X) are highly regulated by post-translational modifications (PTMs), other interacting proteins and the chromatin structure. Therefore, this was not an ideal system to conduct biochemical studies.

The SbcCD complex from *E. coli* could be obtained in large amounts with a high purity. Since it is a mesophilic organism, the protein has full activity at 37 °C. SbcCD is not regulated by PTMs and its activity does not dependent on other interacting proteins or the state of chromatin. Therefore, it is an ideal system to conduct biochemical studies to obtain precise data about MR's or SbcCD's molecular mechanisms.

The biochemical studies in this thesis illustrated that SbcCD has very defined biochemical activities, which are equal to its eukaryotic homologs. In the absence of dsDNA, SbcCD has low basal ATPase rates and is activated 25 fold in the presence of dsDNA. The ATPase activity is further stimulated by DNA ends, as it has been reported for the human MRN complex (Deshpande et al., 2017). In contrast to the T4 MR complex (Hill coefficient of 2.4), the ATP hydrolysis by SbcCD is not cooperative (Herdendorf et al., 2011).

SbcCD incises both DNA strands approximately 25 base pairs from a DNA end. This activity requires ATP hydrolysis and is highly stimulated by a protein block on a DNA end. Similar activities were observed for the human and yeast MR(N/X) complex and the distances were in the same range for human (18 bp) and yeast (20-25 bp) (Anand et al., 2016; Cannavo and Cejka, 2014).

SbcCD binds to double-stranded DNA in the presence of ATP (or ATPγS) with a dissociation constant of K_d = 50 nM. In the absence of ATP, SbcCD does not bind to dsDNA. It does not bind to single-stranded DNA in the presence or absence of ATP. Therefore, SbcCD strictly requires ATP-binding and the helical structure of dsDNA to associate with nucleic acids. Therefore, the dimerized NBDs of SbcC can be considered as the major dsDNA binding platform in SbcCD.

The DNA binding groove of eukaryotic Rad50 is considered as the main DNA binding site. Depending on the study, Mre11 binds double-stranded with a K_d of 5 µM, whereas full length MR(N/X) binds dsDNA in an ATP dependent manner with a K_d in the low nM range (Liu et al., 2016; Paull and Gellert, 1999; Rojowska et al., 2014; Seifert et al., 2016; Sung et al., 2014; Williams et al., 2008). The MR complex from the T4 phage has a K_d s of 0.15 µM in the presence of ATP, 0.69 µM in the absence of ATP, and also binds ssDNA with 0.5 µM affinity (Albrecht et al., 2012).

SbcCD's core functions and activities were characterized and they match with the enzymatic activities of MR(N/X) from other species. Therefore, the obtained data have implications in the general working mechanism of the MR(N/X) and SMC-like proteins from other organisms.

5.2 ATP hydrolysis by SbcCD and ATPase stimulation by dsDNA

The SbcC/Rad50 ATPase domain belongs to the ATP-binding cassette (ABC)-type ATPase family. ABC-proteins are chemomechanical engines for diverse biological pathways. A common feature is that the two nucleotide binding domains (NBDs) cooperate to form two composite active sites. NTPs are then sandwiched in the NBD dimer interfaces and NTP-binding and -hydrolysis lead to conformational

changes between the two NBDs, which is referred to as the “powerstroke” of ABC proteins. The hydrolysis of NTPs to NDPs and Pi and the conformational changes of the NBDs are translated to conformational changes in associated domains.

ABC transporters use the process of ATP-binding and -hydrolysis to transport molecules across membranes. The energy conversion of ABC proteins involved in the repair of DNA damage and mismatch recognition, DNA cleavage, sister-chromatid cohesion is less clear. In general, ABC proteins can be considered as NTP-controlled “molecular machines” or “molecular switches” (Hopfner, 2016).

Several ABC-proteins are involved in the segregation and recombination of the genetic material. These proteins are referred as the SMC/Rad50/RecN/RecF family. A common feature of these proteins is that the NBDs can directly bind to DNA, but also interact with other subunits and domains, including a long coiled-coil domain that is characteristic of most members of this family. Most proteins of this family have low basal ATPase rates which are stimulated by double-stranded DNA (Cobbe and Heck, 2006).

DNA-stimulated ATPase activity was observed with SMC proteins of cohesins and condensins. The *Pyrococcus furiosus* SMC catalytic domains exhibited a 14-fold stimulated ATPase in the presence dsDNA oligonucleotides (Lammens et al., 2004). The *Deinococcus radiodurans* (*Dr*) recombination protein RecN, which is similar to SMC proteins except for a shorter coiled coil, exhibits a 3–4-fold increase in ATPase upon addition of linear plasmid DNA (Pellegrino et al., 2012; Reyes et al., 2010) similar for *Dr*RecF, which possesses the conserved ABC ATPase domains but lacks the coiled-coil of Rad50 or SMC proteins (Koroleva et al., 2007). The ATPase of the postreplicative mismatch proteins from human (hMutSα) and *E.coli* (MutS) were stimulated by 6-fold by dsDNA (Dufner et al., 2000; Lamers et al., 2004) and the recognition of a mismatch of the human hMutSα generated a further 3.5-fold stimulation (Gradia et al., 1997).

A dsDNA dependent ATPase stimulation was also observed for the MR(N/X) from all domains of life. Linear DNA stimulated ATP hydrolysis from archaea (20 fold), yeast (10 fold), human (40 fold) and T4 phage (22-fold) (Deshpande et al., 2017; Herdendorf et al., 2011; Trujillo et al., 2003). The human protein requires the presence of long DNA duplexes (>1 kb) to efficiently induce the ATP hydrolysis than short oligonucleotide substrates (Deshpande et al., 2017).

Although the DNA induced stimulation is a common feature in SMC proteins and ABC-type ATPases, a precise molecular activation mechanism has not been resolved for any of these proteins. It is likely that a minimal conformational change or a differently positioned water molecule convert the protein into an

activated state. Biophysical investigation of the T4 MR and MR-DNA complex identified either chemistry or a conformational change prior to catalysis as a rate-limiting step (Herdendorf and Nelson, 2014).

The characterization of SbcCD's ATPase stimulation revealed that SbcCD requires 30 consecutive base pairs for efficient ATP-hydrolysis activation. The activation is increased stepwise with longer DNA and reaches a maximum at 50 and 60 base pairs. These results were rather unexpected, since structural analysis of Rad50 would predict a DNA binding footprint of about 20 base pairs (Liu et al., 2016; Rojowska et al., 2014; Seifert et al., 2016). Consistent with the ATPase data, efficient DNA binding is obtained with 30 bp and longer and does not increase with longer DNA. It remains speculative what kind of features are provided by 30 bp DNA. Structural modeling with the closed heterotetrameric MR complex of *Thermotoga maritima* (PDB: 3THO) and 30 bp DNA showed that two SbcCD complexes could bind in a staggered arrangement. Preliminary DNA binding experiments with SbcCD at stoichiometric titration conditions indicated that two protein complexes assemble on one DNA molecule (data not shown). An array formation of SbcCD on DNA could be visualized by rotary shadowing electron microscopy or cryo-EM.

Despite its dependence on DNA length, the SbcCD ATPase stimulation is also sensitive to DNA ends. The ATPase activity was increased 25 fold by relaxed, circular plasmid DNA. Linearization of the plasmid DNA did not yield in a higher maximum ATPase rate, but the k_{act} was significantly lower (2.6 nM for linear DNA, 10.8 for circular DNA). This could either be due to a higher affinity to DNA ends or have structural reasons. Negative supercoiling of the circular plasmid DNA negatively affected the ATPase stimulation and the ATP hydrolysis was only activated 9 fold. This is likely due to an altered secondary structure in the underwound state of DNA. This conformation would then not fit in the SbcC DNA binding groove. The remaining 9 fold activation could be due to transient formation of B-DNA due to internal structural dynamics of the supercoiled DNA molecules.

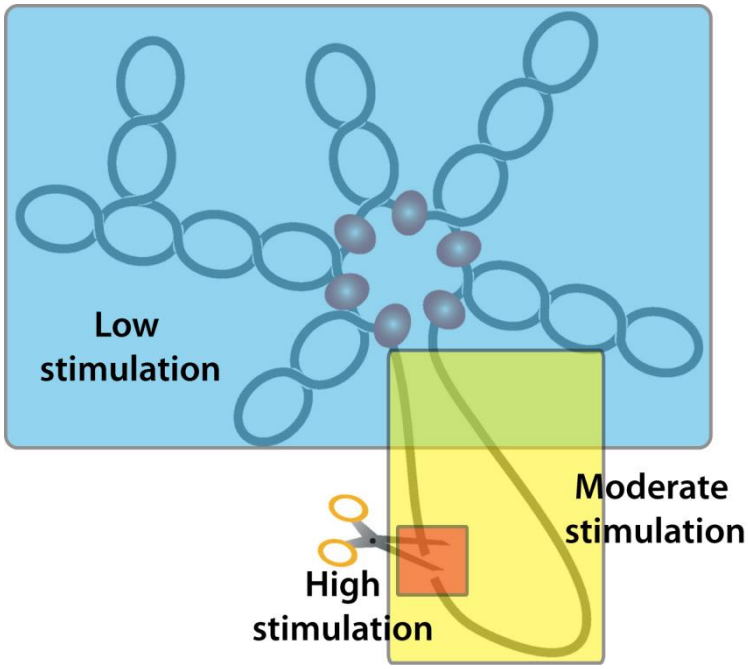

Figure 27 Model of SbcCD's ATPase stimulation upon DNA strand breaks in a bacterial chromosome. DNA is compacted into individual supercoiled domains that are topologically unlinked from each other because of supercoil diffusion barriers (red circles). Introduction of DNA strand breaks as a result of cellular processes or DNA damage (indicated by scissors) relaxes a single domain without affecting the topological state of the remaining chromosome. SbcCD is stimulated step by step by relaxed DNA and DNA ends. Adapted and modified from (Thanbichler et al., 2005).

In the context of a DNA break in an *E. coli* cell, these data would make sense. The *E. coli* genome is a single, circular chromosome with a size of 4.6 Mb, which is embedded in the cytoplasm. An important contribution to chromosome compaction in prokaryotes is made by negative DNA supercoiling which is maintained by topoisomerases. Negative supercoiling is essential for proper functioning of cellular processes that require DNA strand separation, such as transcription, recombination and DNA repair.

The supercoiled state induces the formation of plectonemes that coil up around themselves. At the base of the plectonemes, specific proteins attach to form supercoil diffusion barriers. These unlink the looped DNA topologically from the rest of the genome (Rybenkov et al., 2014; Thanbichler et al., 2005). The number of the isolated supercoiled domains is dependent on the growth phase of *E.coli* and estimated to be in the range of 400 having roughly a size of 10 kb each.

The Michaelis-Menten kinetics with SbcCD showed that SbcCD complexes well with ATP and has a K_M of 50 µM to ATP. The physiological *E. coli* ATP concentration is ~ 1.5 mM (Yaginuma et al., 2014) and SbcCD would preferentially be in an ATP-bound closed conformation in the presence of intact, supercoiled DNA. Normal supercoiled nucleoid DNA activates SbcCD only at a low rate.

The presence of a single-strand or double-strand break would locally relax DNA, without affecting the topological state of the remaining chromosome. The persistent relaxed state of DNA can be considered as a hallmark for broken chromatin and serve as long-range signaling of a DNA strand break. The higher affinity to relaxed DNA could then facilitate the recruitment of SbcCD to DNA damage sites.

Nuclease experiments showed that SbcCD does not cleave or degrade relaxed circular DNA. The *E. coli* genome is organized by small proteins, which bind approximately 10% of the genomic DNA and serve as internal protein block. The presence of an internally-bound protein did not stimulate incision of circular DNA, also when the dsDNA was nicked next to the block, what would provide the ability for SbcCD to structurally distort DNA. The experiments suggest that SbcCD strictly requires DNA ends to process dsDNA. How SbcCD distinguishes between internal and terminal protein blocks remains a matter of future studies.

It is not known if SbcCD requires the DNA ends to load onto DNA. Studies with single molecule DNA curtains proposed that human MRN can load internally onto DNA and diffuse along the DNA in an ATP-bound manner (Myler et al., 2017). Similar experiments with the SMC proteins cohesion (*S. cerevisiae*) and condensing (*S. pombe*) showed internal loading onto dsDNA (Stigler et al., 2016; Terakawa et al., 2017).

If SbcCD would have an ATP-dependent motor protein activity, it could specifically locate to the DNA break through stimulation of its ATPase until DNA terminal structures are encountered to which SbcCD can bind with a higher affinity. The ATPase activity is further stimulated and depending on the structure of the terminal DNA, SbcCD would then perform end resection accordingly.

5.3 SbcCD's nuclease activities, the role of DNA-duplex melting

MR(N/X) and SbcCD have nuclease functions that are conserved amongst bacteria, yeast and human. Conserved activities are (i) 3'->5' exonuclease (ii) cleavage of dsDNA adjacent to a protein blocked DNA end (iii) cleavage of hairpin structures on the 5' side of a hairpin and (iv) cleavage of 3' overhangs (Connelly et al., 1999, 2003; Paull and Gellert, 1999; Trujillo and Sung, 2001).

Leach and Co-workers have extensively investigated SbcCD's nuclease activities (Connelly et al., 2003; Connelly et al., 1997; Connelly et al., 1998). Most data in my study matched with their observations, although I worked with an approximately 100 fold higher DNA and protein concentration and the DNA end was labeled with a fluorophore instead of a radioactive label. In addition to their results, I observed that SbcCD clips approximately six nucleotides from the 5' DNA end on a 60 bp DNA and SbcCD strictly requires ATP hydrolysis to cleave DNA internally.

The ATP-dependent endonuclease activity is a highly conserved function in the MR(N/X) complex. In eukaryotes, the endonuclease activity is required to remove proteins from DNA ends such as Spo11, poisoned and trapped Topo II – DNA adducts, or the high-affinity binding protein ring protein Ku70/Ku80 (Mimitou and Symington, 2010; Stingele et al., 2017). This activity is required to enable downstream DNA processing enzymes to act on the DSB. In bacteria, SbcCD is involved in the processing of quinolone-trapped gyrase-DNA complexes (Aedo and Tse-Dinh, 2013). Furthermore, SbcCD internally cleaves both DNA strands at palindromic sequences and stimulates recombination (Eykelenboom et al., 2008). These data emphasize the central role of the endonuclease activity of MR(N/X) and SbcCD.

My study revealed that SbcCD cleaves both DNA strands of a protein-bound DNA end 27 nucleotides from the 3' end and 23 nucleotides from the 5' end. Minor cleavage products appeared at 15 and 35 nucleotides relative to the 3' end. The distances matched with a recent study where SbcCD was assayed with a plasmid carrying a cruciform secondary structure. SbcCD cut from the top of a cruciform DNA by making initial incisions on both strands and continued cleaving the dsDNA stem at ~10-bp intervals. The initial, most prominent cut appeared at 25 bp from the top of the cruciform (Lim et al., 2015). These similar observations suggest that the cleavage mode on a protein bound DNA end and cruciform structures are identical. After the initial SbcCD cleavage, it is likely that other DNA processing enzymes, such as RecBCD, associate with the free DNA end to continue homologous recombination.

SbcCD's ATPase activity is stimulated by dsDNA and DNA ends. However, to degrade or internally cleave one molecule of DNA, SbcCD hydrolyses approximately 200 (with a protein blocked DNA end) to 1000

(with a free DNA end) ATP-molecules. This has several implications on the relationship between ATPase and nuclease activities: (i) SbcCD's DNA cleavage is an inefficient process, (ii) the ATPase rate and nuclease activity do not directly correlate with each other and (iii) a protein-bound DNA end increases the cleavage efficiency.

The function of ATP-hydrolysis by Rad50 or SbcC and how the released energy is converted into functional activities of the Mre11 protein remains obscure. ABC transporters use the process of ATP-binding and ATP-hydrolysis to transport molecules across membranes. *S. cerevisiae* condensin has ATP-hydrolysis-dependent translocation activity along double-stranded DNA (Terakawa et al., 2017).

SbcCD or MR(N/X) could convert the released energy from ATP hydrolysis into structural distortions in B-DNA. Previous studies proposed that human MRN unwinds dsDNA at the end of the duplex in an ATP-dependent manner (Cannon et al., 2013; Paull and Gellert, 1999).

The mechanism of the dsDNA cleavage by Mre11 has long been discussed since its active site is concealed in the enzyme. Structures of *P. furiosus* Mre11 with dsDNA revealed that B-DNA is 5 Å apart from a position which is productive for cleavage (Hopfner et al., 2001; Williams et al., 2008). Therefore, DNA cleavage requires either a conformational rearrangement of the Mre11 active site or melting of the dsDNA. The advantage of single-stranded DNA in the process of the phosphate backbone cleavage is that the DNA strand can flexibly enter the active site and the approach of the nucleophile (in the case of Mre11 the nucleophile is a water molecule) is sterically not restricted.

MR(N/X) from all domains of life cleaves at the 5' side of a hairpin structure and 3' overhangs (Connelly et al., 1998; Paull and Gellert, 1999; Trujillo and Sung, 2001). These secondary structures have the common feature to contain transitions from dsDNA to ssDNA in 5' -> 3' direction. If one considers spontaneous conformational fluctuations at DNA ends ("fraying"), a blunt-ended DNA would also provide a short 3' overhang for ATP-independent exonucleolytic degradation by Mre11.

In this work, it was tested if dsDNA unwinding and nuclease activities could be functionally connected with each other.

FRET-quenching experiments showed that SbcCD separates DNA at the end of a duplex in the presence of ATPγS and therefore requires ATP-binding. Internal DNA melting was monitored by the addition of potassium permanganate which oxidizes cytosine in structurally distorted regions. These experiments showed that internal DNA melting by SbcCD requires ATP-hydrolysis. A protein-blocked DNA end did not further stimulate unwinding of dsDNA. Since the endonuclease is highly stimulated by a protein-blocked

DNA end, the number of endonucleolytic incisions does not directly correlate with the level of structural distortions in dsDNA.

To correlate DNA melting and endonuclease activity, the local thermodynamic stability of the 60 bp cleavage substrate was tuned by introducing stretches with different A/T- and G/C-contents. Subsequently, the internal SbcCD cleavage products were analyzed. SbcCD cleaves the A/T-rich DNA with higher efficiency than G/C-rich DNA. Therefore, the internal cleavage efficiency correlates with the thermodynamic stability of the DNA duplex. This correlation is overcome when the DNA ends are blocked. Additionally, SbcCD has an increased binding affinity to A/T-rich DNA over G/C-rich DNA whereas the ATPase stimulation was not affected. This implies that the SbcCD endonuclease could either be stimulated by a higher ability to structurally distort DNA or that prolonged location of SbcCD leads to more internal cleavage events.

A binding preference for A/T-rich regions was also shown for *S. pombe* cohesin and *S. cerevisiae* condensin by single-tethered DNA curtain assays (Stigler et al., 2016; Terakawa et al., 2017). This could imply a conserved DNA binding mode of SMC-like proteins.

E. coli has two structurally conserved arginines (R102 and R113) which are located on the top of the Rad50 beta-sheet I. They are in close proximity to the position, where SbcC/Rad50 would potentially bind dsDNA. Arginines are known to insert into the minor groove of dsDNA and stabilize deformation and distortion of DNA (Wang et al., 2010). Therefore, these residues could stabilize structural distortions in the position of around 25 base pairs.

As a follow-up experiment, 60 bp DNA substrates with pre-melted stretches were designed. Three unpaired nucleotides did not have an effect on the cleavage pattern and seven unpaired nucleotides drastically decreased SbcCD's cutting efficiency. The length of five unpaired nucleotides DNA affected SbcCD's cutting pattern by not decreasing the cutting efficiency.

The internal cleavage position of SbcCD directly correlated with the position of the pre-melted DNA stretch and was located at the 5' side of the melted DNA stretch. This is in accordance with the hairpin-opening and the 3'-overhang-cleaving activity of MR(N/X)/SbcCD and suggests that the cleavage mechanisms are conserved to the dsDNA internal cleavage and generally requires a dsDNA – ssDNA transition state. SbcCD generates this substrate by internally melting the DNA in an ATP-dependent manner. If only one complex is involved in internal DNA cleavage or two or more complexes work in concert remains a matter of future experiments.

5.4 Distinct cleavage chemistries and its implications for dsDNA processing

The MR(N/X)/SbcCD complex has a shared endo- and exonuclease activity. When processing dsDNA, SbcCD cleaves the scissile phosphate from either the 3' or 5' side to leave a free 5'-PO_4^{2-} or 5'-OH as cleavage product. These different cleavage chemistries are specific for the different nuclease activity and distinct for each strand. If SbcCD degrades dsDNA with its exonuclease activity, it cleaves the P-O_3'-bond on the 5' strand and the P-O_5'-bond on the 3' strand. Therefore, both DNA strands are then hydroxylated. For the endonucleolytic cleavage, the cleavage chemistry is reversed and SbcCD performs a P-O_3'-cleavage on the 3' strand and a P-O_5'-cleavage on the 5' strand, leaving a fully phosphorylated DNA end.

Mre11's nucleolytic cleavage is an S_N2-reaction which requires an in-line nucleophilic attack of a water molecule, which is coordinated by one Mn^{2+} (Hopfner et al., 2001). The water molecule has to attack from the 5'-side to generate a 5'-PO_4^{2-} and 3'-OH, and from the 3'-side to generate a 5'-OH and 3'-PO_4^{2-}. To produce cleavage products with different cleavage chemistries, either the position of the water molecule is different or the scissile phosphate is coordinated in a reversed orientation.

A reversed cleavage chemistry could be also obtained by a double inversion, which returns the phosphorus to its original configuration by a two-step reaction *via* a covalent enzyme-DNA intermediate. However, this mechanism is unusual for metal-catalyzed nuclease reactions and a Ser, Tyr or His side chain as nucleophile has not been identified for Mre11/SbcD.

A possible explanation for SbcCD's distinct cleavage products could be different polarities of each DNA strand in SbcD's active site. The attacking water molecule would be coordinated at a defined position by one Mn^{2+} and due to the different orientation of the scissile phosphate, a different cleavage product is obtained. To approach the active site in different orientations, the DNA would require the flexibility of single-stranded DNA.

Mre11's/SbcD's *in vitro* nuclease activities are dependent on the presence Mn^{2+}. In SbcD's active site, two Mn^{2+}-ions are octahedrally coordinated by seven conserved residues (Asp8, Asp58, Asn83, His84, His184, His222, His224). The preferred coordination of Mn^{2+} over Mg^{2+} is due to the four histidine ligands, Mg^{2+} preferentially coordinates oxygen containing ligands.

In most cases, Mg^{2+} is the choice for two-metal-ion catalysis because of its stringent coordination geometry and charge requirements, leading to a highly selective nuclease reaction. SbcCD's cleavage efficiency was highly reduced if Mn^{2+} was substituted by Mg^{2+}. Mn^{2+} tends to relax the substrate

specificity of nucleases and polymerases and can rescue defective enzymes (Yang et al., 2006). Mn^{2+} broadens the substrate range of nucleases, likely due to Mn^{2+} being a transitional element with less stringent coordination requirements than Mg^{2+} (Yang, 2011). This could be a key feature to permit the different cleavage chemistries and enable the diverse nuclease functions of SbcD/Mre11.

The cleavage chemistry of a hairpin opening has been characterized by Leach and Co-workers. They found, that SbcCD performs a P-O_5'-cleavage at the 5' side of the hairpin to leave products with 5'- PO_4^{2-} and 3'-OH termini. This is consistent to the observations from this study and claims, that the protein-blocked stimulated endonuclease and hairpin opening activities have the same cleavage- mechanism.

It remains matter of future studies if this activity is conserved for MR(N/X) complexes from other organisms. However, since the nuclease activities are conserved and specific for the same secondary structures, it is likely that the DNA-cleavage follows a similar mechanism.

That one enzyme cleaves the phosphate backbone with different cleavage chemistries is rarely observed. In general, the cleavage products of nucleases are 5'-PO_4^{2-} and 3'-OH groups. The advantage of these products is that the 3'-OH can be passed onto other nucleic acid enzymes and be used as nucleophiles for DNA polymerases or DNA ligases. Furthermore, the 5'-PO_4^{2-} is a common substrate for DNA ligation at the end of replication, DNA repair and recombination (Yang, 2011).

For both, endo- and exonuclease activity, SbcCD produces DNA ends which are not directly compatible for downstream enzymes such as DNA-Ligases or DNA-Polymerases. Therefore, the ends are not suitable for a direct end joining reaction and would require further modifications. The distinct cleavage products This could be a protection mechanism over uncontrolled end joining reaction after nucleolytic degradation of DNA ends by MR(N/X) or SbcCD.

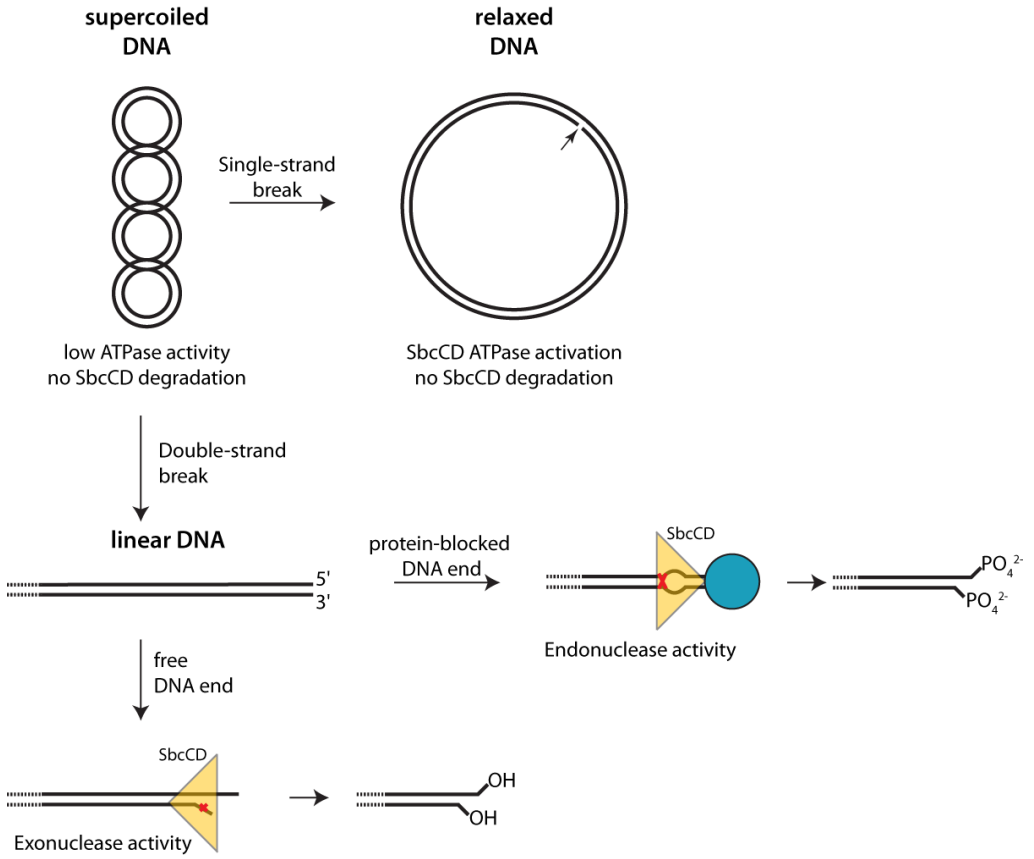

Figure 28 Model to summarize the activities of the SbcCD complex: SbcCD is in an inactive state in the presence of negative supercoiled DNA. SbcCD's ATPase becomes activated in the presence of relaxed DNA, which occurs for example due to single-strand or double-strand breaks, during DNA-replication or transcription. SbcCD's nuclease is exclusively activated by DNA ends. Free DNA ends are processed by SbcCD's exonuclease, which produces a hydroxylated DNA ends. If the DNA end is protein-blocked, SbcCD's endonuclease cleaves off the protein obstacle to leave both DNA strands phosphorylated. These ends are not compatible for the direct end-ligation reactions and require further downstream-processing.

5.5 SbcD dimer organization during DNA processing

The Mre11-Mre11 homodimeric interface is mediated by a conserved four-helix bundle motif. Functional investigation of the Mre11 interface emphasized a high importance of an unmodified interface. A destabilized *S. pombe* Mre11 dimer interface resembled *mre11Δ* in being very sensitive to genotoxins. *In vitro* studies with the nuclease and capping domain of *P. furiosus* Mre11 showed that an intact Mre11 dimer is important to bind dsDNA, but dispensable for the incision of ssDNA (Williams et al., 2008). Biochemical investigation with the T4 phage MR complex showed that the Mre11 dimer interface disruption reduces the DNA-stimulated ATPase activity of Rad50 and slows down the MR-exonuclease (Albrecht et al., 2012).

The SbcD nuclease and capping domain forms a weak dimer, 4% of SbcD forms a dimer during size-exclusion chromatography coupled right angle light scattering (SEC-RALS). It is likely that SbcD forms a dimer in the full-length SbcCD complex, since the two SbcD protomers should be in close proximity due to the SbcC Zinc-hook.

The introduction of the SbcD^{V68D} mutation destabilizes the SbcD dimer-interface, and the fraction of dimeric SbcD during SEC-RALS vanishes. The ssDNA endonuclease activity is not affected by the nuclease and capping domain SbcD^{V68D}. Therefore, this mutation does not affect the overall fold of SbcD and the nuclease active site appears to be properly folded.

The SbcD^{V68D} mutation affects SbcCD's nuclease- and ATPase-activities in a defined manner. Full-length SbcCD^{V68D} retains its dsDNA exonuclease and ssDNA endonuclease activities in the presence of ATP, however, SbcCD^{V68D} is dsDNA endonuclease-deficient. The endonuclease activity is rescued by introducing bubbles into the dsDNA, a structure which was previously discussed to be an intermediate during endonucleolytic cleavage. In the presence of ATPγS, SbcCD^{V68D} loses all of its nuclease activities. Michelis-Menten kinetics showed that SbcCD^{V68D} has similar k_{cat} and K_M values to SbcC alone.

Form these data, one could hypothesize that SbcCD^{V68D} is not able to form a DNA intermediate which is in a productive structure for SbcD cleavage. If the dimer is directly involved in DNA melting or the SbcD-dimer destabilization introduces an allosteric defect into the SbcCD complex is not clear yet. Since the endonuclease is ATP-hydrolysis dependent and the SbcC ATPase was highly affected by the SbcD^{V68D}, the defect in the SbcCD^{V68D} complex could have allosteric reasons.

However, the crystal structure of *P. furiosus* and *M. jannashii* Mre11-DNA complexes show a minor groove widening of B-DNA. Additionally, DNA-binding of the *M. jannashii* Mre11 induces a rigid body rotation of the two Mre11 protomers, and the authors of this work hypothesized that this movement could directly induce DNA melting (Sung et al., 2014; Williams et al., 2008).

The N-terminal fusion of the LisH domain to SbcD would inhibit an opening of the SbcD dimer but allow minor conformational changes. The SbcCD^{LisH} complex retains full exonuclease activity. However, the endonuclease on a protein-blocked dsDNA was reduced 2-5 fold, depending on the linker-length between LisH and SbcD. The presence of a bubble restores the endonuclease activity to almost SbcCD^{wt}-level. Covalent crosslinking of the SbcD-dimer counteracts any plasticity of the dimer-interface. This rigid conformation of SbcD favors the exonuclease activity compared to SbcCD^{wt}, depletes endonuclease activity which is only partially restored by the presence of a bubble.

Collectively, these data propose that a native SbcD dimer interface is crucial for endonuclease activity, but not for exonuclease activity. The exonuclease activity remained robust for all introduced SbcD modifications and was enhanced for the crosslinked SbcD dimer, which hints towards that the SbcD dimer, remains in a rigid organization.

The endonuclease appears to be a finely tuned activity, which requires an intact allosteric cascade within SbcCD. A precise sequence of mechanisms could be necessary between dsDNA binding and internal dsDNA cleavage. A crucial step appears to generate a DNA intermediate with an unpaired DNA-stretch which is productive for cleavage. Since the endonuclease activity of the dimer interface mutants could be rescued by the presence of a bubble, the wild-type SbcD dimer is crucial to generating this substrate. The obtained data contradict a SbcD-dimer opening during endonuclease activity but emphasize that plasticity is essential for the proper function of the SbcCD complex.

6. References

Adkins, N.L., Niu, H., Sung, P., and Peterson, C.L. (2013). Nucleosome dynamics regulates DNA processing. Nature structural & molecular biology *20*, 836-842.

Aedo, S., and Tse-Dinh, Y.C. (2013). SbcCD-mediated processing of covalent gyrase-DNA complex in Escherichia coli. Antimicrobial agents and chemotherapy *57*, 5116-5119.

Aguilera, A., and Gomez-Gonzalez, B. (2008). Genome instability: a mechanistic view of its causes and consequences. Nature reviews. Genetics *9*, 204-217.

Albrecht, D.W., Herdendorf, T.J., and Nelson, S.W. (2012). Disruption of the bacteriophage T4 Mre11 dimer interface reveals a two-state mechanism for exonuclease activity. The Journal of biological chemistry *287*, 31371-31381.

Anand, R., Ranjha, L., Cannavo, E., and Cejka, P. (2016). Phosphorylated CtIP Functions as a Co-factor of the MRE11-RAD50-NBS1 Endonuclease in DNA End Resection. Molecular cell *64*, 940-950.

Anderson, D.G., and Kowalczykowski, S.C. (1997). The recombination hot spot chi is a regulatory element that switches the polarity of DNA degradation by the RecBCD enzyme. Genes & development *11*, 571-581.

Aparicio, T., and Gautier, J. (2016). BRCA1-CtIP interaction in the repair of DNA double-strand breaks. Molecular & cellular oncology *3*, e1169343.

Aylon, Y., Liefshitz, B., and Kupiec, M. (2004). The CDK regulates repair of double-strand breaks by homologous recombination during the cell cycle. The EMBO journal *23*, 4868-4875.

Ayora, S., Carrasco, B., Cardenas, P.P., Cesar, C.E., Canas, C., Yadav, T., Marchisone, C., and Alonso, J.C. (2011). Double-strand break repair in bacteria: a view from Bacillus subtilis. FEMS microbiology reviews *35*, 1055-1081.

Bauerschmidt, C., Arrichiello, C., Burdak-Rothkamm, S., Woodcock, M., Hill, M.A., Stevens, D.L., and Rothkamm, K. (2010). Cohesin promotes the repair of ionizing radiation-induced DNA double-strand breaks in replicated chromatin. Nucleic acids research *38*, 477-487.

Berkovich, E., Monnat, R.J., Jr., and Kastan, M.B. (2007). Roles of ATM and NBS1 in chromatin structure modulation and DNA double-strand break repair. Nature cell biology *9*, 683-690.

Betermier, M., Bertrand, P., and Lopez, B.S. (2014). Is non-homologous end joining really an inherently error-prone process? PLoS genetics *10*, e1004086.

Bidnenko, V., Seigneur, M., Penel-Colin, M., Bouton, M.F., Dusko Ehrlich, S., and Michel, B. (1999). sbcB sbcC null mutations allow RecF-mediated repair of arrested replication forks in rep recBC mutants. Molecular microbiology *33*, 846-857.

Blier, P.R., Griffith, A.J., Craft, J., and Hardin, J.A. (1993). Binding of Ku protein to DNA. Measurement of affinity for ends and demonstration of binding to nicks. The Journal of biological chemistry *268*, 7594-7601.

Bonetti, D., Martina, M., Falcettoni, M., and Longhese, M.P. (2013). Telomere-end processing: mechanisms and regulation. Chromosoma.

Buis, J., Wu, Y., Deng, Y., Leddon, J., Westfield, G., Eckersdorff, M., Sekiguchi, J.M., Chang, S., and Ferguson, D.O. (2008). Mre11 Nuclease Activity Has Essential Roles in DNA Repair and Genomic Stability Distinct from ATM Activation. Cell *135*, 85-96.

Bunting, S.F., Callen, E., Wong, N., Chen, H.T., Polato, F., Gunn, A., Bothmer, A., Feldhahn, N., Fernandez-Capetillo, O., Cao, L.*, et al.* (2010). 53BP1 inhibits homologous recombination in Brca1-deficient cells by blocking resection of DNA breaks. Cell *141*, 243-254.

Cadet, J., Berger, M., Douki, T., and Ravanat, J.L. (1997). Oxidative damage to DNA: formation, measurement, and biological significance. Reviews of physiology, biochemistry and pharmacology *131*, 1-87.

Callen, E., Di Virgilio, M., Kruhlak, M.J., Nieto-Soler, M., Wong, N., Chen, H.T., Faryabi, R.B., Polato, F., Santos, M., Starnes, L.M.*, et al.* (2013). 53BP1 mediates productive and mutagenic DNA repair through distinct phosphoprotein interactions. Cell *153*, 1266-1280.

Cannavo, E., and Cejka, P. (2014). Sae2 promotes dsDNA endonuclease activity within Mre11-Rad50-Xrs2 to resect DNA breaks. Nature *514*, 122-125.

Cannavo, E., Cejka, P., and Kowalczykowski, S.C. (2013). Relationship of DNA degradation by Saccharomyces cerevisiae exonuclease 1 and its stimulation by RPA and Mre11-Rad50-Xrs2 to DNA end resection. Proceedings of the National Academy of Sciences of the United States of America *110*, E1661-1668.

Cannon, B., Kuhnlein, J., Yang, S.H., Cheng, A., Schindler, D., Stark, J.M., Russell, R., and Paull, T.T. (2013). Visualization of local DNA unwinding by Mre11/Rad50/Nbs1 using single-molecule FRET. Proceedings of the National Academy of Sciences of the United States of America *110*, 18868-18873.

Carreira, A., Hilario, J., Amitani, I., Baskin, R.J., Shivji, M.K., Venkitaraman, A.R., and Kowalczykowski, S.C. (2009). The BRC repeats of BRCA2 modulate the DNA-binding selectivity of RAD51. Cell *136*, 1032-1043.

Chalker, A.F., Leach, D.R., and Lloyd, R.G. (1988). Escherichia coli sbcC mutants permit stable propagation of DNA replicons containing a long palindrome. Gene *71*, 201-205.

Chapman, J.R., and Jackson, S.P. (2008). Phospho-dependent interactions between NBS1 and MDC1 mediate chromatin retention of the MRN complex at sites of DNA damage. EMBO Rep *9*, 795-801.

Chapman, J.R., Sossick, A.J., Boulton, S.J., and Jackson, S.P. (2012). BRCA1-associated exclusion of 53BP1 from DNA damage sites underlies temporal control of DNA repair. Journal of cell science *125*, 3529-3534.

Chappell, C., Hanakahi, L.A., Karimi-Busheri, F., Weinfeld, M., and West, S.C. (2002). Involvement of human polynucleotide kinase in double-strand break repair by non-homologous end joining. The EMBO journal *21*, 2827-2832.

Chen, H., Donnianni, R.A., Handa, N., Deng, S.K., Oh, J., Timashev, L.A., Kowalczykowski, S.C., and Symington, L.S. (2015). Sae2 promotes DNA damage resistance by removing the Mre11-Rad50-Xrs2 complex from DNA and attenuating Rad53 signaling. Proceedings of the National Academy of Sciences of the United States of America *112*, E1880-1887.

Chen, J., and Stubbe, J. (2005). Bleomycins: towards better therapeutics. Nature reviews. Cancer *5*, 102-112.

Chen, L., Nievera, C.J., Lee, A.Y., and Wu, X. (2008). Cell cycle-dependent complex formation of BRCA1.CtIP.MRN is important for DNA double-strand break repair. The Journal of biological chemistry *283*, 7713-7720.

Chen, X., Cui, D., Papusha, A., Zhang, X., Chu, C.D., Tang, J., Chen, K., Pan, X., and Ira, G. (2012). The Fun30 nucleosome remodeller promotes resection of DNA double-strand break ends. Nature *489*, 576-580.

Ciccia, A., and Elledge, S.J. (2010). The DNA damage response: making it safe to play with knives. Molecular cell *40*, 179-204.

Cobbe, N., and Heck, M.M. (2006). The evolution of ATPase activity in SMC proteins. Proteins *63*, 685-696.

Connelly, J.C., de Leau, E.S., and Leach, D.R. (1999). DNA cleavage and degradation by the SbcCD protein complex from Escherichia coli. Nucleic acids research *27*, 1039-1046.

Connelly, J.C., de Leau, E.S., and Leach, D.R. (2003). Nucleolytic processing of a protein-bound DNA end by the E. coli SbcCD (MR) complex. DNA repair *2*, 795-807.

Connelly, J.C., de Leau, E.S., Okely, E.A., and Leach, D.R. (1997). Overexpression, purification, and characterization of the SbcCD protein from Escherichia coli. The Journal of biological chemistry *272*, 19819-19826.

Connelly, J.C., Kirkham, L.A., and Leach, D.R. (1998). The SbcCD nuclease of Escherichia coli is a structural maintenance of chromosomes (SMC) family protein that cleaves hairpin DNA. Proceedings of the National Academy of Sciences of the United States of America *95*, 7969-7974.

Cordeiro-Stone, M., Makhov, A.M., Zaritskaya, L.S., and Griffith, J.D. (1999). Analysis of DNA replication forks encountering a pyrimidine dimer in the template to the leading strand. Journal of molecular biology *289*, 1207-1218.

Cortez, D. (2015). Preventing Replication Fork Collapse to Maintain Genome Integrity, Vol 32.

Cox, M.M. (2007). Motoring along with the bacterial RecA protein. Nat Rev Mol Cell Biol *8*, 127-138.

Crisalli, P., and Kool, E.T. (2011). Multi-path quenchers: efficient quenching of common fluorophores. Bioconjugate chemistry *22*, 2345-2354.

Cromie, G.A., Millar, C.B., Schmidt, K.H., and Leach, D.R. (2000). Palindromes as substrates for multiple pathways of recombination in Escherichia coli. Genetics *154*, 513-522.

Darmon, E., Lopez-Vernaza, M.A., Helness, A.C., Borking, A., Wilson, E., Thacker, Z., Wardrope, L., and Leach, D.R. (2007). SbcCD regulation and localization in Escherichia coli. Journal of bacteriology *189*, 6686-6694.

Davison, A., and Leach, D.R. (1994). The effects of nucleotide sequence changes on DNA secondary structure formation in Escherichia coli are consistent with cruciform extrusion in vivo. Genetics *137*, 361-368.

De Bont, R., and van Larebeke, N. (2004). Endogenous DNA damage in humans: a review of quantitative data. Mutagenesis *19*, 169-185.

de Jager, M., Trujillo, K.M., Sung, P., Hopfner, K.-P., Carney, J.P., Tainer, J.A., Connelly, J.C., Leach, D.R.F., Kanaar, R., and Wyman, C. (2004). Differential Arrangements of Conserved Building Blocks among Homologs of the Rad50/Mre11 DNA Repair Protein Complex. Journal of molecular biology *339*, 937-949.

de Jager, M., van Noort, J., van Gent, D.C., Dekker, C., Kanaar, R., and Wyman, C. (2001). Human Rad50/Mre11 Is a Flexible Complex that Can Tether DNA Ends. Molecular cell *8*, 1129-1135.

De Vlaminck, I., van Loenhout, M.T., Zweifel, L., den Blanken, J., Hooning, K., Hage, S., Kerssemakers, J., and Dekker, C. (2012). Mechanism of homology recognition in DNA recombination from dual-molecule experiments. Molecular cell *46*, 616-624.

DeFazio, L.G., Stansel, R.M., Griffith, J.D., and Chu, G. (2002). Synapsis of DNA ends by DNA-dependent protein kinase. The EMBO journal *21*, 3192-3200.

Deng, Sarah K., Yin, Y., Petes, Thomas D., and Symington, Lorraine S. (2015). Mre11-Sae2 and RPA Collaborate to Prevent Palindromic Gene Amplification. Molecular cell *60*, 500-508.

Desai-Mehta, A., Cerosaletti, K.M., and Concannon, P. (2001). Distinct functional domains of nibrin mediate Mre11 binding, focus formation, and nuclear localization. Molecular and cellular biology *21*, 2184-2191.

Deshpande, R.A., Lee, J.H., Arora, S., and Paull, T.T. (2016). Nbs1 Converts the Human Mre11/Rad50 Nuclease Complex into an Endo/Exonuclease Machine Specific for Protein-DNA Adducts. Molecular cell *64*, 593-606.

Deshpande, R.A., Lee, J.H., and Paull, T.T. (2017). Rad50 ATPase activity is regulated by DNA ends and requires coordination of both active sites. Nucleic acids research *45*, 5255-5268.

Deshpande, R.A., Williams, G.J., Limbo, O., Williams, R.S., Kuhnlein, J., Lee, J.H., Classen, S., Guenther, G., Russell, P., Tainer, J.A*., et al.* (2014). ATP-driven Rad50 conformations regulate DNA tethering, end resection, and ATM checkpoint signaling. The EMBO journal *33*, 482-500.

Dexheimer, T.S. (2013). DNA Repair Pathways and Mechanisms. In DNA Repair of Cancer Stem Cells, L.A. Mathews, S.M. Cabarcas, and E.M. Hurt, eds. (Dordrecht: Springer Netherlands), pp. 19-32.

Dillingham, M.S., and Kowalczykowski, S.C. (2008). RecBCD enzyme and the repair of double-stranded DNA breaks. Microbiology and molecular biology reviews : MMBR *72*, 642-671, Table of Contents.

Dimitrova, N., and de Lange, T. (2009). Cell cycle-dependent role of MRN at dysfunctional telomeres: ATM signaling-dependent induction of nonhomologous end joining (NHEJ) in G1 and resection-mediated inhibition of NHEJ in G2. Molecular and cellular biology *29*, 5552-5563.

Dufner, P., Marra, G., Raschle, M., and Jiricny, J. (2000). Mismatch recognition and DNA-dependent stimulation of the ATPase activity of hMutSalpha is abolished by a single mutation in the hMSH6 subunit. The Journal of biological chemistry *275*, 36550-36555.

Dupre, A., Boyer-Chatenet, L., and Gautier, J. (2006). Two-step activation of ATM by DNA and the Mre11-Rad50-Nbs1 complex. Nature structural & molecular biology *13*, 451-457.

Errico, A., and Costanzo, V. (2010). Differences in the DNA replication of unicellular eukaryotes and metazoans: known unknowns. EMBO reports *11*, 270-278.

Eykelenboom, J.K., Blackwood, J.K., Okely, E., and Leach, D.R. (2008). SbcCD causes a double-strand break at a DNA palindrome in the Escherichia coli chromosome. Molecular cell *29*, 644-651.

Falck, J., Coates, J., and Jackson, S.P. (2005). Conserved modes of recruitment of ATM, ATR and DNA-PKcs to sites of DNA damage. Nature *434*, 605-611.

Ferrari, M., Dibitetto, D., De Gregorio, G., Eapen, V.V., Rawal, C.C., Lazzaro, F., Tsabar, M., Marini, F., Haber, J.E., and Pellicioli, A. (2015). Functional interplay between the 53BP1-ortholog Rad9 and the Mre11 complex regulates resection, end-tethering and repair of a double-strand break. PLoS genetics *11*, e1004928.

Forget, A.L., and Kowalczykowski, S.C. (2012). Single-molecule imaging of DNA pairing by RecA reveals a three-dimensional homology search. Nature *482*, 423-427.

Fradet-Turcotte, A., Canny, M.D., Escribano-Diaz, C., Orthwein, A., Leung, C.C., Huang, H., Landry, M.C., Kitevski-LeBlanc, J., Noordermeer, S.M., Sicheri, F.*, et al.* (2013). 53BP1 is a reader of the DNA-damage-induced H2A Lys 15 ubiquitin mark. Nature *499*, 50-54.

Furuse, M., Nagase, Y., Tsubouchi, H., Murakami-Murofushi, K., Shibata, T., and Ohta, K. (1998). Distinct roles of two separable in vitro activities of yeast Mre11 in mitotic and meiotic recombination. The EMBO journal *17*, 6412-6425.

Gatei, M., Kijas, A.W., Biard, D., Dork, T., and Lavin, M.F. (2014). RAD50 phosphorylation promotes ATR downstream signaling and DNA restart following replication stress. Hum Mol Genet *23*, 4232-4248.

Gibson, F.P., Leach, D.R., and Lloyd, R.G. (1992). Identification of sbcD mutations as cosuppressors of recBC that allow propagation of DNA palindromes in Escherichia coli K-12. Journal of bacteriology *174*, 1222-1228.

Gilhooly, N.S., Carrasco, C., Gollnick, B., Wilkinson, M., Wigley, D.B., Moreno-Herrero, F., and Dillingham, M.S. (2016). Chi hotspots trigger a conformational change in the helicase-like domain of AddAB to activate homologous recombination. Nucleic acids research *44*, 2727-2741.

Gobbini, E., Cesena, D., Galbiati, A., Lockhart, A., and Longhese, M.P. (2013). Interplays between ATM/Tel1 and ATR/Mec1 in sensing and signaling DNA double-strand breaks. DNA repair *12*, 791-799.

Goudsouzian, L.K., Tuzon, C.T., and Zakian, V.A. (2006). S. cerevisiae Tel1p and Mre11p are required for normal levels of Est1p and Est2p telomere association. Molecular cell *24*, 603-610.

Gradia, S., Acharya, S., and Fishel, R. (1997). The human mismatch recognition complex hMSH2-hMSH6 functions as a novel molecular switch. Cell *91*, 995-1005.

Green, S. (2012). Molecular Cloning: A laboratory Manual (4th Edition) (Cold Spring Harbor Laboratory Press).

Grimes, E., Busby, S., and Minchin, S. (1991). Different thermal energy requirement for open complex formation by Escherichia coli RNA polymerase at two related promoters. Nucleic acids research *19*, 6113-6118.

Haber, J.E. (2008). Alternative endings. Proceedings of the National Academy of Sciences of the United States of America *105*, 405-406.

Haber, J.E. (2012). Mating-type genes and MAT switching in Saccharomyces cerevisiae. Genetics *191*, 33-64.

Handa, N., Yang, L., Dillingham, M.S., Kobayashi, I., Wigley, D.B., and Kowalczykowski, S.C. (2012). Molecular determinants responsible for recognition of the single-stranded DNA regulatory sequence, chi, by RecBCD enzyme. Proceedings of the National Academy of Sciences of the United States of America *109*, 8901-8906.

Hauer, M.H., and Gasser, S.M. (2017). Chromatin and nucleosome dynamics in DNA damage and repair. Genes & development *31*, 2204-2221.

Herdendorf, T.J., Albrecht, D.W., Benkovic, S.J., and Nelson, S.W. (2011). Biochemical characterization of bacteriophage T4 Mre11-Rad50 complex. The Journal of biological chemistry *286*, 2382-2392.

Herdendorf, T.J., and Nelson, S.W. (2014). Catalytic mechanism of bacteriophage T4 Rad50 ATP hydrolysis. Biochemistry *53*, 5647-5660.

Heyer, W.D. (2015). Regulation of recombination and genomic maintenance. Cold Spring Harb Perspect Biol *7*, a016501.

Hirano, Y., Fukunaga, K., and Sugimoto, K. (2009). Rif1 and rif2 inhibit localization of tel1 to DNA ends. Molecular cell *33*, 312-322.

Hoa, N.N., Shimizu, T., Zhou, Z.W., Wang, Z.Q., Deshpande, R.A., Paull, T.T., Akter, S., Tsuda, M., Furuta, R., Tsutsui, K.*, et al.* (2016). Mre11 Is Essential for the Removal of Lethal Topoisomerase 2 Covalent Cleavage Complexes. Molecular cell *64*, 580-592.

Hoeijmakers, J.H. (2009). DNA damage, aging, and cancer. The New England journal of medicine *361*, 1475-1485.

Hohl, M., Kochanczyk, T., Tous, C., Aguilera, A., Krezel, A., and Petrini, J.H. (2015). Interdependence of the rad50 hook and globular domain functions. Molecular cell *57*, 479-491.

Hohl, M., Kwon, Y., Galvan, S.M., Xue, X., Tous, C., Aguilera, A., Sung, P., and Petrini, J.H. (2011). The Rad50 coiled-coil domain is indispensable for Mre11 complex functions. Nature structural & molecular biology *18*, 1124-1131.

Hopfner, K.P. (2016). Invited review: Architectures and mechanisms of ATP binding cassette proteins. Biopolymers *105*, 492-504.

Hopfner, K.P., Craig, L., Moncalian, G., Zinkel, R.A., Usui, T., Owen, B.A., Karcher, A., Henderson, B., Bodmer, J.L., McMurray, C.T*., et al.* (2002). The Rad50 zinc-hook is a structure joining Mre11 complexes in DNA recombination and repair. Nature *418*, 562-566.

Hopfner, K.P., Karcher, A., Craig, L., Woo, T.T., Carney, J.P., and Tainer, J.A. (2001). Structural biochemistry and interaction architecture of the DNA double-strand break repair Mre11 nuclease and Rad50-ATPase. Cell *105*, 473-485.

Hopfner, K.P., Karcher, A., Shin, D., Fairley, C., Tainer, J.A., and Carney, J.P. (2000a). Mre11 and Rad50 from Pyrococcus furiosus: cloning and biochemical characterization reveal an evolutionarily conserved multiprotein machine. Journal of bacteriology *182*, 6036-6041.

Hopfner, K.P., Karcher, A., Shin, D.S., Craig, L., Arthur, L.M., Carney, J.P., and Tainer, J.A. (2000b). Structural biology of Rad50 ATPase: ATP-driven conformational control in DNA double-strand break repair and the ABC-ATPase superfamily. Cell *101*, 789-800.

Huertas, P., Cortes-Ledesma, F., Sartori, A.A., Aguilera, A., and Jackson, S.P. (2008). CDK targets Sae2 to control DNA-end resection and homologous recombination. Nature *455*, 689-692.

Hustedt, N., and Durocher, D. (2016). The control of DNA repair by the cell cycle. Nature cell biology *19*, 1-9.

Inagaki, A., Schoenmakers, S., and Baarends, W.M. (2010). DNA double strand break repair, chromosome synapsis and transcriptional silencing in meiosis. Epigenetics *5*, 255-266.

Ira, G., Pellicioli, A., Balijja, A., Wang, X., Fiorani, S., Carotenuto, W., Liberi, G., Bressan, D., Wan, L., Hollingsworth, N.M*., et al.* (2004). DNA end resection, homologous recombination and DNA damage checkpoint activation require CDK1. Nature *431*, 1011-1017.

Isono, M., Niimi, A., Oike, T., Hagiwara, Y., Sato, H., Sekine, R., Yoshida, Y., Isobe, S.Y., Obuse, C., Nishi, R*., et al.* (2017). BRCA1 Directs the Repair Pathway to Homologous Recombination by Promoting 53BP1 Dephosphorylation. Cell reports *18*, 520-532.

Iwabuchi, K., Hashimoto, M., Matsui, T., Kurihara, T., Shimizu, H., Adachi, N., Ishiai, M., Yamamoto, K., Tauchi, H., Takata, M*., et al.* (2006). 53BP1 contributes to survival of cells irradiated with X-ray during G1 without Ku70 or Artemis. Genes to cells : devoted to molecular & cellular mechanisms *11*, 935-948.

Jeggo, P., and O'Neill, P. (2002). The Greek Goddess, Artemis, reveals the secrets of her cleavage. DNA repair *1*, 771-777.

Kahl, B.F., and Paule, M.R. (2008). The Use of Diethyl Pyrocarbonate and Potassium Permanganate as Probes for Strand Separation and Structural Distortions in DNA #. In T DNA-Protein Interactions, pp. 73-85.

Kahl, B.F., and Paule, M.R. (2009). The use of diethyl pyrocarbonate and potassium permanganate as probes for strand separation and structural distortions in DNA. Methods in molecular biology *543*, 73-85.

Keeney, S. (2008). Spo11 and the Formation of DNA Double-Strand Breaks in Meiosis. Genome dynamics and stability *2*, 81-123.

Keeney, S., and Kleckner, N. (1995). Covalent protein-DNA complexes at the 5' strand termini of meiosis-specific double-strand breaks in yeast. Proceedings of the National Academy of Sciences of the United States of America *92*, 11274-11278.

Kibbe, W.A. (2007). OligoCalc: an online oligonucleotide properties calculator. Nucleic acids research *35*, W43-46.

Kijas, A.W., Lim, Y.C., Bolderson, E., Cerosaletti, K., Gatei, M., Jakob, B., Tobias, F., Taucher-Scholz, G., Gueven, N., Oakley, G.*, et al.* (2015). ATM-dependent phosphorylation of MRE11 controls extent of resection during homology directed repair by signalling through Exonuclease 1. Nucleic acids research *43*, 8352-8367.

Kim, J.H., Grosbart, M., Anand, R., Wyman, C., Cejka, P., and Petrini, J.H.J. (2017). The Mre11-Nbs1 Interface Is Essential for Viability and Tumor Suppression. Cell reports *18*, 496-507.

Kim, M.H., Cooper, D.R., Oleksy, A., Devedjiev, Y., Derewenda, U., Reiner, O., Otlewski, J., and Derewenda, Z.S. (2004). The structure of the N-terminal domain of the product of the lissencephaly gene Lis1 and its functional implications. Structure *12*, 987-998.

Kironmai, K.M., and Muniyappa, K. (1997). Alteration of telomeric sequences and senescence caused by mutations in RAD50 of Saccharomyces cerevisiae. Genes to cells : devoted to molecular & cellular mechanisms *2*, 443-455.

Kobayashi, M., Hayashi, N., Takata, M., and Yamamoto, K. (2013). NBS1 directly activates ATR independently of MRE11 and TOPBP1. Genes to cells : devoted to molecular & cellular mechanisms *18*, 238-246.

Kolinjivadi, A.M., Sannino, V., De Antoni, A., Zadorozhny, K., Kilkenny, M., Techer, H., Baldi, G., Shen, R., Ciccia, A., Pellegrini, L.*, et al.* (2017). Smarcal1-Mediated Fork Reversal Triggers Mre11-Dependent Degradation of Nascent DNA in the Absence of Brca2 and Stable Rad51 Nucleofilaments. Molecular cell *67*, 867-881 e867.

Koroleva, O., Makharashvili, N., Courcelle, C.T., Courcelle, J., and Korolev, S. (2007). Structural conservation of RecF and Rad50: implications for DNA recognition and RecF function. The EMBO journal *26*, 867-877.

Koster, D.A., Palle, K., Bot, E.S., Bjornsti, M.A., and Dekker, N.H. (2007). Antitumour drugs impede DNA uncoiling by topoisomerase I. Nature *448*, 213-217.

Kowalczykowski, S.C. (2015). An Overview of the Molecular Mechanisms of Recombinational DNA Repair. Cold Spring Harb Perspect Biol *7*.

Kowalczykowski, S.C., Dixon, D.A., Eggleston, A.K., Lauder, S.D., and Rehrauer, W.M. (1994). Biochemistry of homologous recombination in Escherichia coli. Microbiol Rev *58*, 401-465.

Krasich, R., Wu, S.Y., Kuo, H.K., and Kreuzer, K.N. (2015). Functions that protect Escherichia coli from DNA-protein crosslinks. DNA repair *28*, 48-59.

Lafrance-Vanasse, J., Williams, G.J., and Tainer, J.A. (2015). Envisioning the dynamics and flexibility of Mre11-Rad50-Nbs1 complex to decipher its roles in DNA replication and repair. Progress in biophysics and molecular biology *117*, 182-193.

Lamers, M.H., Georgijevic, D., Lebbink, J.H., Winterwerp, H.H., Agianian, B., de Wind, N., and Sixma, T.K. (2004). ATP increases the affinity between MutS ATPase domains. Implications for ATP hydrolysis and conformational changes. The Journal of biological chemistry *279*, 43879-43885.

Lammens, A., Schele, A., and Hopfner, K.P. (2004). Structural biochemistry of ATP-driven dimerization and DNA-stimulated activation of SMC ATPases. Current biology : CB *14*, 1778-1782.

Lammens, K., Bemeleit, D.J., Mockel, C., Clausing, E., Schele, A., Hartung, S., Schiller, C.B., Lucas, M., Angermuller, C., Soding, J*., et al.* (2011). The Mre11:Rad50 structure shows an ATP-dependent molecular clamp in DNA double-strand break repair. Cell *145*, 54-66.

Lee, J., and Dunphy, W.G. (2013). The Mre11-Rad50-Nbs1 (MRN) complex has a specific role in the activation of Chk1 in response to stalled replication forks. Molecular biology of the cell *24*, 1343-1353.

Lee, J.H., and Paull, T.T. (2005). ATM activation by DNA double-strand breaks through the Mre11-Rad50-Nbs1 complex. Science *308*, 551-554.

Lengsfeld, B.M., Rattray, A.J., Bhaskara, V., Ghirlando, R., and Paull, T.T. (2007). Sae2 is an endonuclease that processes hairpin DNA cooperatively with the Mre11/Rad50/Xrs2 complex. Molecular cell *28*, 638-651.

Liao, S., Tammaro, M., and Yan, H. (2016). The structure of ends determines the pathway choice and Mre11 nuclease dependency of DNA double-strand break repair. Nucleic acids research *44*, 5689-5701.

Lieber, M.R. (2010). The mechanism of double-strand DNA break repair by the nonhomologous DNA end joining pathway. Annual review of biochemistry *79*, 181-211.

Lim, C.T., Lai, P.J., Leach, D.R., Maki, H., and Furukohri, A. (2015). A novel mode of nuclease action is revealed by the bacterial Mre11/Rad50 complex. Nucleic acids research *43*, 9804-9816.

Limbo, O., Chahwan, C., Yamada, Y., de Bruin, R.A., Wittenberg, C., and Russell, P. (2007). Ctp1 is a cell-cycle-regulated protein that functions with Mre11 complex to control double-strand break repair by homologous recombination. Molecular cell *28*, 134-146.

Lindahl, T., and Nyberg, B. (1972). Rate of depurination of native deoxyribonucleic acid. Biochemistry *11*, 3610-3618.

Lisby, M., Barlow, J.H., Burgess, R.C., and Rothstein, R. (2004). Choreography of the DNA damage response: spatiotemporal relationships among checkpoint and repair proteins. Cell *118*, 699-713.

Liu, Y., Sung, S., Kim, Y., Li, F., Gwon, G., Jo, A., Kim, A.K., Kim, T., Song, O.K., Lee, S.E.*, et al.* (2016). ATP-dependent DNA binding, unwinding, and resection by the Mre11/Rad50 complex. The EMBO journal *35*, 743-758.

Lloyd, J., Chapman, J.R., Clapperton, J.A., Haire, L.F., Hartsuiker, E., Li, J., Carr, A.M., Jackson, S.P., and Smerdon, S.J. (2009). A supramodular FHA/BRCT-repeat architecture mediates Nbs1 adaptor function in response to DNA damage. Cell *139*, 100-111.

Lu, H., Schwarz, K., and Lieber, M.R. (2007). Extent to which hairpin opening by the Artemis:DNA-PKcs complex can contribute to junctional diversity in V(D)J recombination. Nucleic acids research *35*, 6917-6923.

Ma, Y., Pannicke, U., Schwarz, K., and Lieber, M.R. (2002). Hairpin opening and overhang processing by an Artemis/DNA-dependent protein kinase complex in nonhomologous end joining and V(D)J recombination. Cell *108*, 781-794.

Mahaney, B.L., Meek, K., and Lees-Miller, S.P. (2009). Repair of ionizing radiation-induced DNA double-strand breaks by non-homologous end joining. The Biochemical journal *417*, 639-650.

Marras, S.A., Kramer, F.R., and Tyagi, S. (2002). Efficiencies of fluorescence resonance energy transfer and contact-mediated quenching in oligonucleotide probes. Nucleic acids research *30*, e122.

McCulloch, S.D., and Kunkel, T.A. (2008). The fidelity of DNA synthesis by eukaryotic replicative and translesion synthesis polymerases. Cell research *18*, 148-161.

McIlwraith, M.J., Vaisman, A., Liu, Y., Fanning, E., Woodgate, R., and West, S.C. (2005). Human DNA polymerase eta promotes DNA synthesis from strand invasion intermediates of homologous recombination. Molecular cell *20*, 783-792.

Mehta, A., and Haber, J.E. (2014). Sources of DNA Double-Strand Breaks and Models of Recombinational DNA Repair. Cold Spring Harb Perspect Biol.

Milo, R., Jorgensen, P., Moran, U., Weber, G., and Springer, M. (2010). BioNumbers--the database of key numbers in molecular and cell biology. Nucleic acids research *38*, D750-753.

Mimitou, E.P., and Symington, L.S. (2010). Ku prevents Exo1 and Sgs1-dependent resection of DNA ends in the absence of a functional MRX complex or Sae2. The EMBO journal *29*, 3358-3369.

Möckel, C., Lammens, K., Schele, A., and Hopfner, K.P. (2012). ATP driven structural changes of the bacterial Mre11:Rad50 catalytic head complex. Nucleic acids research *40*, 914-927.

Moncalian, G., Lengsfeld, B., Bhaskara, V., Hopfner, K.P., Karcher, A., Alden, E., Tainer, J.A., and Paull, T.T. (2004). The rad50 signature motif: essential to ATP binding and biological function. Journal of molecular biology *335*, 937-951.

Moreno-Herrero, F., de Jager, M., Dekker, N.H., Kanaar, R., Wyman, C., and Dekker, C. (2005). Mesoscale conformational changes in the DNA-repair complex Rad50/Mre11/Nbs1 upon binding DNA. Nature *437*, 440-443.

Morimatsu, K., and Kowalczykowski, S.C. (2003). RecFOR proteins load RecA protein onto gapped DNA to accelerate DNA strand exchange: a universal step of recombinational repair. Molecular cell *11*, 1337-1347.

Myler, L.R., Gallardo, I.F., Soniat, M.M., Deshpande, R.A., Gonzalez, X.B., Kim, Y., Paull, T.T., and Finkelstein, I.J. (2017). Single-Molecule Imaging Reveals How Mre11-Rad50-Nbs1 Initiates DNA Break Repair. Molecular cell *67*, 891-898 e894.

Nakamura, K., Sakai, W., Kawamoto, T., Bree, R.T., Lowndes, N.F., Takeda, S., and Taniguchi, Y. (2006). Genetic dissection of vertebrate 53BP1: a major role in non-homologous end joining of DNA double strand breaks. DNA repair *5*, 741-749.

Noirot, P., and Noirot-Gros, M.F. (2004). Protein interaction networks in bacteria. Current opinion in microbiology *7*, 505-512.

Oh, J., Al-Zain, A., Cannavo, E., Cejka, P., and Symington, L.S. (2016). Xrs2 Dependent and Independent Functions of the Mre11-Rad50 Complex. Molecular cell *64*, 405-415.

Park, Y.B., Chae, J., Kim, Y.C., and Cho, Y. (2011). Crystal structure of human Mre11: understanding tumorigenic mutations. Structure *19*, 1591-1602.

Park, Y.B., Hohl, M., Padjasek, M., Jeong, E., Jin, K.S., Krezel, A., Petrini, J.H., and Cho, Y. (2017). Eukaryotic Rad50 functions as a rod-shaped dimer. Nature structural & molecular biology *24*, 248-257.

Paudyal, S.C., Li, S., Yan, H., Hunter, T., and You, Z. (2017). Dna2 initiates resection at clean DNA double-strand breaks. Nucleic acids research *45*, 11766-11781.

Paull, T.T., and Gellert, M. (1998). The 3' to 5' exonuclease activity of Mre 11 facilitates repair of DNA double-strand breaks. Molecular cell *1*, 969-979.

Paull, T.T., and Gellert, M. (1999). Nbs1 potentiates ATP-driven DNA unwinding and endonuclease cleavage by the Mre11/Rad50 complex. Genes & development *13*, 1276-1288.

Pellegrino, S., Radzimanowski, J., de Sanctis, D., Boeri Erba, E., McSweeney, S., and Timmins, J. (2012). Structural and functional characterization of an SMC-like protein RecN: new insights into double-strand break repair. Structure *20*, 2076-2089.

Persky, N.S., and Lovett, S.T. (2008). Mechanisms of recombination: lessons from E. coli. Critical reviews in biochemistry and molecular biology *43*, 347-370.

Polo, S.E., Kaidi, A., Baskcomb, L., Galanty, Y., and Jackson, S.P. (2010). Regulation of DNA-damage responses and cell-cycle progression by the chromatin remodelling factor CHD4. The EMBO journal *29*, 3130-3139.

Quinet, A., Lemacon, D., and Vindigni, A. (2017). Replication Fork Reversal: Players and Guardians. Molecular cell *68*, 830-833.

Rahal, E.A., Henricksen, L.A., Li, Y., Williams, R.S., Tainer, J.A., and Dixon, K. (2010). ATM regulates Mre11-dependent DNA end-degradation and microhomology-mediated end joining. Cell cycle *9*, 2866-2877.

Ravanat, J.L., Douki, T., and Cadet, J. (2001). Direct and indirect effects of UV radiation on DNA and its components. Journal of photochemistry and photobiology. B, Biology *63*, 88-102.

Reginato, G., Cannavo, E., and Cejka, P. (2017). Physiological protein blocks direct the Mre11-Rad50-Xrs2 and Sae2 nuclease complex to initiate DNA end resection. Genes & development *31*, 2325-2330.

Reyes, E.D., Patidar, P.L., Uranga, L.A., Bortoletto, A.S., and Lusetti, S.L. (2010). RecN is a cohesin-like protein that stimulates intermolecular DNA interactions in vitro. The Journal of biological chemistry *285*, 16521-16529.

Rojowska, A., Lammens, K., Seifert, F.U., Direnberger, C., Feldmann, H., and Hopfner, K.P. (2014). Structure of the Rad50 DNA double-strand break repair protein in complex with DNA. The EMBO journal *33*, 2847-2859.

Rybenkov, V.V., Herrera, V., Petrushenko, Z.M., and Zhao, H. (2014). MukBEF, a chromosomal organizer. Journal of molecular microbiology and biotechnology *24*, 371-383.

Rydberg, B., and Lindahl, T. (1982). Nonenzymatic methylation of DNA by the intracellular methyl group donor S-adenosyl-L-methionine is a potentially mutagenic reaction. The EMBO journal *1*, 211-216.

Sartori, A.A., Lukas, C., Coates, J., Mistrik, M., Fu, S., Bartek, J., Baer, R., Lukas, J., and Jackson, S.P. (2007). Human CtIP promotes DNA end resection. Nature *450*, 509-514.

Schatz, D.G., and Swanson, P.C. (2011). V(D)J recombination: mechanisms of initiation. Annual review of genetics *45*, 167-202.

Schiller, C.B., Lammens, K., Guerini, I., Coordes, B., Feldmann, H., Schlauderer, F., Mockel, C., Schele, A., Strasser, K., Jackson, S.P*., et al.* (2012). Structure of Mre11-Nbs1 complex yields insights into ataxia-telangiectasia-like disease mutations and DNA damage signaling. Nature structural & molecular biology *19*, 693-700.

Schiller, C.B., Seifert, F.U., Linke-Winnebeck, C., and Hopfner, K.P. (2014). Structural studies of DNA end detection and resection in homologous recombination. Cold Spring Harb Perspect Biol *6*, a017962.

Schlapschy, M., Binder, U., Borger, C., Theobald, I., Wachinger, K., Kisling, S., Haller, D., and Skerra, A. (2013). PASylation: a biological alternative to PEGylation for extending the plasma half-life of pharmaceutically active proteins. Protein engineering, design & selection : PEDS *26*, 489-501.

Schneider, C.A., Rasband, W.S., and Eliceiri, K.W. (2012). NIH Image to ImageJ: 25 years of image analysis. Nature methods *9*, 671-675.

Seeber, A., Hauer, M., and Gasser, S.M. (2013). Nucleosome remodelers in double-strand break repair. Current opinion in genetics & development *23*, 174-184.

Seifert, F.U., Lammens, K., and Hopfner, K.P. (2015). Structure of the catalytic domain of Mre11 from Chaetomium thermophilum. Acta crystallographica. Section F, Structural biology communications *71*, 752-757.

Seifert, F.U., Lammens, K., Stoehr, G., Kessler, B., and Hopfner, K.P. (2016). Structural mechanism of ATP-dependent DNA binding and DNA end bridging by eukaryotic Rad50. The EMBO journal *35*, 759-772.

Shim, E.Y., Chung, W.H., Nicolette, M.L., Zhang, Y., Davis, M., Zhu, Z., Paull, T.T., Ira, G., and Lee, S.E. (2010). Saccharomyces cerevisiae Mre11/Rad50/Xrs2 and Ku proteins regulate association of Exo1 and Dna2 with DNA breaks. The EMBO journal *29*, 3370-3380.

Simoneau, A., Robellet, X., Ladouceur, A.M., and D'Amours, D. (2014). Cdk1-dependent regulation of the Mre11 complex couples DNA repair pathways to cell cycle progression. Cell cycle *13*, 1078-1090.

So, S., Davis, A.J., and Chen, D.J. (2009). Autophosphorylation at serine 1981 stabilizes ATM at DNA damage sites. J Cell Biol *187*, 977-990.

Spies, M., Bianco, P.R., Dillingham, M.S., Handa, N., Baskin, R.J., and Kowalczykowski, S.C. (2003). A molecular throttle: the recombination hotspot chi controls DNA translocation by the RecBCD helicase. Cell *114*, 647-654.

Stigler, J., Camdere, G.O., Koshland, D.E., and Greene, E.C. (2016). Single-Molecule Imaging Reveals a Collapsed Conformational State for DNA-Bound Cohesin. Cell reports *15*, 988-998.

Stingele, J., Bellelli, R., and Boulton, S.J. (2017). Mechanisms of DNA-protein crosslink repair. Nat Rev Mol Cell Biol *18*, 563-573.

Stracker, T.H., and Petrini, J.H.J. (2011). The MRE11 complex: starting from the ends. Nat Rev Mol Cell Biol *12*, 90-103.

Sung, P., and Klein, H. (2006). Mechanism of homologous recombination: mediators and helicases take on regulatory functions. Nat Rev Mol Cell Biol *7*, 739-750.

Sung, S., Li, F., Park, Y.B., Kim, J.S., Kim, A.K., Song, O.K., Kim, J., Che, J., Lee, S.E., and Cho, Y. (2014). DNA end recognition by the Mre11 nuclease dimer: insights into resection and repair of damaged DNA. The EMBO journal *33*, 2422-2435.

Symington, L.S., and Gautier, J. (2011). Double-Strand Break End Resection and Repair Pathway Choice. Annual review of genetics *45*, 247-271.

Takai, H., Smogorzewska, A., and de Lange, T. (2003). DNA damage foci at dysfunctional telomeres. Current biology : CB *13*, 1549-1556.

Tang, J., Cho, N.W., Cui, G., Manion, E.M., Shanbhag, N.M., Botuyan, M.V., Mer, G., and Greenberg, R.A. (2013). Acetylation limits 53BP1 association with damaged chromatin to promote homologous recombination. Nature structural & molecular biology *20*, 317-325.

Taylor, A.F., and Smith, G.R. (1985). Substrate specificity of the DNA unwinding activity of the RecBC enzyme of Escherichia coli. Journal of molecular biology *185*, 431-443.

Terakawa, T., Bisht, S., Eeftens, J.M., Dekker, C., Haering, C.H., and Greene, E.C. (2017). The condensin complex is a mechanochemical motor that translocates along DNA. Science *358*, 672-676.

Thanbichler, M., Viollier, P.H., and Shapiro, L. (2005). The structure and function of the bacterial chromosome. Current opinion in genetics & development *15*, 153-162.

Thompson, L.H. (2012). Recognition, signaling, and repair of DNA double-strand breaks produced by ionizing radiation in mammalian cells: the molecular choreography. Mutation research *751*, 158-246.

Tomimatsu, N., Mukherjee, B., Catherine Hardebeck, M., Ilcheva, M., Vanessa Camacho, C., Louise Harris, J., Porteus, M., Llorente, B., Khanna, K.K., and Burma, S. (2014). Phosphorylation of EXO1 by CDKs 1 and 2 regulates DNA end resection and repair pathway choice. Nature communications *5*, 3561.

Tonegawa, S. (1983). Somatic generation of antibody diversity. Nature *302*, 575.

Trujillo, K.M., Roh, D.H., Chen, L., Van Komen, S., Tomkinson, A., and Sung, P. (2003). Yeast xrs2 binds DNA and helps target rad50 and mre11 to DNA ends. The Journal of biological chemistry *278*, 48957-48964.

Trujillo, K.M., and Sung, P. (2001). DNA structure-specific nuclease activities in the Saccharomyces cerevisiae Rad50*Mre11 complex. The Journal of biological chemistry *276*, 35458-35464.

Trujillo, K.M., Yuan, S.S., Lee, E.Y., and Sung, P. (1998). Nuclease activities in a complex of human recombination and DNA repair factors Rad50, Mre11, and p95. The Journal of biological chemistry *273*, 21447-21450.

Usui, T., Ohta, T., Oshiumi, H., Tomizawa, J., Ogawa, H., and Ogawa, T. (1998). Complex formation and functional versatility of Mre11 of budding yeast in recombination. Cell *95*, 705-716.

Uziel, T., Lerenthal, Y., Moyal, L., Andegeko, Y., Mittelman, L., and Shiloh, Y. (2003). Requirement of the MRN complex for ATM activation by DNA damage. The EMBO journal *22*, 5612-5621.

van der Linden, E., Sanchez, H., Kinoshita, E., Kanaar, R., and Wyman, C. (2009). RAD50 and NBS1 form a stable complex functional in DNA binding and tethering. Nucleic acids research *37*, 1580-1588.

Walker, J.R., Corpina, R.A., and Goldberg, J. (2001). Structure of the Ku heterodimer bound to DNA and its implications for double-strand break repair. Nature *412*, 607-614.

Wang, D., and Lippard, S.J. (2005). Cellular processing of platinum anticancer drugs. Nature reviews. Drug discovery *4*, 307-320.

Wang, D., Ulyanov, N.B., and Zhurkin, V.B. (2010). Sequence-dependent Kink-and-Slide deformations of nucleosomal DNA facilitated by histone arginines bound in the minor groove. J Biomol Struct Dyn *27*, 843-859.

Wang, W., Daley, J.M., Kwon, Y., Krasner, D.S., and Sung, P. (2017). Plasticity of the Mre11-Rad50-Xrs2-Sae2 nuclease ensemble in the processing of DNA-bound obstacles. Genes & development *31*, 2331-2336.

Ward, J.F. (1994). The complexity of DNA damage: relevance to biological consequences. International journal of radiation biology *66*, 427-432.

Watson, J.D., and Crick, F.H. (1953). Molecular structure of nucleic acids; a structure for deoxyribose nucleic acid. Nature *171*, 737-738.

Wendel, B.M., Cole, J.M., Courcelle, C.T., and Courcelle, J. (2018). SbcC-SbcD and ExoI process convergent forks to complete chromosome replication. Proceedings of the National Academy of Sciences of the United States of America *115*, 349-354.

White, M.A., Eykelenboom, J.K., Lopez-Vernaza, M.A., Wilson, E., and Leach, D.R. (2008). Non-random segregation of sister chromosomes in Escherichia coli. Nature *455*, 1248-1250.

Williams, G.J., Williams, R.S., Williams, J.S., Moncalian, G., Arvai, A.S., Limbo, O., Guenther, G., SilDas, S., Hammel, M., Russell, P*., et al.* (2011). ABC ATPase signature helices in Rad50 link nucleotide state to Mre11 interface for DNA repair. Nature structural & molecular biology *18*, 423-431.

Williams, R.S., Dodson, G.E., Limbo, O., Yamada, Y., Williams, J.S., Guenther, G., Classen, S., Glover, J.N., Iwasaki, H., Russell, P*., et al.* (2009). Nbs1 flexibly tethers Ctp1 and Mre11-Rad50 to coordinate DNA double-strand break processing and repair. Cell *139*, 87-99.

Williams, R.S., Moncalian, G., Williams, J.S., Yamada, Y., Limbo, O., Shin, D.S., Groocock, L.M., Cahill, D., Hitomi, C., Guenther, G*., et al.* (2008). Mre11 dimers coordinate DNA end bridging and nuclease processing in double-strand-break repair. Cell *135*, 97-109.

Wiltzius, J.J., Hohl, M., Fleming, J.C., and Petrini, J.H. (2005). The Rad50 hook domain is a critical determinant of Mre11 complex functions. Nature structural & molecular biology *12*, 403-407.

Wong, A.K., Ormonde, P.A., Pero, R., Chen, Y., Lian, L., Salada, G., Berry, S., Lawrence, Q., Dayananth, P., Ha, P*., et al.* (1998). Characterization of a carboxy-terminal BRCA1 interacting protein. Oncogene *17*, 2279-2285.

Wyatt, H.D., and West, S.C. (2014). Holliday junction resolvases. Cold Spring Harb Perspect Biol *6*, a023192.

Wyrobek, A.J., Schmid, T.E., and Marchetti, F. (2005). Relative susceptibilities of male germ cells to genetic defects induced by cancer chemotherapies. Journal of the National Cancer Institute. Monographs, 31-35.

Xu, C., Wu, L., Cui, G., Botuyan, M.V., Chen, J., and Mer, G. (2008). Structure of a second BRCT domain identified in the nijmegen breakage syndrome protein Nbs1 and its function in an MDC1-dependent localization of Nbs1 to DNA damage sites. Journal of molecular biology *381*, 361-372.

Yaginuma, H., Kawai, S., Tabata, K.V., Tomiyama, K., Kakizuka, A., Komatsuzaki, T., Noji, H., and Imamura, H. (2014). Diversity in ATP concentrations in a single bacterial cell population revealed by quantitative single-cell imaging. Scientific reports *4*, 6522.

Yakovchuk, P., Protozanova, E., and Frank-Kamenetskii, M.D. (2006). Base-stacking and base-pairing contributions into thermal stability of the DNA double helix. Nucleic acids research *34*, 564-574.

Yang, W. (2011). Nucleases: diversity of structure, function and mechanism. Quarterly reviews of biophysics *44*, 1-93.

Yang, W., Lee, J.Y., and Nowotny, M. (2006). Making and breaking nucleic acids: two-Mg2+-ion catalysis and substrate specificity. Molecular cell *22*, 5-13.

You, Z., Chahwan, C., Bailis, J., Hunter, T., and Russell, P. (2005). ATM activation and its recruitment to damaged DNA require binding to the C terminus of Nbs1. Molecular and cellular biology *25*, 5363-5379.

Zahra, R., Blackwood, J.K., Sales, J., and Leach, D.R. (2007). Proofreading and secondary structure processing determine the orientation dependence of CAG x CTG trinucleotide repeat instability in Escherichia coli. Genetics *176*, 27-41.

Zeman, M.K., and Cimprich, K.A. (2014). Causes and consequences of replication stress. Nature cell biology *16*, 2-9.

Zimmermann, M., Lottersberger, F., Buonomo, S.B., Sfeir, A., and de Lange, T. (2013). 53BP1 regulates DSB repair using Rif1 to control 5' end resection. Science *339*, 700-704.

7. Abreviations

°C	degree celsius
6-FAM	6-carboxyfluorescein
Å	Angstrom
aa	amino acid
ABC	ATP binding cassette
ADP	adenosine diphosphate
alt-NHEJ	alternative non-homologous end joining
AT	adenine - thymine base pair
ATP	adenosine triphosphate
ATPγS	adenosine 5´-[γ-thio]triphosphate
BER	base-excision repair
BMOE	bis-maleimidoethane
bp	base pair
BRCT	breast cancer carboxy terminus
cNHEJ	classical non-homologous end joining
CSR	class switch recombination
C-terminus	carboxy terminus
CuSO4	copper sulfate
DNA	deoxyribonucleic acid
DNA-PKcs	catalytic subunit of DNA-dependent protein kinase
DSB	DNA double strand break
DSBR	DNA double strand break repair
dsDNA	double-stranded DNA
EDTA	ethylenediaminetetraacetic acid
EMSA	electrophoretic mobility shift assay
FHA	forkhead associated
GC	guanine - cytidine base pair
h	hour
HEX	6-Hexachloro-Fluorescein

HLH	helix-loop-helix
HR	homologous recombination
IPTG	isopropyl-ß-D-thiogalactopyranosid
IR	ionizing radiation
kDa	kilo dalton
LB	Lysogeny Broth
Mg	magnesium
min	minute
MMEJ	microhomology-mediated end joining
MMS	methyl methanesulfonate
Mn	manganese
Mre11	meiotic recombination 11
NBD	nucleotide binding domain
Nbs1	Nijmegen breakage syndrome 1
nt	nucleotide
N-terminus	amino terminus
OD_{600}	optical density at 600 nm
PAGE	polyacrylamide gelelectrophoresis
PCR	polymerase chain reaction
PDB	protein data bank
pH	potential of hydrogen
Rad50	radiation sensitive 50
ROS	reactive oxygen species
RPA	replication protein A
rpm	rotation per min
RT	room temperature
sc	single-chain variable fragment
SDS	sodium dodecyl-sulfate
sec	second
SMC	structural maintenance of chromosomes
SSB	DNA single strand break
ssDNA	single-stranded DNA

Tris	tris(hydroxymethyl)aminomethane
UV	ultraviolet
wt	wild type
Zn	zinc

8. Acknowledgements

First of all, I want to thank Prof. Karl-Peter Hopfner for his supervision of my work. You gave me not only the opportunity to work within this nice team but also permanently supported me during the last few years. You infected me with your enthusiasm about this project and you gave me at the time and the freedom to explore new ideas.

I am very thankful to Prof. Dr. Klaus Förstemann for being the second reviewer of this thesis as well as PD Dr. D. Martin, Prof. Dr. J. Stingele, Prof. Dr. R. Beckmann and PD Dr. Gregor Witte for accepting to be co-reviewers.
I am very grateful to Robert Byrne, Katja Lammens and Charlotte Lässig for careful proofreading of this work.

Many thanks go to all the members of the Hopfner group. I really enjoyed the friendly and inspiring working atmosphere. Thank you, for all your support with experiments and helpful scientific discussions. Special thanks goes to Katja for the steady support and help during the thesis and for the expertise in X-ray crystallography. Thank you Rob for the support, your broad and precise scientific expertise and always taking your time to share it! I also want to thank Aaron Alt and Sebastian Eustermann for many ideas and inspiring discussions.

I also want to thank all the members from the DNA repair group for the discussions, in particular Lisa Käshammer, my fellow on the SbcCD project. Thank you for fruitful conversations, the productive and collaborative working atmosphere, I really enjoyed working with you!

I want to acknowledge in particular also Alexandra Schele, Brigitte Keßler, Manuela Moldt and Olga Fettscher for the excellent organization of the laboratory.

I am very thankful to my students Benjamin Demarco Vargaras, Jennifer Willmann, Tiana Hanelt, Tobias Becker, Felix Metzner for their enthusiasm and hard work.

Most importantly I want to thank my beloved wife, Daniela, for your patience, love and support throughout my thesis. I am also deeply grateful to my family for the love and never-ending support!